# The Effect of Pre-Bond Moisture on In-Service Composite Bonded Repairs

by

**Nadine H. Auda**

Department of Mechanical Engineering

McGill University, Montreal

A thesis submitted to McGill University in partial fulfillment of the requirements of the degree of Master's in Engineering

15th April 2015

# Abstract

The increasing use of composite materials, namely carbon–fibre reinforced plastic (CFRP) composites, in commercial and military aerospace applications has led to new challenges, amongst which is developing robust composite repair methodologies. Bonded repairs are one of the methods employed by service depots to restore the original strength and stiffness of a composite component. In-service bonded repairs are accomplished by co-bonding a repair patch and adhesive layer onto the damaged structure and curing it by means of a heating blanket. However, composite parts absorb moisture over time as the aircraft is exposed to periods of high temperature and humidity, the effects of which could be detrimental during the bonding process and hence must be removed. Another source of moisture that is of concern is the atmospheric exposure of the uncured repair patch and film adhesive during the repair process, as well as absorbed humidity during storage. To effectively understand the effects of moisture on the repair, the problem was divided in three sections; first, the thermochemical behaviour of the film adhesive used in structural repairs was studied, then then the effects of moisture entrapped in the film adhesive and uncured repair patch was determined, and finally the effects of moisture entrapped in the parent laminate (the aircraft structure itself) due to years of service was assessed. Through this study, it was determined that the presence of pre-bond moisture in the repair affects the final quality of the part and reduces the strength of the repair. The experimental results show a cure gradient through the thickness of the repair laminate due to the one-sided heating nature of the repair that leads to increased void content. Additionally, the presence of pre-bond moisture in the repair was found to further increase the percentage void content and lead to a reduction in the tensile strength of the repaired laminate. Nevertheless, the repair procedures were found to be repeatable and robust as all repairs restored above 80% of the original laminate's strength.

# Résumé

L'utilisation croissante de matériaux composites, tels que ceux renforcés par des fibres de carbone dans l'industrie aérospatiale commerciale et militaire comporte de nouveaux défis, parmi lesquels on trouve le développement de méthodes de réparations robustes. Les réparations collées sont une des méthodes employées par les centres de réparation pour rétablir la résistance initiale et la rigidité d'une structure en matériau composite. Les réparations collées en service sont effectuées par le collage d'une pièce de réparation et d'une couche d'adhésif sur la structure endommagée suivie d'une cuisson à l'aide d'une couverture chauffante. Cependant, les éléments de la réparation peuvent absorber de l'humidité lorsque l'avion est exposé à des périodes de haute température et d'humidité. Cette exposition à un milieu humide peut engendrer des effets néfastes durant le processus de collage. Il est donc important de mieux comprendre ces effets afin de les éliminer. Une autre source d'humidité peut provenir de l'exposition de la pièce de réparation non polymérisée ou du film d'adhésif aux conditions atmosphériques. Pour comprendre de manière efficace les effets de l'humidité sur la réparation, le problème a été divisé en trois sections; en premier lieu, le comportement thermochimique du film d'adhésif utilisé dans les réparations structurelles a été étudié, ensuite les effets du taux d'humidité du film d'adhésif et de la pièce de réparation non polymérisée ont été déterminés, et finalement les effets du taux d'humidité de la structure primaire (la structure de l'avion même ) ont été évalués. Grâce à cette étude, on a déterminé que la présence d'humidité dans la réparation modifie la qualité finale de la pièce et réduit la résistance de la réparation. Les résultats expérimentaux montrent un gradient de réticulation à travers l'épaisseur du stratifié de réparation en raison du chauffage sur la surface de la réparation qui entraîne une augmentation de la teneur en vide. En outre, la présence d'humidité avant la polymérisation de la réparation a augmenté le pourcentage de vide et a entrainé une réduction de la résistance à la traction du stratifié réparé.

Néanmoins, les procédures de réparation se sont avérées reproductible et robuste alors que toutes les réparations ont restauré à plus de 80% de la résistance initiale du laminé.

# Acknowledgements

I would like to express my deepest gratitude to my advisor, Professor Pascal Hubert, for his guidance through the learning process of my master's thesis. His patience and support taught me to overcome obstacles and think critically and independently.

I would like to thank Natural Sciences and Engineering Research Council of Canada (NSERC) for their financial support, as well as all the industrial and academic partners for their funding and resources on this project, mainly CRIAQ for organizing and arranging the funding; Bombardier, L3, and CNRC for their invaluable industry experience; as well as Université Laval and Ecole Polytechnique de Montréal for their feedback and collaboration; and McGill University for the use of their facilities.

I am thankful for the wonderful friendship I cultivated with my collaborators on the project; Mathieu Préau and Kavish Bujun; I truly appreciate their invaluable contributions throughout the course of my research. A big Thank You goes to Lucie Riffard for her support with the test equipment and methods and Marie Romedenne for her help with the thermomechanical testing.

The very interactive and involved atmosphere created by the members of Structures and Composites Materials Laboratory made my graduate experience smooth and enjoyable, for which I am really thankful.

I would like to thank my team and management at Bombardier for affording me the time and flexibility that allowed me to complete my research.

Finally, I would like to extend my gratitude to all the people who supported me throughout my master's journey. I am grateful to my wonderful husband and loving family for their endless patience and support.

# Table of Contents

# List of Figures

# List of Tables

# Chapter 1

# Introduction and Literature Review

## 1.1 Introduction

The use of composite materials in the aerospace industry has seen a sharp upwards trend over the past two decades, as more aircraft manufacturers began using composites for primary structure. Composite materials have shown to have high potential in areas of weight savings, optimization, toughness and resistance to fatigue degradation enabling application to many large aircraft components such as the fuselage and wing. Combining composite materials' properties with advanced layup and manufacturing technologies, manufacturers estimate operational efficiency improvement by means of increased range, reduced operation and maintenance costs which are highly desirable by the airline operators [1]. With these advantages, the industry has seen an increase in implementation of composites in more commercial aircraft starting with Boeing's 787 aircraft's extensive implementation at 50% of the structure being manufactured using multiple forms of composites followed by other aircraft manufacturers like Airbus A-350 and Bombardier's CSeries aircraft. Figure 1-1 shows the increasing usage of composites in commercial aircraft over the past two decades, exceeding those in military applications.

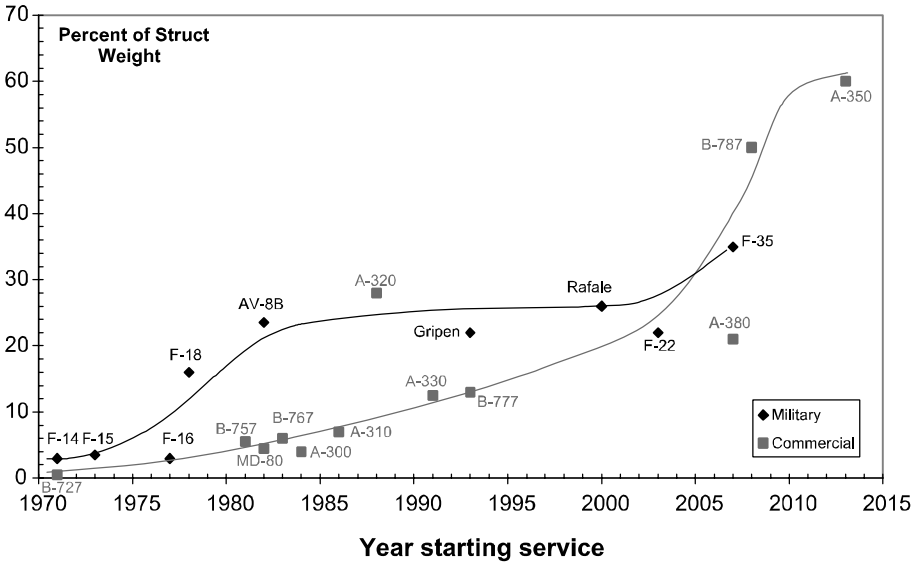


**Figure 1-1: Evolution in the application of composites in military and civilian aircraft structures [1]**

The main focus in the aerospace industry is to take advantage of composites to reduce the scheduled maintenance requirements of the aircraft. Damage tolerance and damage resistance analysis of aircraft components are required to consider in-service threats, which for most part, remain unchanged between metallic or composite components. Damage tolerance analysis of composite typically involves damage threat assessment and residual strength analysis while metallic components are traditionally analyzed using Linear Elastic Fracture Mechanics (LEFM) crack growth analysis. Fracture mechanics based approaches can be used for composites; however their use is currently limited due to insufficient in-service data, lack of experience and applicability under only limited scenarios. Since composites are semi-brittle materials, their strength can reduce sharply with flaws, defects and damages. However they usually have very high fatigue life under typical flight loadings.

Aircraft components, even those manufactured using high stiffness and strength materials, require maintenance and repair in-service due to various unforeseen events. In early production days, composites were limited to secondary structures such as fairings; these structures are removable so they can be repaired at a service depot, or in the case of large damages these fairings can be economically replaced. Recently, with more knowledge and rigorous processes, composite repairs are more easily achievable, as they

are necessary for larger components that cannot be removed or replaced. To develop repair procedures, one must consider the selection of materials and a methodology that would restore the strength of the structure while respecting the certification criteria of strength, stiffness, process repeatability and robustness.

The objective of a composite repair is to rebuild the primary load path throughout the structure; ideally a repair would match the original strength, stiffness and weight. In many instances, it is not feasible to reproduce exactly the same original structure, but it is still imperative that the overall stiffness and strength of the repair patch to be as close to parent structure. This ensures continuity of the original load path. It is difficult to match the exact original properties (strength and stiffness) of the parent structure once a repair is implemented, therefore acceptable trade-offs are utilized in the repair design. The trade-offs in the repair design and its impact on the structural behaviour should be well understood.

There are two primary methods of repairing composite structures in the industry; bolted and bonded repairs. Bolted repairs have been historically selected due to prior industry experience, readily available repair materials and minimum influence on the repair quality due to in-field processing parameters. In addition, many guidelines already exist for repair depots to use in designing a bolted repair, with relatively accurate tools in place to predict the repair's final strength. Many of these guidelines have been developed and documented by the industry and government authorities in the Composites Materials Handbook, [2]. However, bolted repairs do come with a weight penalty, as these repairs tend to be heavier with a higher Bill of Materials (BOM) cost. It is also possible to develop fatigue-cracking issues over time. The selection of the fasteners used in the repair is also crucial as galvanic corrosion is a concern in a hybrid composite-metallic structure. Since bolted repairs require a structure of a certain minimum thickness, protruding head fasteners are used to accommodate for thickness requirements of countersunk fastener and hence a protruding repair (non-flush) which may cause aerodynamic inefficiencies.

On the other hand, adhesively bonded repairs have some significant advantages over bolted repairs. The repair is usually more fatigue resistant as the damage initiation sites and stress concentrations caused by drilling are removed. Bonded repairs are considerably lighter as eliminating fasteners along with the associated galvanic corrosion concerns reduces the part count. Furthermore, bonded repairs can be used for any thickness substrate while respecting the aerodynamic requirements of the aircraft. However, better understanding of the bonded repair process is vital to ensure a good quality repair joint as adhesively bonded repairs are process dependent and sensitive to harsh environments. Robust Non-Destructive Inspection methods are yet to be developed to accurately detect weak bonds in the joint.

## 1.2 Bonded Repair Overview

In recent years, the civil aerospace industry has recognized the need for standardized bonded repair process due to heavy use of composites in new aircraft designs evident by the aircrafts entering into service. An industry driven group (airliners, OEMs, and repair depots) working with regulatory authorities has been formed to develop and improve maintenance procedures, inspection methods and in-service repair processes of commercial aircraft composite structure and components known as the “Commercial Aircraft Composite Repair Committee” (CACRC), [3]. A typical CACRC-recommended adhesively bonded repair requires the removal of the damaged plies by sanding to gradually expose the laminates. Usually a drying procedure is required prior to the application of the repair patch to remove all the moisture entrapped in the skin throughout the service life of the aircraft. The prepared location is then cleaned and the repair laminates are placed. The repair patch is then cured on top of the original parent structure (aircraft part) using a heating blanket under vacuum as in most cases the part cannot be placed in an oven. A summary repair workflow is shown in Figure 1-2, and an industry example is shown in Figure 1-3, [3]. These repairs are typically done on the field with no access to an environmentally controlled hanger or cleanroom.


**Figure 1-2: Typical in-service repair process flow**

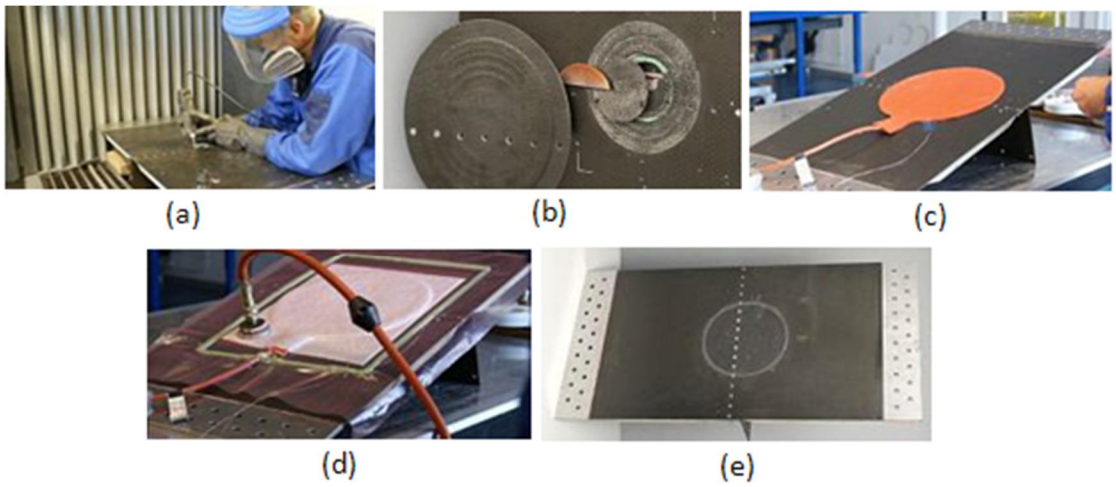


**Figure 1-3: Example of a repair prepared at a service depot; (a) damage removal, (b) repair patch application, (c) heating blanket placement, (d) bagging and vacuum application, (e) repaired part ready for inspection [4]**

In typical maintenance and repair cases, the operator has to ground the aircraft for the duration of the repair. Unscheduled downtime due to repairs increases maintenance cost of an aircraft, thus reducing operational profit for airlines. For example, An airbus A320 delay costs approximately $7,400 an hour in revenue which turns to hefty profit losses compounded by additional delay costs for the duration of lengthy or complex repairs [5, 6]. It is in the airliner's best interest to produce a good quality repair in the most efficient way possible namely by ensuring the implementation of a robust and low cost repair process.

## 1.3 Background and Literature Review

All composite components of aircrafts are exposed to moisture during the course of their service life, which is then typically absorbed by the polymer matrix of the composite structure. A survey carried out by Collings [7] of climatic records taken from six geographical locations, presented in Table 1-1, shows the most severe environmental conditions likely to be met by composite materials in service.

**Table 1-1: Survey of climate records (relative humidity) for six geographical locations [7]**

| | **%RH throughout the year** | | | |
|---|---|---|---|---|
| | January-March | April-June | July-September | October-December |
| **Port Harcourt in Nigeria** | 58-95% | 70-95% | 75-95% | 61-96% |
| **Schleswig in Germany** | 72-91% | 61-92% | 66-93% | 78-94% |
| **Woodbridge in UK** | 66-83% | 61-83% | 60-84% | 68-82% |
| **Singapore** | 69-92% | 68-95% | 70-90% | 68-93% |
| **Guam** | 75-84% | 75-88% | 78-89% | 70-87% |
| **Bahrain** | 57-81% | 49-74% | 50-77% | 56-82% |

During a typical bonded repair operation, it is recommended for the composite structure to be dried prior to the beginning of the repair, which could take from hours up to several days depending on the level of moisture content in the structure. Typical levels of moisture in components in service is found to be 0.8-1.0% by weight [8]. However, in-service environmental exposure is not the only concern in a repair environment as moisture can be absorbed into the joint in different ways. In fact, a problem well acknowledged in the industry is that of the moisture that might be absorbed by uncured composites (prepreg or film adhesive) during storage, especially when taken out from the freezer, as condensation forms on the surface as it warmed to room temperature. Finally, repair materials that are left uncovered during the multi-step process of bonded repairs may also absorb and trap atmospheric moisture.

It has been found that once moisture enters an adhesive joint, the effects can be complex, as presence of moisture proved to have detrimental effects on the bond quality, joint strength, and presented some detrimental effects on the fracture toughness of the film adhesive depending on the adhesive system used. For example, it was found that moisture of 1% could drastically reduce the fracture toughness of some adhesive joint systems while others are not affected or even experience a slight increase in the fracture toughness, [9], which can be attributed to the extra energy being absorbed due to plasticization of the adhesive. Blackman et al noted that results were not always consistent for all adhesives; the observations show that effects of pre-bond moisture are complex and heavily dependent on the adhesive's sensitivity to moisture, [10].

The majority of the findings related to bonded joints and moisture ingress recommend drying the substrate prior to bonding. Typical repair procedures recommend implementing a drying step before bonding. As drying of composites may take up to several days depending on the thickness and initial moisture levels, this step may increase the repair costs because of the energy required for the drying process and the down time causing revenue loss for the airline operator, hence not always desirable.

### 1.3.1 Moisture Sources in the Repair

Presence of moisture in composites may affect the properties of the repair as it can cause an increase in bond line porosity and a decrease in joint strength. Research has shown that joints prepared with composite substrates exhibited lower fracture toughness than those bonded with metallic substrate which can be attributed to the moisture in the substrate. This is suspected to be due to the pre-bond moisture in the composite substrates diffused into the adhesive during the curing process of the joint.

One of the early research into the effects of the substrate on the joint quality was done by Sage et. al described the "bubble problem" as large voids were found to be caused by the emission of water vapor from the composite when bonding previously cured composites at high temperature, this phenomena was not noted for non-CFRP substrate, [11]. In composite substrates, water and volatile components previously absorbed by the

composite begin to boil off during the high temperature phase of the cure cycle. Spectrophotometric analysis was done and concluded that the emissions were mostly water vapor with small traces of other compounds. Static tension strength and fatigue life were significantly reduced due to the bubble effect.

- Large bubbles: 40-60% of static strength, fatigue average of 35,000 cycles (R= -1)
- Small bubbles: 70% of static strength, fatigue average of 130,000 cycles (R= -1)
- No bubbles: 100% of static strength, fatigue average of 775,000 cycles (R= -1)

It was found by Blackman that the substrate material could affect the fracture toughness of the film adhesive; this is likely due to the moisture absorbed by the composites, a trend no present for metallic substrate, [12]. This effect is due to the moisture trapped in the composites that diffuse into the film adhesive during the cure cycle of the repair. This moisture would then interfere with the phase separation of the rubber toughening agent during the cure of this adhesive hence reducing the glass transition temperature of the adhesive and the strain energy release rate of the joint. The results in Table 1-2 shows that the fracture toughness of an adhesive bonded to a metallic substrate was almost up to four times higher than that bonded to a composite substrate.

**Table 1-2: Fracture toughness results for film adhesive bonded to aluminum, steel, and composite substrates**

| Substrate | $G_c$ ($Jm^{-2}$) | $T_g$ (°C) |
|---|---|---|
| **Aluminum alloy** | 0% | 0% |
| **Mild steel** | 30% | 2% |
| **Composite "dry"** | 35% | 3% |
| **Composite "as received"** | -71% | -13% |
| **Composite "wet"** | -85% | -18% |

Blackman had further investigation into the effects of pre-bond moisture in composite substrate; that exposure to moisture was found to lead to significant reductions in joint

strength and change in the locus of the joint failure from cohesive in the adhesive to interfacial between the adhesive-substrate interface, [12].

The effects of drying the substrate prior to bonding were studied as well, a threshold of pre-bond moisture up to 0.5% by weight was found to have little effect on the final joint strength. However, pre-bond moisture of about 1.3% would cause a 20% loss in the tensile strength of the joint, whereas the flexural strength of the joints was not affected. Robson et al also found that surface moisture is more critical than the total absorbed moisture for the final strength of the joint, hence long exposure to low humidity less detrimental than short exposure to high humidity, [8].

All literature sources studied, [8-10, 12], showed that an increase in the pre-bond moisture of the composite substrate yielded an increase in the void content of the joint , further supporting the "bubble theory" by Sage et al, [11].

To further isolate the effects of the moisture in the substrate, a few studies looked into the effects of the moisture on the film adhesive only. Dodiuk [13] studied the effect of moisture on cured film adhesives to isolate the moisture problem from substrate effects. It was shown that when the moisture level in the film adhesive is above a certain threshold value (0.3% by weight), the strength of the adhesive was partially regained by drying. However, it was noted that above this critical moisture level an irreversible change occurred in the adhesive that resulted in a permanent loss of properties.

More studies specifically on the effect of moisture on cured FM300 adhesive showed that moisture can penetrate into the adhesive and weaken the joint by plasticization or hydrolysis of the adhesive, [14]. Dynamic Mechanical Analysis (DMA) was used to determine the glass transition temperature ($T_g$) of the film adhesive. It was noted that the $T_g$ value decreased with moisture, as moisture is known to plasticize epoxies which lead to a reduction in the glass transition temperature and softening of the adhesive. To verify the reversibility of hygrothermal ageing of the adhesive, DMA samples were immersed in water then oven dried. The reversal of moisture effects on the glass transition temperature by means of drying was also studied. It was found that the moisture effect on the mobility

of the crosslink network was almost completely reversible after specimen drying. This reversal of the moisture effect on the $T_g$ indicates that changes associated to moisture exposure were due to plasticization rather than hydrolysis.

Further studies of FM300 bonded joints were conducted by Mohan et al, focusing on moisture content in the prepreg due to storage conditions and their effects on the fracture toughness of the adhesive, [15]. This moisture was released during the co-curing cycle which plasticized the adhesive and also resulted in interfacial failure. Effect of moisture content in the prepreg had very different effects depending on the test method. For example, Mode I loading conditions lead to a reduction of 20% in fracture toughness at the highest humidity level, whereas Mode II lead to a reduction of 50% of the fracture toughness. While the locus of failure was primarily interfacial in nature for the as-received co-cured joint system, when humidity levels increased, there was a noticeable increase in the degree of cohesive failure of fracture toughness specimens at the higher humidity levels.

### 1.3.2 Void Formation in Prepregs

Since the typical in-service bonded repair procedure does not permit the use of an autoclave, a vacuum-bag-only (VBO) atmospheric pressure bagging configuration is used to consolidate the repair patch during cure. Therefore, the repair material selection is restricted to those engineered for Out-of Autoclave (OOA) applications. OOA prepregs can be cured at lower pressures and temperatures (vacuum pressure vs. a typical autoclave pressure of 85 psi and cure at 200°F/93°C or 250°F/121°C vs. a traditional 350°F/ 177°C autoclave cure), therefore reducing high capital and operating costs. Additionally, mismatches between tool and part coefficients of thermal expansion (CTEs) are smaller at lower temperatures; therefore, potential part cracking caused by cure-temperature differentials is reduced, [16-18]. However, a high percentage of void content has been observed in cured OOA laminates due to entrapped air which cannot be collapsed by the lower compaction pressure of a VBO system.

Voids are defects found in cured composite laminates that can be described as small cavities of different shapes and sizes that are found in resin rich regions (between the plies or between the fibre tows. The void content of a composite part can be calculated as the ratio between the volume occupied by voids and the total volume of the composite.

Many sources of void formation are a byproduct of air or gas entrapped in the laminate during the fabrication process, shown in Figure 1-4, most of which is evacuated via the vacuum pump during cure. Air entrapped in or between the prepreg plies during the layup or volatiles generated by the resin's chemical reaction during cure could be sources of void formation. In some cases, moisture in the laminate was found to generate voids as the water turns into vapor during the cure, [18, 19].

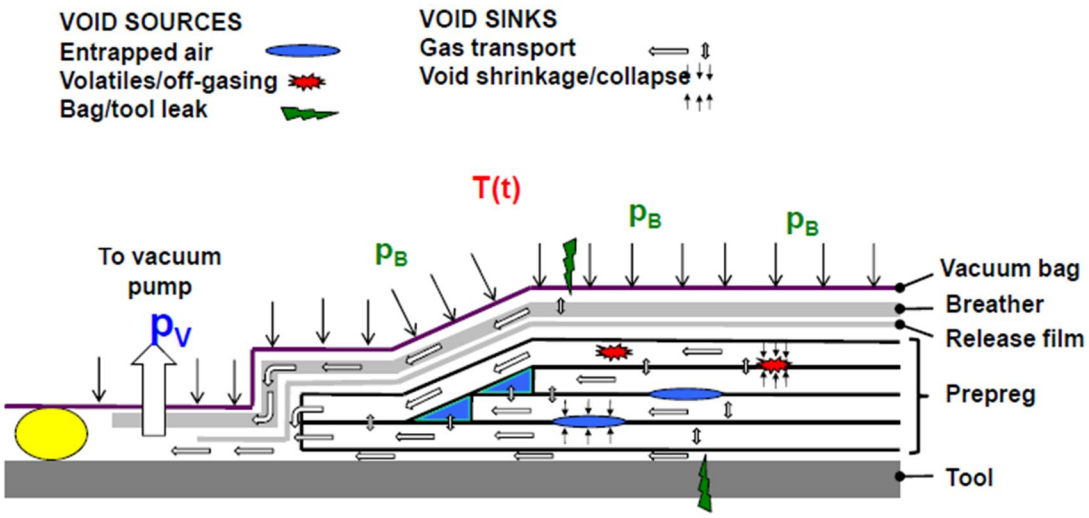


**Figure 1-4: Void sources and sinks in a composite laminate. Entrapped air, volatiles and off-gassing of the resin chemical reaction, and bag leaks are all sources of possible void formation. The breather layer provides a path for the gasses to be evacuated via the vacuum pump [19]**

The evolution of the void depends on the pressure differential between the gas in the void and the resin surrounding the void, and the surface tension at the interface. Pressure applied by autoclave cure is high enough to collapse the voids. However, pressure applied by out-of-autoclave technology might not be sufficient to remove all the voids entrapped in the laminate.

Since moisture is one source of voids in a laminate, an analytical model was developed by Grunenfelder et al [20] to predict the void formation in the laminate as a function of humidity exposure. The experimental framework showed a clear correlation between the void content formed in the laminate and the moisture level within the laminate pre-cure. The results of the study clearly demonstrate the effectiveness of the autoclave pressure in eliminating voids when compared to the void content results of an out-of-autoclave pressure (for the same moisture content samples). Equation (1-1) was used to predict the percentage void content (Vol%) as a function of relative humidity.

$$Vol\% = \frac{\pi\left[4\beta(Dt)^{1/2}\right]^3}{6V_m} \quad \textbf{(1-1)}$$

where $V_m$ is the unit matrix volume, β is the growth driving force, t is time, and D is the diffusion coefficient of water in the prepreg.

### 1.3.3 Environmental Conditioning

As previously stated, most polymeric materials are capable of absorbing small, but potentially significant amounts of moisture from their surrounding environment. Generally, the moisture gain mechanism is mass diffusion following Fick's Law, assuming no cracks or other absorption paths are present in the structure. The moisture gain through the thickness of a composite laminate is slow, however as time progresses (in the order of weeks to months) a significant amount of water will be absorbed in the structure. Absorbed moisture in many aerospace applications is considered a design concern; hence evaluation of the material properties is often conducted after representative moisture exposure, [2].

The environmental conditions of most concern is hot/wet hygrothermal conditioning simulating the effects of long term environmental exposure. The hygrothermal conditioning of composites involves three main variables; temperature, moisture conditions and time, [21].

The amount of water absorbed in a composite laminate is thickness and time dependent, therefore a fixed-time conditioning method is not recommended. Instead, conditioning procedures should be based on the final moisture content in the laminate. One such standardized method is captured in ASTM D 5229/5229M, [22], that documents the weight gain of an initially dry sample exposed to a hot and humid environment. During early weighing, the mass-time relation that determines the diffusion constant is linear. As the sample approaches equilibrium, the weight increase between weighing approaches zero. The diffusion constant is a material property that controls the rate of moisture absorption and is a function of the temperature. Whereas moisture equilibrium content of a laminate is a function of the humidity.

The most common approach taken to determine environmentally induced changes in materials is to expose the material to a particular environment and then compare the properties of the material before and after exposure. The amount of absorbed water in the composite has significant effects on the property reduction with increasing temperature as shown in Figure 1-5, [2]. To achieve this comparison, tests are performed with preconditioned specimens with moisture content representative to that found at the design service life (end-of-life). The upper bound humidity level used for environmental testing was determined from historical aircraft data and was found to be 85%RH [2]. The second variable in environmental conditioning is the temperature at which conditioning is performed. As matrix-dominated properties of a composite laminate decrease with increasing temperatures, care must be taken when determining the upper bound of test temperatures as to not artificially degrade the material. A reasonable upper bound temperature for environmental conditioning is the material operational limit (MOL). Many criteria for selecting the MOL exists, one of the most popular is using the glass transition temperature; the MOL is considered 50°C below the $T_g$ of the material.

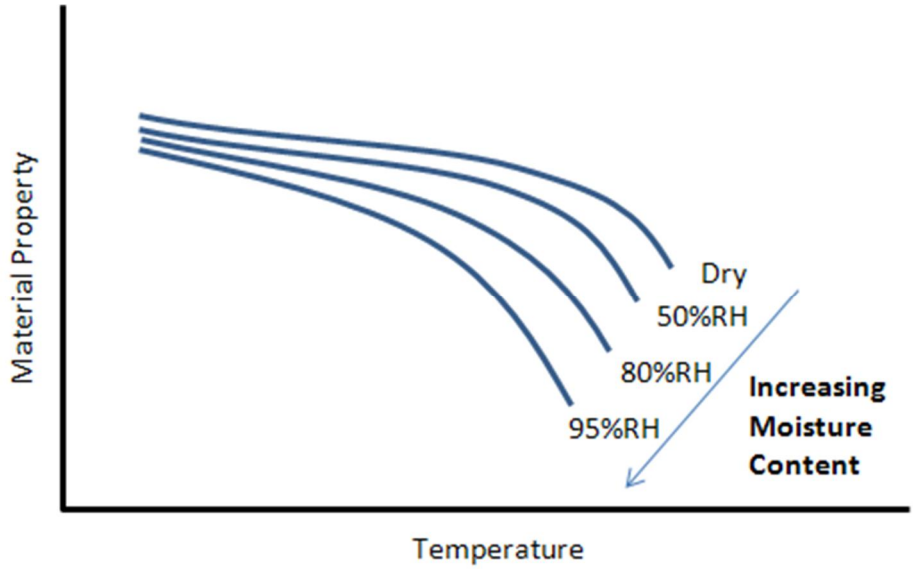


**Figure 1-5: Influence of the temperature and moisture on the matrix-dependent material property[2]**

Many industrial grade environmental chambers exist that are used for sample conditioning; their main function is to act as a closed environment kept at constant temperature and humidity. Simpler conditioning apparatus have been found in the literature capable of achieving the same objectives. This apparatus, shown in Figure 1-6, uses a closed container partially filled with saturated salt solution; the amount of air above the salt solution is kept to a minimum. Humid air above saturated salt solutions provide a constant and well-defined humidity level, [21]. There is a wide variety of salt solutions that produce different humidity levels depending on the temperature, [23]. For example, a closed container half-filled with a saturated solution of sodium chloride and distilled water will provide a constant humidity level of around 75% at 25°C, [21].


**Figure 1-6: Experimental setup for maintaining constant humidity environments for coupon conditioning**

## 1.4 Research Motivation

The majority of research papers recommend drying the composite substrates before bonding to prevent the diffusion of moisture in the substrate into the joint during repair cure cycle. However, the effects of moisture are not always reversible by drying. Research is needed to establish whether the effect of pre-bond moisture is always detrimental or whether a small percentage of moisture in the composite is acceptable.

The content of a selected number of relevant research papers was summarized to identify potential gaps in knowledge that is of relevance to the topic at hand, shown in Table 1-3. Fracture toughness of the film adhesive has been studies along with moisture effects in the substrate and the uncured prepregs. An opportunity was identified to further implement these research ideas for an in-service representative repair scenario as most of these papers address a small component of an adhesively bonded joint.

**Table 1-3: Summary of relevant results from select research papers**

| Author | Conditioning | | | Effects of Drying | Voids | Takeaway Result |
|---|---|---|---|---|---|---|
| | S | FA | P | | | |
| Robson et al [8] | Yes | - | - | - | Yes | A threshold of moisture content less than 0.5% w/w was found below which drying is not required |
| Sage et al [11] | Yes | - | - | - | Yes | Static strength and fatigue life reduction due to pre-bond moisture in composite substrates causing the "bubble problem" |
| Blackman et al [10, 12] | Yes | - | - | Yes | Yes | Large voids were found in the adhesive for high levels of pre-bond moisture associated with low toughness values. Results dependent on adhesive's sensitivity to moisture. |
| LaPlante et al [14] | - | Yes | - | Yes | - | Reduction of the adhesive's glass transition temperature due to moisture; effects could be reversible by drying |
| Dodiuk et al [13] | - | Yes | - | Yes | - | Strength can be partially regained by drying of samples with moisture content less than 0.3% w/w |
| Grunenfelder et al [20] | - | - | Yes | - | Yes | Analytical model predicting void formation in the resulting laminate as a function of moisture content |
| Parker et al [24, 25] | - | - | Yes | - | Yes | Strength reduction of the joint due to prebond moisture due to storage conditions |

*S = cured substrate, FA = Film Adhesive, P = uncured prepreg*

## 1.5 Research Objectives

The objective of this research project is driven from the industry's need to better understand the effects of moisture on bonded joints in in-service representative conditions. This thesis will focus on studying the effect of prebond moisture for three separate scenarios; in the parent laminate (cured substrate), in the film adhesive, and in the repair prepreg (uncured). The main research tasks are summarized below.

1. First, the effect of moisture on the cure behaviour of the structural film adhesive used in the bonded repairs will be investigated.
2. Second, a moisture content threshold below which material and strength degradation due to moisture is negligible will be determined.
3. Finally, the quality and strength of the resulting environmentally conditioned repairs will be assessed and a correlation between the moisture content, resulting void content, and final strength of the repair will be determined.

## 1.6 Thesis Structure

The thesis is organized in the following chapters:

Chapter 2: the thermochemical behaviour of the film adhesive is presented. Cure kinetics and viscosity models are developed and the glass transition temperature of the adhesive is calculated. The effects of moisture are then taken into account and the results are compared to the nominal “as-received” conditions.

Chapter 3: a summary of the sample manufacturing techniques are discussed. The parent laminate manufacturing methods were detailed, as well as the typical bonded repair method and apparatus. The laboratory scale environmental conditioning techniques were discussed, and the final specimen void content is presented.

Chapter 4: the mechanical testing methods are discussed. The final strength of the specimens are presented. The effect of the void content on the failure mode and strength is presented.

Chapter 5: a conclusion on the main findings of the research and proposed future work are presented.

Chapter 2

# Cure Behaviour of Adhesive Film

To fully understand the effect of moisture in a bonded repair, it is imperative to first understand the cure behaviour of the adhesive and to study the effects of moisture on the cure. Therefore, the curing behaviour of the FM300-2M is investigated in order to obtain the evolution of the degree-of-cure as a function of time and temperature, and the adhesive's glass transition temperature was also measured as a function of the degree-of-cure. A select number of samples of film adhesive were then conditioned and the curing behaviour and viscosity were investigated against the nominal results. The following sections describe the equipment and experimental procedure used to perform the tests.

## 2.1 Cure Kinetics

The extent of the reaction of the adhesive is known as the degree of cure; a characteristic that is used in physical property models such as the glass transition temperature and viscosity models. To determine the degree of cure experimentally, the heat flow of small amounts of adhesive is monitored at given temperatures for long periods of time. These experimental results can be mathematically modelled in an equation used to determine the degree of cure of the material at any given temperature. This mathematical equation is also known as the cure kinetics model,

which could be a helpful tool used to design or alter the cure cycles for thermosetting composites.

### 2.1.1 Experimental Procedure

A calibrated TA Instruments Q100 Dynamic Scanning Calorimeter (DSC) was used to measure the heat flow of the film adhesive in isothermal and dynamic conditions. The dynamic scans measure the total heat of reaction released during the cure, whereas isothermal scans are used to monitor the heat flow during a series of cures at constant temperature.

Isothermal tests were performed between 80°C and 140°C to determine the isothermal heat of reaction, after which the sample was cooled to room temperature and then ramped at 2°C/min to determine the residual heat of reaction. Dynamic scans at 2°C/min from room temperature up to 300°C were conducted to determine the total (exothermic) heat of reaction of the adhesive. Summary of the DSC tests for as-received samples (unconditioned) is shown in Table 2-1.

**Table 2-1: DSC test matrix for as-received samples of FM300-2 adhesive**

| Conditioning | DSC Test | Temperature (°C) | Time (min) | Ramp Rate (°C/min) | Residual Temperature (°C) | Number of samples |
|---|---|---|---|---|---|---|
| | Dynamic | 300 | - | 2 | - | 2 |
| **As-Received** | Isothermal | 80 | 990 | 2 | 250 | 2 |
| (nominal | Isothermal | 100 | 600 | 2 | 250 | 2 |
| conditions) | Isothermal | 120 | 240 | 2 | 250 | 2 |
| | Isothermal | 140 | 120 | 2 | 250 | 2 |

The measured heat of reaction generated by the adhesive is then converted into cure rate based on the assumption that the rate of reaction is proportional to the rate of the heat flow, as shown in Equation (2-1),

$$\frac{d\alpha}{dt} = \frac{1}{H_T}\frac{dH}{dT} \quad \textbf{(2-1)}$$

The degree-of-cure of the adhesive can be obtained by integrating the area under the curve of cure rate versus time, Equation (2-2), where α in the degree of cure and $H_T$ is the total heat of reaction.

$$\alpha = \frac{1}{H_T}\int_0^t \left(\frac{dH}{dt}\right) dt \quad \textbf{(2-2)}$$

The total heat released during a complete reaction was calculated using the dynamic tests, shown in Table 2-1. The total heat of reaction was determined as the area between the heat flow curve and the baseline curve. The baseline curve is obtained from the heat flow results and is the linear line between the start and end of the reaction as shown in Figure 2-1. Using this technique, the average total heat of reaction for an as-received FM300-2M adhesive film sample was 311.7 J/g with a standard deviation of 3.4 J/g.

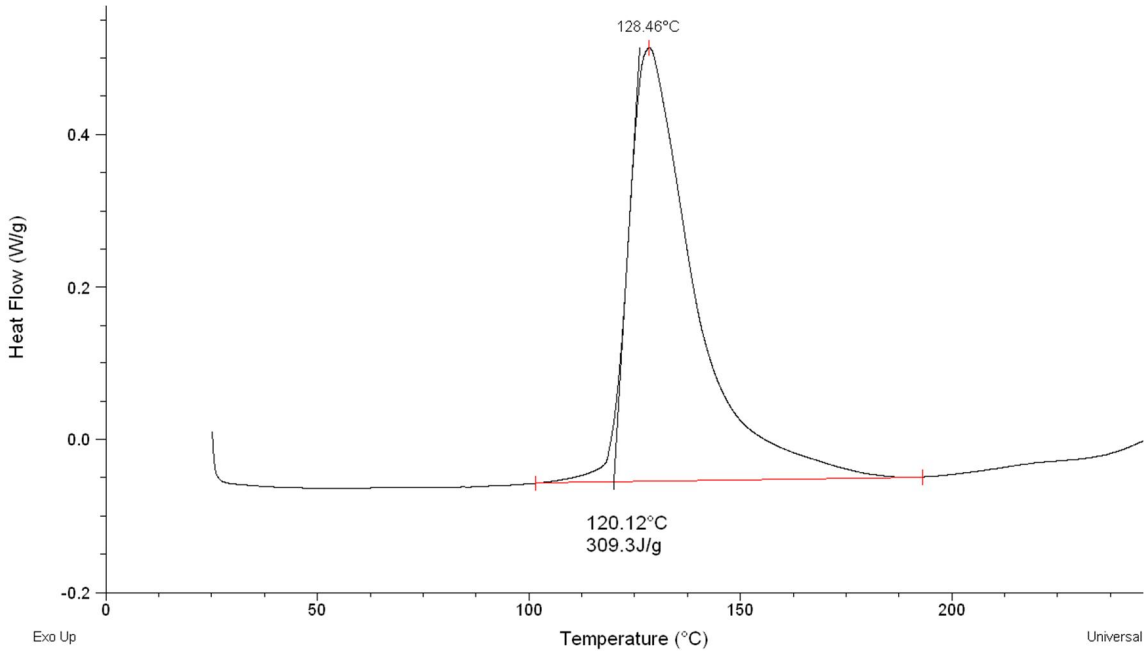


**Figure 2-1: Heat flow from a dynamic scan at 2°C/min up to 400°C. Example shown for an as-received (unconditioned) sample of FM300-2M**

### 2.1.2 Cure Kinetics Model

To determine the cure kinetics model, only data obtained from as-received (unconditioned) samples of FM300-2M were used in the process herein.

The experimental cure rate determined in Equation (2-1) is used to fit constants to several diffusion controlled autocatalytic equations obtained from literature. Equations (2-3) and (2-4) shown below, obtained from Khoun et al [26], best describe the curing behaviour of the FM300-2M film adhesive.

$$\left(\frac{d\alpha}{dt}\right)_{model} = K\frac{\alpha^m(1-\alpha)^n}{1 + exp\left(C\left(\alpha - (\alpha_{C0} + \alpha_{CT}T)\right)\right)} \quad \textbf{(2-3)}$$

$$K = A\, exp\left(\frac{-E_A}{RT}\right) \quad \textbf{(2-4)}$$

where K is the rate constant, A is the experimentally determined Arrhenius constant for the adhesive, $E_A$ is the activation energy determined by calculating the slope of ln(dα/dt) versus (1/T) at low degree-of-cure ($\alpha = 0.1$) as shown in Figure 2-2 and Equation (2-5), where R is the universal gas constant, and T is the absolute temperature.

$$ln\left(\frac{d\alpha}{dt}\right) = lnA - \frac{E_A}{RT} \quad \textbf{(2-5)}$$

$$\alpha_{max} = \alpha_{CT}T + \alpha_{C0} \quad \textbf{(2-6)}$$

The constants $\alpha_{C0}$ and $\alpha_{CT}$ which correspond to the critical degree of cure at absolute zero and the increase in critical degree of cure with temperature were experimentally calculated using Equation (2-6) and Figure 2-2.

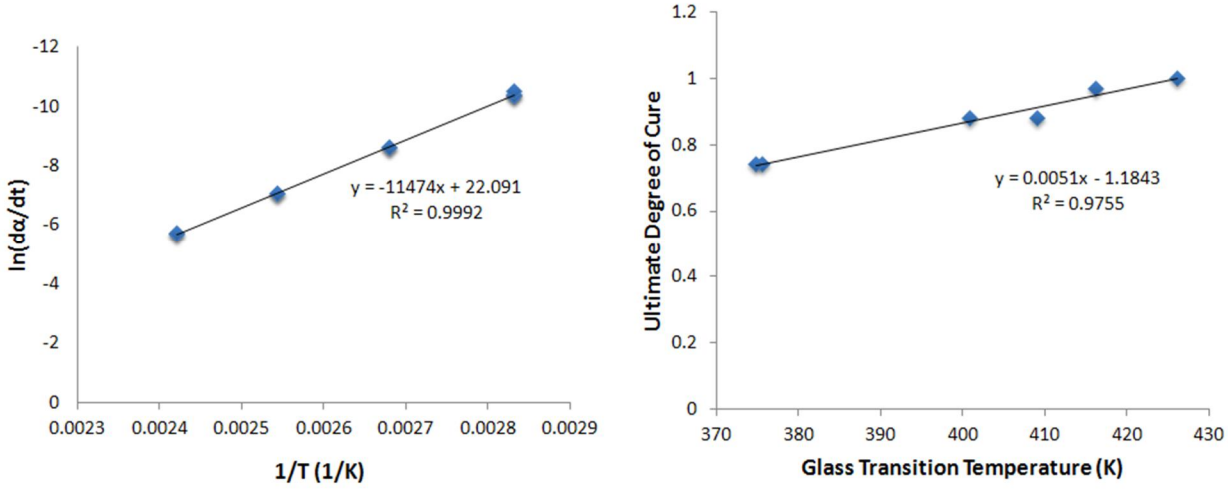


**Figure 2-2: Determination of cure kinetics model constants; left: Arrhenius plot to determine the activation energy $E_a$, right: $\alpha_{C0}$ and $\alpha_{CT}$ are determined from the slope of $T_g$ (Table 2-3) and the final degree of cure**

Finally, the material constants m and n, the diffusion constant C, and the Arrhenius constant A were experimentally determined and optimized using sum of least square, their values along with the activation energy ($E_a$) are summarized below;

| | |
|---|---|
| $\alpha_{C0}$ = -1.184 | $\alpha_{CT} = 5.10 \times 10^3$ (1/K) |
| $R$ = 8.314 J/(mol.K) | $E_A$ = 95395 (J/mol) |
| $A = 3.37 \times 10^{10}$(1/s) | $C$ = 25.0 |
| $m$ = 0.923 | $n$ = 2.41 |

The model is in acceptable agreement with the experimental results assessed by the goodness of fit of the model, reflected by $R^2$ values. The $R^2$ values are well above 0.8 for the 100°C, 120°C and 140°C isothermal runs, as shown in Figure 2-3. Figure 2-4 shows the evolution of the degree of cure. The model slightly over predicts the degree of cure for the 100°C and 120°C isotherm samples, and slightly under predicts the degree of cure for the 140°C samples. However, the model under-estimates the degree of cure for the 80°C isotherm until $\alpha = 0.6$. This behaviour, however imperfect, can be tolerated for extreme temperatures, as the as 80°C isotherm falls well below the manufacturer's recommended processing window of the FM300-2M film adhesive.

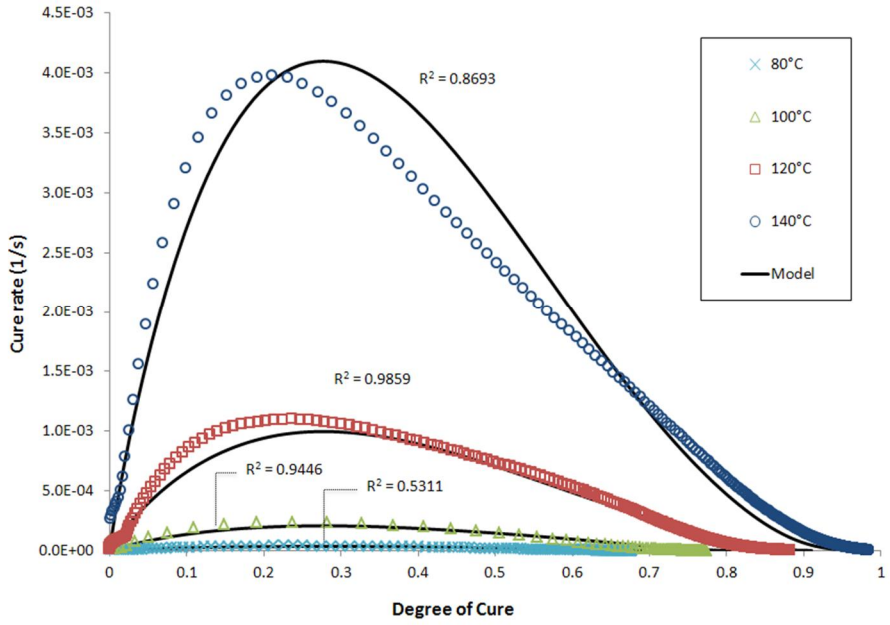


**Figure 2-3: Isothermal progression of the cure rate with increasing degree of cure for as-received FM300-2M samples. The experimental data (symbols) is compared with the model predictions (solid lines)**

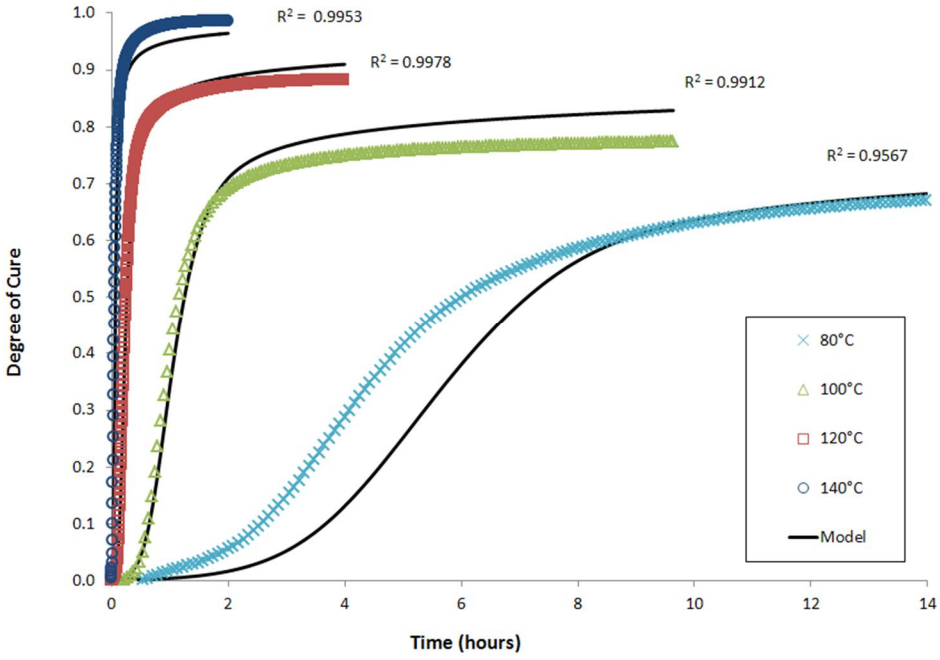


**Figure 2-4: The evolution of the degree of cure during the cure for as-received FM300-2M samples. The experimental data (symbols) is compared with the model predictions (solid lines)**

## 2.2 Glass Transition Temperature

The glass transition temperature ($T_g$) is an important parameter to study as it represents the temperature when a polymer goes from a hard glassy state to a rubbery state; above which the polymer exhibits the properties of a rubbery solid that transforms into a hard, brittle glass-like material as it's cooled down, which in turn has an increased stiffness. The temperature at which this rubber to glass transformation occurs defines the glass transition temperature (or $T_g$) of the polymer, [27].

### 2.2.1 Experimental Procedure

Techniques such as differential scanning calorimetry (DSC), dynamic mechanical analysis (DMA), and thermo mechanical analysis (TMA) have been recognized as valid instrumentation supported by several standardized test methods to test for the glass transition temperature [27].

A TA instruments Q800 DMA (dynamic mechanical analyzer) was used to oscillate a 1.0 mm thick beam to determine the $T_g$. The DMA instrument operates with forced oscillation and applies a flexural loading mode to the test specimen. A dual cantilever configuration was selected for the $T_g$ tests in this section per ASTM D7028 standards, [28]. A fixed frequency of 1 Hz and a heating rate of 5°C/min were selected to conduct the tests. A summary of the tests conducted for $T_g$ determination for as-received (unconditioned) adhesive specimens is shown in Table 2-2.

**Table 2-2: DMA test matrix for as-received (unconditioned) FM300-2M samples**

| **Conditioning** | **Test Method** | **Cure Temperature (°C)** | **Degree of Cure** *Equation **(2-9)*** | **Number of samples** |
|---|---|---|---|---|
| **As-Received** *(nominal conditions)* | DMA | 80 | 0.74 | 2 |
| | | 100 | 0.88 | 2 |
| | | 120 | 0.96 | 1 |
| | | 140 | 1 | 1 |

The test sample was manufactured from four layers of as-received (unconditioned) FM300-2M adhesive film and cured at 120°C. The final test samples were cut to 35 ± 4 mm length, and 12 ± 1 mm width in compliance with the standard [28].

During the glass transition, the storage modulus of the adhesive is significantly reduced. The $T_g$ is determined by the intersection of two tangent lines from the storage modulus, where the first tangent line is selected at a temperature before the transition and the second tangent line is constructed at the inflection point to approximately the midpoint of the storage modulus drop, as shown in Figure 2-5. A summary of the measured $T_g$ values is shown in Table 2-3.

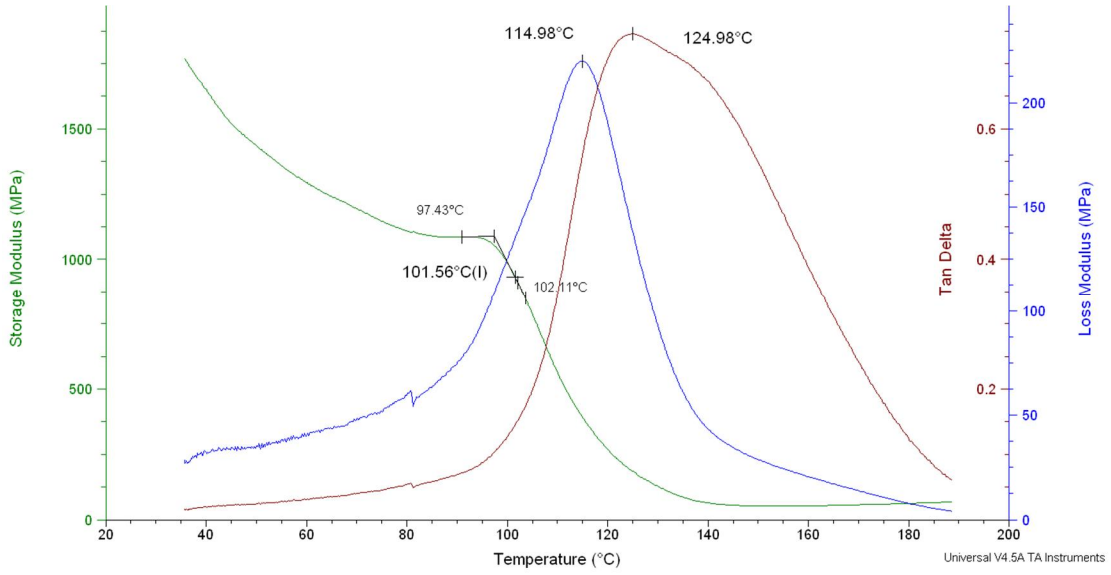


**Figure 2-5: DMA test at 5°C/min of 4 layers of as-received (unconditioned) FM300-2M adhesive film originally cured at 120°C. $T_g$ is determined as the point at which the storage modulus begins to decrease**

**Table 2-3: Measured glass transition temperature for as-received (unconditioned) FM300-2M samples**

| Test Method | Cure Temperature (°C) | Number of samples | Measured $T_g$ (°C) | Standard deviation |
|---|---|---|---|---|
| DMA | 80 | 2 | 102.5 | ±0.62 |
| | 100 | 2 | 131.8 | ±5.84 |
| | 120 | 1 | 143.1 | - |
| | 140 | 1 | 152.9 | - |

### 2.2.2 The Glass Transition Model

The glass transition temperature can be described by the degree of cure of the film adhesive for as-received (unconditioned) FM300-2M film adhesive. The evolution of the $T_g$ can be modelled with the degree of cure with the DiBendetto model, in Equation (2-7), [29].

$$\frac{T_g - T_{g0}}{T_{g\infty} - T_{g0}} = \frac{\lambda\alpha}{1 - (1-\lambda)\alpha} \quad \textbf{(2-7)}$$

where $T_g$ is the glass transition temperature, $T_{g0}$ and $T_{g\infty}$ are the glass transition temperatures of an uncured and fully cured sample of film adhesive respectively, where $T_{g0}$ was measured using the DSC, and $T_{g\infty}$ was the highest recorded value from the DMA tests. Additional parameters in the equation are $\alpha$ which is the degree-of-cure, and $\lambda$ is an experimentally determined constant. These values were experimentally found to be:

$T_{g0}$ = -14.23°C  $T_{g\infty}$ = 152.9°C  $\lambda$ = 0.827

The theoretical maximum degree of cure (also referred to as final or ultimate degree of cure) used in the $T_g$ model was calculated using the average total heat of reaction as shown in Equation (2-8), where $\alpha$ is the maximum degree of cure, $H_T$ is the total heat of reaction, and $H_R$ is the residual heat.

$$\alpha_{max} = \frac{H_T - H_R}{H_T} \quad \textbf{(2-8)}$$

An increase of the $T_g$ with the degree of cure was noted as the $T_g$ is a physical property of the adhesive. The model, Figure 2-6, shows a good correlation between the experimental and the predicted values of $T_g$. The model described in Equation (2-7) allows the determination of the $T_g$ of the cured adhesive at any given degree of cure.

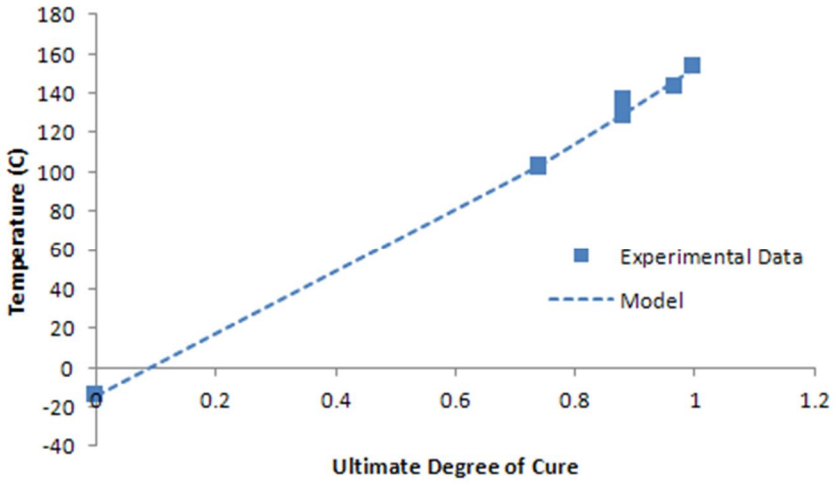


**Figure 2-6: Comparison of the $T_g$ model (dashed line) and the experimental data (symbols) for as-received FM300-2M samples**

## 2.3 Rheology

Viscosity is highly temperature and cure dependent, depending on the temperature ramp rate and the dwell temperature. The ramp rate affect the point at which the minimum viscosity occurs, whereas the dwell temperature affects the duration the film adhesive behaves like a fluid. Understanding the rheological behaviour of the adhesive is important as it could affect void content due to entrapped air in a repaired structure.

### 2.3.1 Experimental Procedure

A dynamic mechanical oscillating instrument, namely an AR2000 rheometer from TA Instruments, was used to determine the viscosity. The viscosity measured in an oscillatory experiment is a Complex Viscosity which contains an elastic component and a term similar to the steady state viscosity, [19]. The complex viscosity is defined in Equation (2-9), where $\eta^*$ is the magnitude of complex viscosity, $G^*$ is the complex modulus, and $\omega$ is the frequency.

$$|\eta^*| = \frac{G^*}{\omega} \quad \textbf{(2-9)}$$

Dynamic and isothermal tests per Table 2-4 were used to monitor the complex viscosity of the adhesive by inducing a small amplitude oscillatory strain in the adhesive sample between two 40 mm parallel plates at 15% strain and 1Hz frequency. The sample is made from 4 plies of uncured adhesive film debulked at room temperature to ensure intimate consolidation of the layers. To properly measure the viscosity, the adhesive must flow between the parallel plates as the sample is heated from room temperature to 40°C.

**Table 2-4: Rheology test matrix for as-received FM300-2M adhesive samples**

| Conditioning | Test Method | Temperature (°C) | Ramp (°C/min) | Number of samples |
|---|---|---|---|---|
| **As-Received** *(nominal conditions)* | Dynamic | - | 1 | 2 |
| | | - | 2 | 2 |
| | | - | 3 | 2 |
| **As-Received** *(nominal conditions)* | Isothermal | 80 | - | 2 |
| | | 100 | - | 2 |
| | | 110 | - | 2 |
| | | 120 | - | 2 |
| | | 140 | - | 2 |

The dynamic rheological behaviour of the adhesive is shown in Figure 2-7. A clear difference in the minimum viscosity can be seen as the ramp rate is increased from 1°C/min to 3°C/min. Since the minimum viscosity is greatly affected by the ramp rate, special care should be take when selecting a cure cycle. Figure 2-8 presents the complex viscosity versus time at each temperature obtained from the isothermal tests. Higher temperatures show a lower initial viscosity, but higher rates of viscosity increase, this indicates the time available for the adhesive to flow, followed by gelation.

These results can be used to alter the dwell temperatures in a cure cycle to manipulate the adhesive's flow during cure, therefore allowing entrapped air in the laminate to be evacuated.

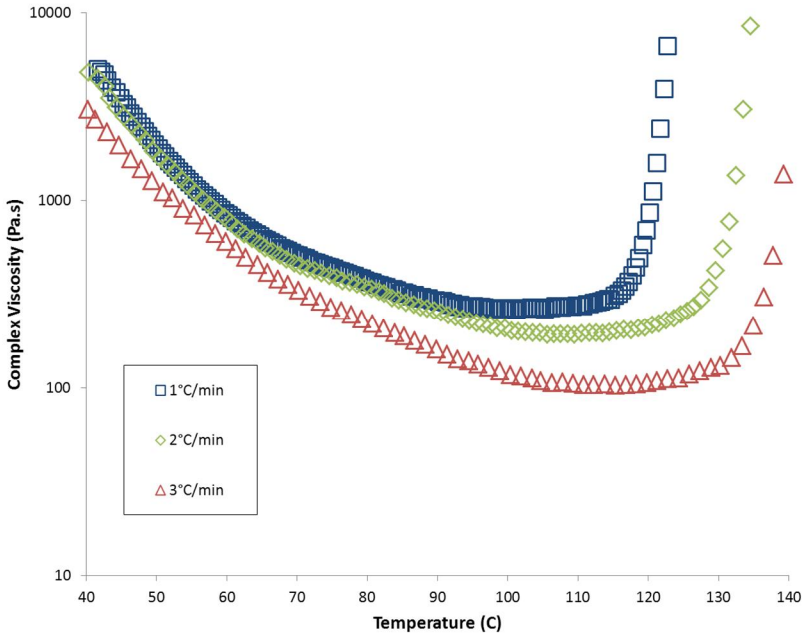


**Figure 2-7 Dynamic viscosity of as-received FM300-2M samples for different ramp rates**

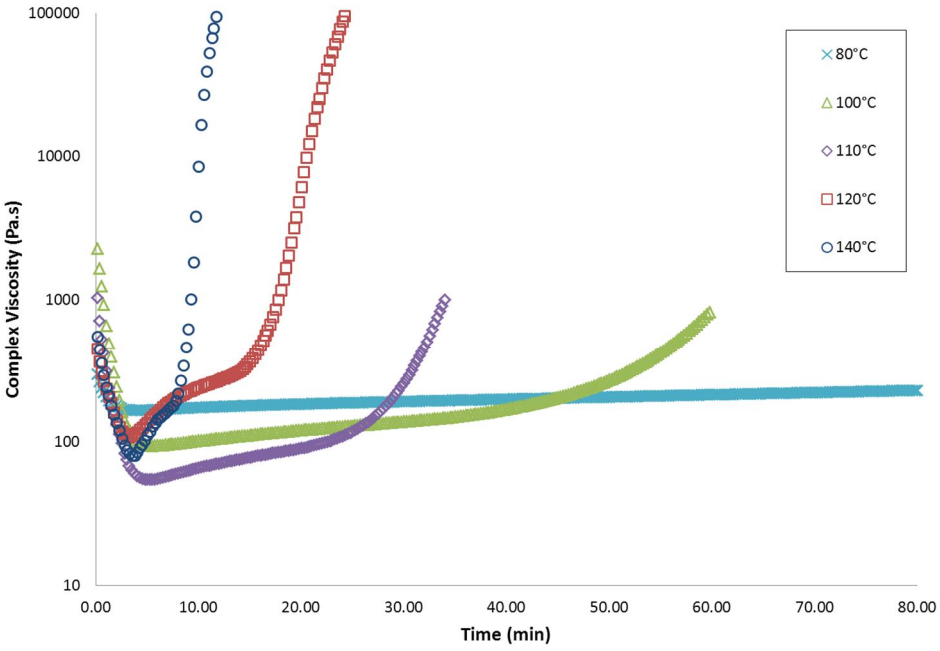


**Figure 2-8: Isothermal viscosity of as-received FM300-2M samples at different temperatures**

### 2.3.2 Viscosity Model

A rheology model was developed using as-received (unconditioned) FM300-2M data, which allows the prediction of the progression of viscosity for any time–temperature history when coupled with the predicted degree of cure obtained from the cure kinetics model, [30]. A rheology model in its simplest form is described in Equation (2-10), where μ is the viscosity, α is the degree of cure, and T is the temperature.

$$\mu = f(\alpha, T) \tag{2-10}$$

A more complex viscosity model, Equation (2-11), was used to present the evolution of viscosity with respect to the degree of cure, [30, 31].

$$\mu = \mu_1(T) + \mu_2(T)\left(\frac{\alpha_{gel}}{\alpha_{gel} - \alpha}\right)^{A' + B'\alpha + C'\alpha^2} \tag{2-11}$$

$$\mu_i(T) = A_i exp\left(\frac{E_{\mu i}}{RT}\right) \quad i = 1 \text{ or } 2 \tag{2-12}$$

where $\alpha_{gel}$ is the degree of cure at gel-point, $E_{\mu i}$ is the viscosity activation energy, $A_{\mu i}$ is the pre-exponential factor, R is the universal gas constant and T is the absolute temperature. The degree of cure at gelation, $\alpha_{gel}$, was determined at the average crossover point between the storage modulus and the loss modulus as shown in Figure 2-9, [32]. The viscosity activation energy, $E_{\mu 1}$, was obtained by plotting ln(μ) versus the inverse of the temperature (1/T) obtained from the dynamic tests from room temperature until the viscosity began increasing. All other constants were calculated using a weighted least squares curve fit with the experimental data. The model constants are summarized below,

$A_{\mu 1}$ = 2.02x10$^{-10}$ (Pa.s) $A_{\mu 2}$ = 41.0 (Pa.s)

$E_{\mu 1}$ = 79337 (J/mol) $E_{\mu 2}$ = 3650 (J/mol)

$\alpha_{gel}$ = 0.77 $A'$ = 0.10

$B'$ = 0.60 $C'$ = 2.4

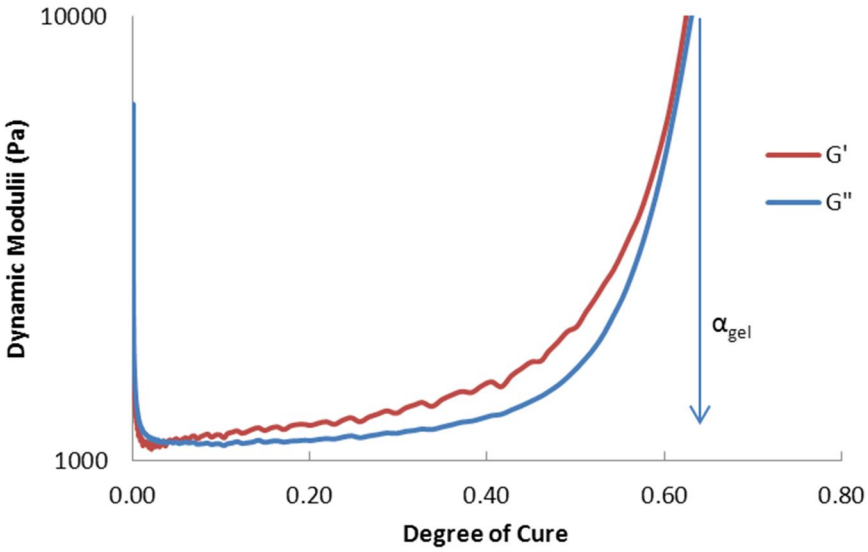


**Figure 2-9: Example of the dynamic moduli for as-received sample of FM300-2M ramped at 1°C/min. The crossover between the storage and loss modulus is defined as the gel point**

The model was compared to the experimental isothermal and dynamic complex viscosity data. Figure 2-11 shows good model correlation with the dynamic complex viscosity and the gelation is well captured, with the model goodness captured via $R^2$ to be above 0.8. Nevertheless, the model over-estimates the viscosity for the 1°C/min and 2°C/min runs, and slightly under-estimates it for the 3°C/min experimental data. The model does not correlate as closely with the isothermal data shown in Figure 2-10; which is an inaccuracy carried over from the cure kinetics model discussed earlier.

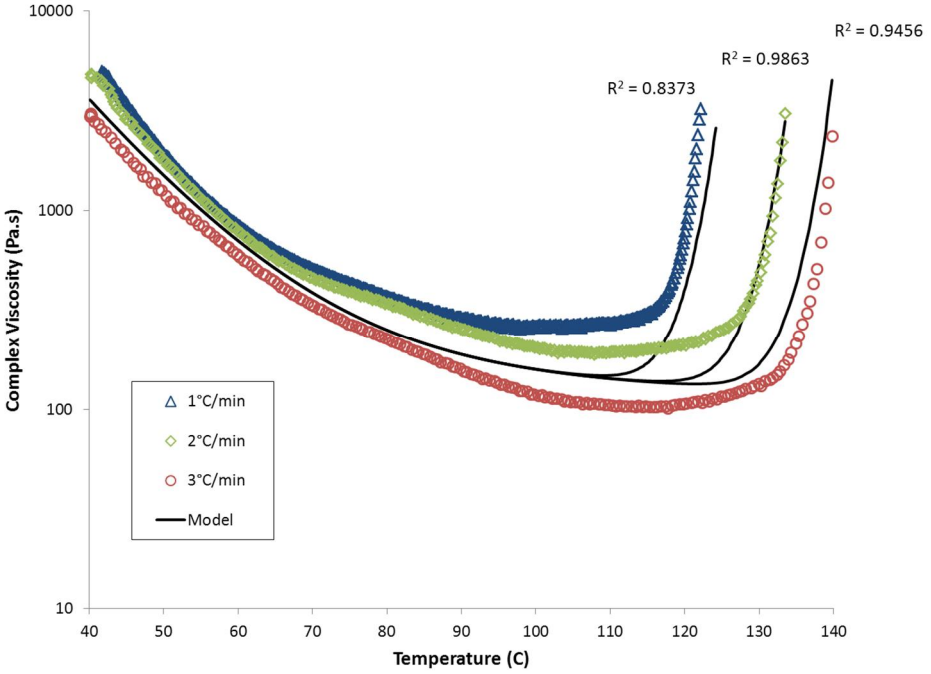


**Figure 2-10: The experimental dynamic viscosity data (symbols) is compared to the model predictions (solid line) for as-received (unconditioned) FM300-2M adhesive samples**

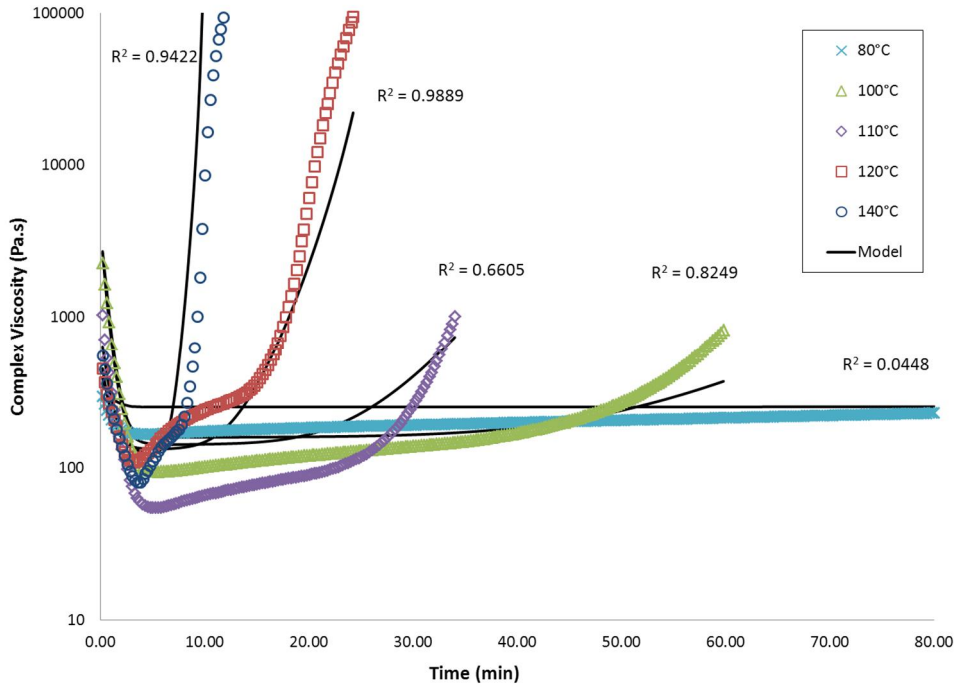


**Figure 2-11: The experimental data for isothermal viscosity (symbols) is compared to the model predictions (solid line) for as-received (unconditioned) FM300-2M adhesive samples**

## 2.4 Moisture Effects on Cure Behaviour

To assess the effects of moisture on the cure behaviour of the adhesive, DSC, TMA, and rheological tests were conducted for conditioned adhesive samples. Conditioning of samples followed the procedure in Section 3.3. For all conditioned scenarios, uncured adhesive samples were conditioned per the apparatus in Figure 3-19, at room temperature and relative humidity above 90% for 4 hours, until moisture content of 0.3% by weight is reached.

### 2.4.1 Effects of Moisture on the Degree of Cure

The effect of moisture on the degree of cure of conditioned samples was experimentally investigated. Similar to previous discussion, the heat flow of conditioned samples of uncured film adhesive for isothermal and dynamic DSC tests were measured by DSC tests per Table 2-5.

**Table 2-5: Test matrix for dynamic and isothermal DSC tests of conditioned FM300-2M samples**

| Conditioning | DSC Test | Temperature (°C) | Time (min) | Ramp Rate (°C/min) | Residual Temperature (°C) | Number of samples |
|---|---|---|---|---|---|---|
| **2 , 4 , 16 hours** >90%RH | Dynamic | 300 | - | 2 | - | 1 per condition |
| **4 hours** >90%RH | Isothermal | 80 | 990 | 2 | 250 | 2 |
| | Isothermal | 100 | 600 | 2 | 250 | 2 |
| | Isothermal | 120 | 240 | 2 | 250 | 2 |
| | Isothermal | 140 | 120 | 2 | 250 | 2 |

Total heat of reaction was evaluated for uncured samples conditioned at room temperature and high humidity (23°C, >90%RH) for a duration of 2, 4, and 16 hours. The resulting average total heat of reaction of the conditioned samples was 317 J/g with a standard deviation of 3.8 J/g. Figure 2-12 shows a comparison of the average total heat of reaction for the conditioned samples to the as-received samples; the moisture conditioning regardless of the duration had insignificant effect on the total heat of reaction.

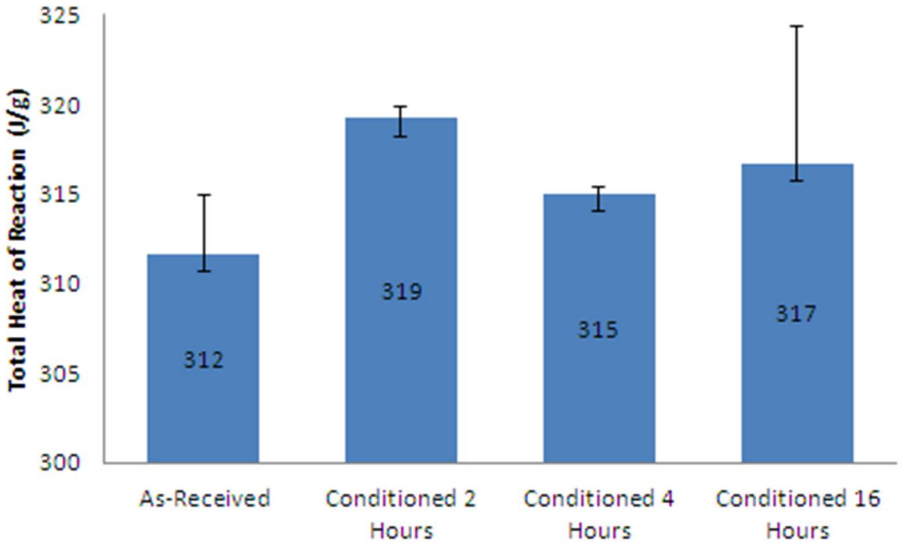


**Figure 2-12: Effect of moisture on the total heat of reaction for FM300-2M samples conditioned for various durations compared to the as-received sample**

Uncured adhesive samples prepared for isothermal tests were conditioned at room temperature (23°C, >90%RH) for a duration of 4 hours until the sample was considered at equilibrium. The residual heat of reaction was determined from the isothermal tests of the conditioned samples.

The theoretical degree of cure for the conditioned FM300-2M samples was then calculated using Equation (2-8) and compared to the theoretical degree of cure of the as-received (unconditioned) results. Figure 2-13 shows a (1-5%) drop in the theoretical degree of cure of the conditioned film adhesive. However, when the plot of the progression of the degree of cure of the experimental results of the conditioned samples was compared to those of the as-received samples, a larger drop in the final degree of cure was noted. As shown in Figure 2-14, the experimental progression of the degree of cure of the conditioned samples is reduced by 8-13%. The maximum reduction of the final degree of cure was noted for the 80°C specimens. This large drop could be associated with the presence of free water particles (unbound to the film adhesive) that affect the final degree of cure due to the low isothermal temperature, [15].

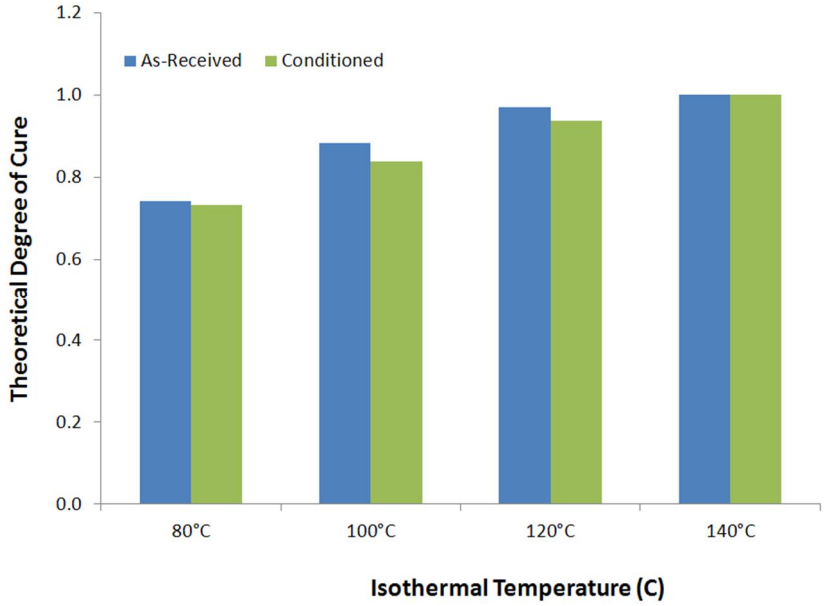


**Figure 2-13: The effect of moisture on the calculated degree of cure**

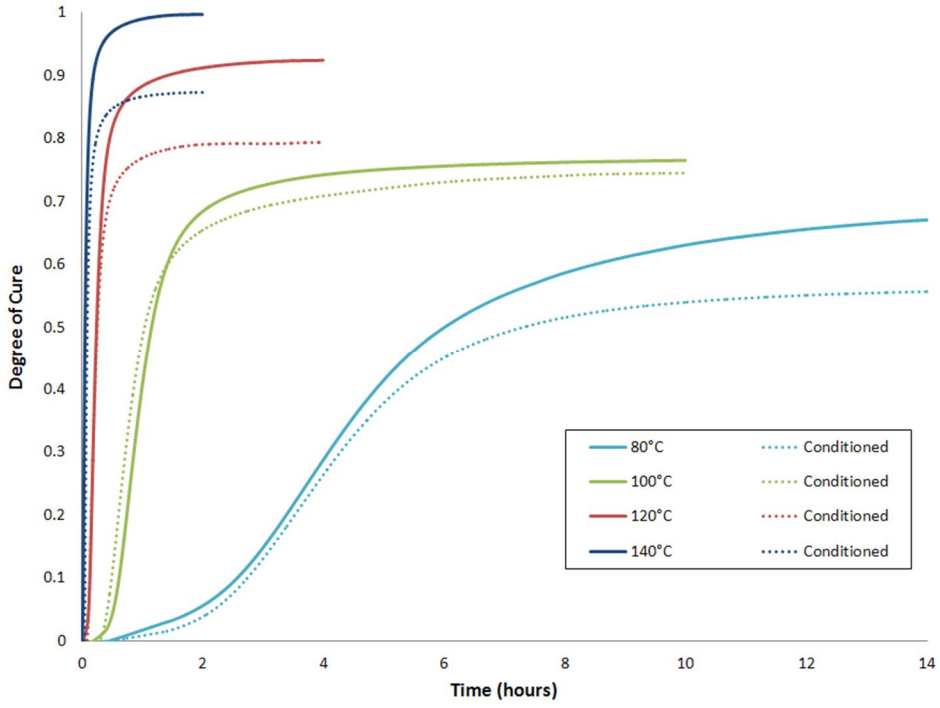


**Figure 2-14: The evolution of the degree of cure during the cure cycle. Experimental data for as-received samples (solid lines) is compared with the experimental data of the conditioned samples (dotted lines)**

### 2.4.2 Effects of Moisture on the Rheological Behaviour

To assess the effect of moisture on the rheological behaviour, conditioned FM300-2M adhesive samples were tested per Table 2-6 and the dynamic viscosity response was recorded.

**Table 2-6: Rheology test matrix for conditioned FM300-2M adhesive samples**

| Conditioning | Test Method | Temperature (°C) | Ramp (°C/min) | Number of samples |
|---|---|---|---|---|
| **Conditioned** 4 hours >90%RH | Dynamic | - | 1 | 1 |
| | | - | 2 | 1 |
| | | - | 3 | 1 |

The results in Figure 2-15 shows reduction in the minimum viscosity of the conditioned samples, however the gelation and ramp behaviour remains unaltered.

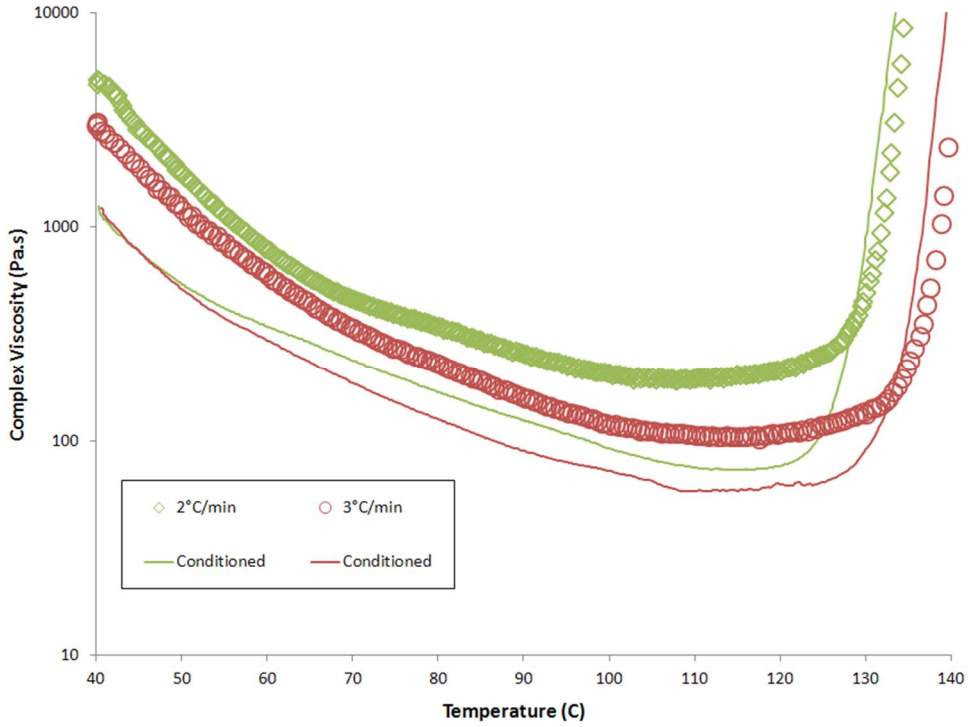


**Figure 2-15: The dynamic viscosity data for conditioned FM300-2M samples (solid lines) is compared to the as-received samples (symbols)**

## 2.5 Summary and Discussion of Cure Behaviour

A cure kinetics model was developed for as-received (unconditioned) FM300-2M adhesive film, which describes the degree of cure of the adhesive based on any time-temperature history. The cure kinetics model was then used to derive the viscosity and glass transition temperature models. The cure kinetics model slightly over-predicts the final degree of cure, but is in general agreement with the experimental results. The glass transition temperature of the adhesive was determined experimentally and the $T_g$ model was accurately modeled as a function of the degree of cure. Finally, the viscosity model was developed which accurately predicts the gel point of the adhesive, however over-estimates the minimum viscosity; which is a result of the cure kinetics model. By understanding the cure behaviour of the adhesive, the repair cure cycle can be altered from that of the manufacturer's recommendation to allow entrapped moisture in the parent laminate to escape during the repair.

The effects of moisture on the cure kinetics and viscosity of the adhesive were studied. Experimental data shows a reduction in the final degree of cure of the adhesive during isothermal DSC tests that could be attributed to the moisture that had penetrated adhesive. However, dynamic tests show an insignificant effect on the total heat of reaction of the adhesive. The viscosity of the adhesive was also evaluated for conditioned adhesive samples. Conditioned samples of FM300-2M were notably more "tacky" or "sticky" than those unconditioned, an observation that support the observed reduction in the complex viscosity obtained during the dynamic rheology tests. Nevertheless, the overall gelation of the adhesive remains consistent with that of unconditioned samples.

Chapter 3

# Manufacturing and Conditioning Procedures

This chapter will elaborate on the procedures used to manufacture the parent laminates and to perform the bonded repairs, which includes the main recommendations documented in the literature as well as industry standards. The experimental investigations discussed in the subsequent chapters will refer to the procedures detailed herein. A description of the materials used to manufacture the parent laminates and to conduct subsequent repairs is summarized below, followed by a description of the repair methodology. This chapter also overviews the apparatus and procedures used to condition the test samples in preparation for thermochemical or mechanical testing.

## 3.1 Manufacturing Procedures

Repaired laminates were manufactured in steps; first, the parent laminate was manufactured, followed by a surface preparation process to expose the fibres and prepare the joint for bonding, the parent laminate was then conditioned depending on the conditioning requirements, finally the repair plies were applied and cured to achieve the final repair product. Depending on the conditioning requirements, some repairs were performed with conditioned adhesive film or

repair prepreg plies prior to the cure process. Sample conditioning details will be discussed in subsequent sections.

### 3.1.1 Materials

**Pre-impregnated carbon fibre plies**

The composite laminates were manufactured from epoxy resin pre-impregnated carbon fibre, namely Cytec's CYCOM® 5320. CYCOM 5320 is a toughened epoxy prepreg system specifically designed for Out of Autoclave (OOA) manufacturing which provides the right balance of performance and processing enabling manufacturers of aircraft primary structures to capitalize on the benefits of vacuum-bag-only processing. These prepregs were specially designed to help evacuate air and volatiles during the debulk and cure phase under OOA processing conditions. The selected material form is plain weave PW T650/3K (fibre type and tow count), with fibre areal weight of 196 g/m$^2$ and resin content of 36% in mass fraction.

**Film adhesive**

To achieve a good quality structural bond, FM300-2M film adhesive was selected for the repairs. FM300-2M is a 250°F (121°C) cure film adhesive that delivers high temperature performance, toughness, and stress/strain properties. FM300-2 family of adhesives was developed specifically for co-curing and secondary composite bonding applications; the material supplier's data also shows excellent moisture and corrosion resistance in high humidity environments with no significant reduction in mechanical properties. The selected form of the adhesive was FM300-2M, 0.25 mm thick film with an aerial weight of 293 g/m².

**Consumable materials**

Various consumable materials, which are made for one-time usage, were required for bagging composite materials. These materials, summarized in Table 3-1, facilitate the evacuation of air and volatiles while transferring the compaction pressure during cure.

**Table 3-1: List of consumables and their function**

| Consumable Material | Function |
|---|---|
| **Perforated release film** | Allows through-thickness resin bleed during cure and prevents the consumables from curing onto the part |
| **Non-perforated release film** | Prevents through-thickness resin bleed during cure and allows easy removal of the part after cure |
| **Breather cloth** | Provides passage for air and volatiles to evacuate from the laminate to the vacuum valve |
| **Fibreglass ply** | Used for edge breathing. Provides passage of air and volatiles from the laminate to the breathing cloth |
| **Sealant tape** | Provides seal of vacuum bag. Prevents in-plane resin bleed. Used as damn to prevent the in-plane evacuation of air and volatiles |

### 3.1.2 Parent Laminate Manufacturing

A summary of the manufactured parent laminates is shown in Table 3-2 below. Two parent laminate layups were chosen; 'L1' panel identification represents an 8-ply quasi-isotropic layup totaling 1.54 mm laminate thickness, whereas 'L2' and 'L3' panel identification represent a 16-ply quasi-isotropic layup totaling 3.1 mm thickness. Note that although panels 'L2' and 'L3' are of the same thickness and layup orientation, they were given different identification numbers because they were manufactured separately and were used for different conditioning configurations (conditioning to be discussed in subsequent sections).

**Table 3-2: Parent laminate panel identification, layup, and quantity**

| Panel ID | Layup | Quantity |
|---|---|---|
| **L1** | 8 plies PW, QI, $(+45,0,-45,90)_S$ | 3 |
| **L2** | 16 plies PW, QI, $(+45,0,-45,90)_{2S}$ | 3 |
| **L3** | 16 plies PW, QI, $(+45,0,-45,90)_{2S}$ | 3 |

Prior to starting the layup process, and to ensure that storage moisture does not form on the prepreg, the sealed prepreg bag taken out of the freezer was left to reach room temperature prior to unsealing it. Once at room temperature, plies of different orientation to achieve a quasi-

isotropic laminate were prepared for layup. The parent laminate was then placed on a clean 6.35 mm aluminum toolplate coated with a release agent and covered with a non-perforated release film to protect the tool and facilitate the removal of the part after cure (demoulding). To simulate the scarf of a repair joint, a slope of 1:20 (0.58 mm ply drop off) was used to manufacture the initial scarf geometry and to ease the complexity of the surface preparation step, as shown in Figure 3-1.

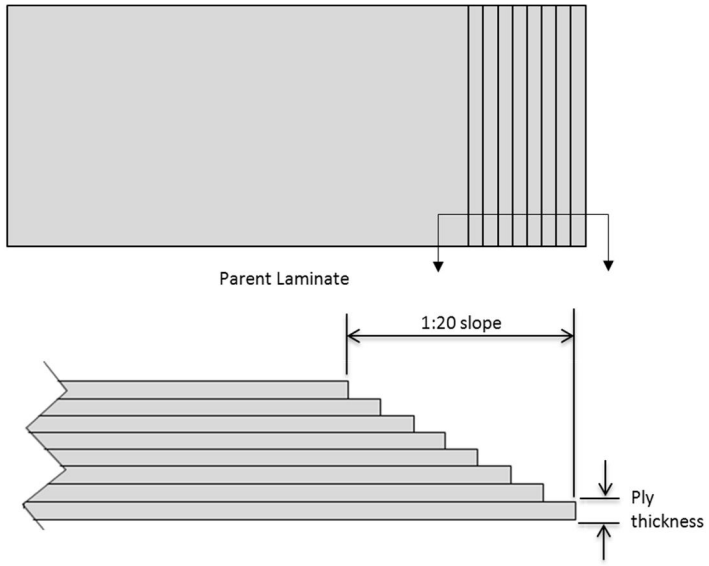


**Figure 3-1: Parent laminate panel size and manufacturing details**

An edge breathing technique was used to facilitate the evacuation of air from the edge of the laminate to the vacuum port for good quality low-porosity aircraft representative laminates. A 76 mm woven fibreglass strip was wrapped around sealant tape and placed around the entire panel. The fibreglass strip was in contact with the edge of each ply of the laminate and the consequent breather cloth. It provided a path for the air to be evacuated through the breather cloth and into the vacuum line, whereas the sealant tape prevented any in-plane resin bleed, as shown in Figure 3-2, [17, 33].

The parent laminates were then bagged per Figure 3-3 and debulked at room temperature overnight to allow the entrapped air to evacuate to ensure good consolidation before resin impregnation during cure. Laminates were then cured in a temperature controlled oven. The cure cycle was selected based on the 5320 prepreg system requirements and comprises of three

phases; ramp up rate of 2°C/min, dwell at 121°C for 4 hours, and finally cool down at 2°C/min to room temperature. During cure, the parent laminate was kept under 1 atm pressure by means of a vacuum pump to ensure good consolidation of the plies during the cure cycle.

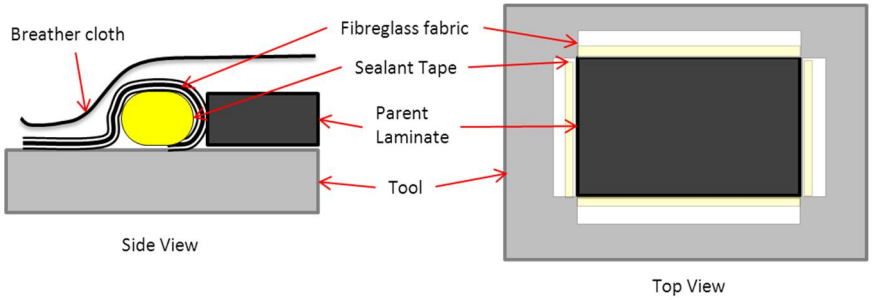


**Figure 3-2: Edge breathing technique used for parent laminate manufacturing**

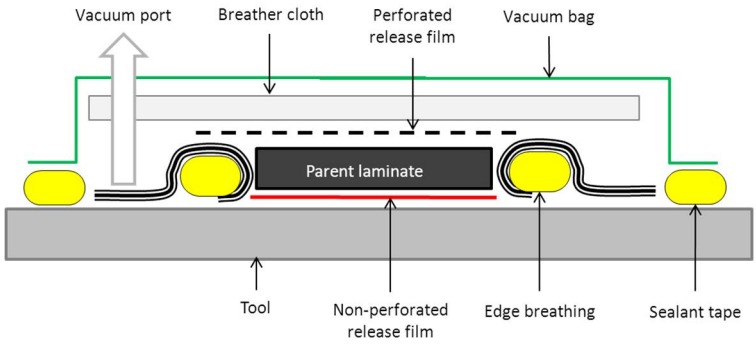


**Figure 3-3: Bagging configuration used during parent laminate manufacturing**

### 3.1.3 Repaired Laminates Configuration and Identification

The resulting repair identification numbering is based on the laminate ID (thickness) and the conditioning requirements; the baseline configuration, denoted as ‘C0’, is a repaired laminate with no conditioning requirements, the repair was performed on a dry substrate (parent laminate) and as-received adhesive film and prepreg plies. Laminates repaired with a conditioned parent laminate are denoted as configuration ‘C1’, laminates repaired with a conditioned adhesive film are denoted as configuration ‘C2’, whereas the laminates repaired with a conditioned prepreg

plies (repair patch) are denoted as configuration ‘C3’. Table 3-3 summarizes the repaired laminate identification.

**Table 3-3: Resulting mechanical test coupon identification and conditioning requirements**

| Coupon ID | Parent laminate panel ID | Conditioning requirements |
|---|---|---|
| **L1-C0** | L1 | Baseline; no conditioning |
| **L1-C1a** | L1 | Conditioned parent laminate for duration ‘a’ |
| **L1-C1b** | L1 | Conditioned parent laminate for duration ‘b’ |
| **L2-C0** | L2 | Baseline; no conditioning |
| **L2-C1a** | L2 | Conditioned parent laminate for duration ‘a’ |
| **L2-C1b** | L2 | Conditioned parent laminate for duration ‘b’ |
| **L3-C2a** | L3 | Conditioned adhesive film for duration ‘a’ |
| **L3-C3a** | L3 | Conditioned repair patch for duration ‘a’ |
| **L3-C3b** | L3 | Conditioned repair patch for duration ‘b’ |

To acquire the final test coupons, the repaired laminates were cut on a water cooled saw with a diamond cutting blade to ensure a good quality edge that is fraying and delamination free. Each repaired laminates yielded four test coupons that were then numbered accordingly to track the test results.

### 3.1.4 Repair Procedure

Once the parent laminates are cured and conditioned as required per the test matrix, the repair process began. The first step of the repair process was to simulate the removal of in-service damage. This step was initiated when the parent laminate was manufactured with ply drop-offs incorporated into the laminate. The steps were then sanded by hand to the required slope of 1:20 starting with 100-grit and finishing with 120-grit sanding paper to ensure a good quality surface finish. Then, a water break free test was performed to ensure a contaminant-free surface. Figure 3-4 shows the water break free test on the scarf region of the parent laminate; when water is sprayed onto prepared surface it should completely spread out and wet the surface for at least 30 seconds, if the water starts to form beads, then the surface is not well prepared for bonding, [34]. The parent laminate is then thoroughly dried by means of lint-free cloths. The laminate is then covered for up to an hour prior to the repair patch application to ensure the surface activation

energy was bond-ready, [34]. To simplify the repair ply placement process, a translucent plastic sheet was used to trace the exposed plies of the parent laminates creating a template for the repair patch; the repair plies were then measured and placed onto the template prior to transferring them onto the film adhesive covered scarf. To ensure a good load transfer between the repair and parent plies, it was imperative that the repair plies overlap with the exposed parent plies as shown in Figure 3-5, this step can be ensured by visually ensuring the alignment of the first and last repair plies with the parent laminate. A butt-joint, also shown in Figure 3-5 should be avoided as it does not provide a good load path between the repair and the parent structure, hence could result in a reduction of the joint's strength.

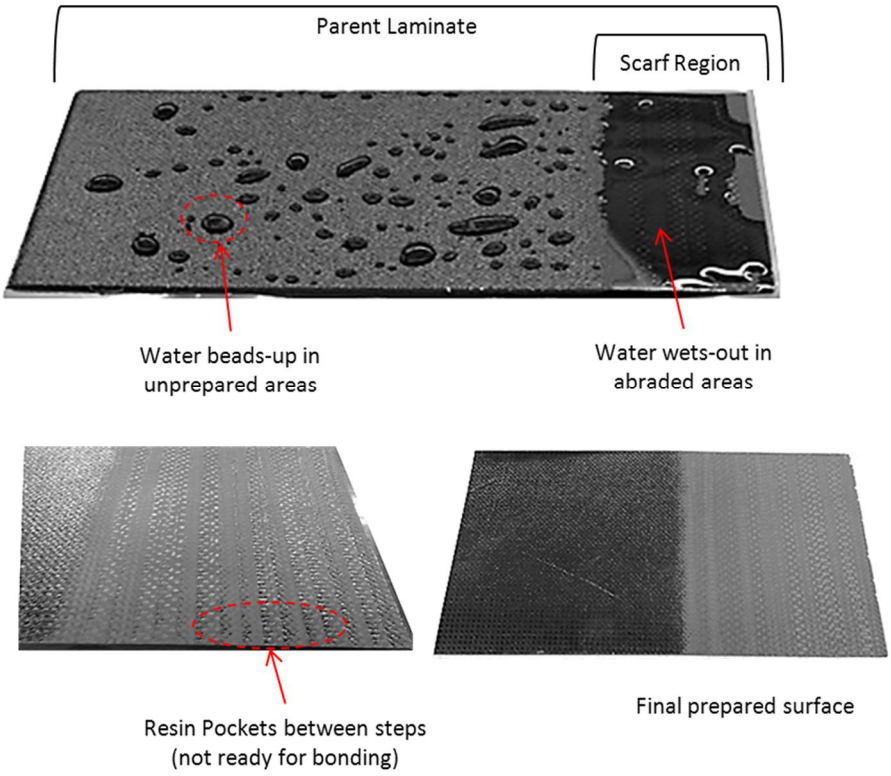


**Figure 3-4: Surface preparation of the parent laminate's scarf region. Top picture shows the water break free technique, bottom left shows a poorly prepped surface, bottom right shows the desired surface preparation for good bond quality**

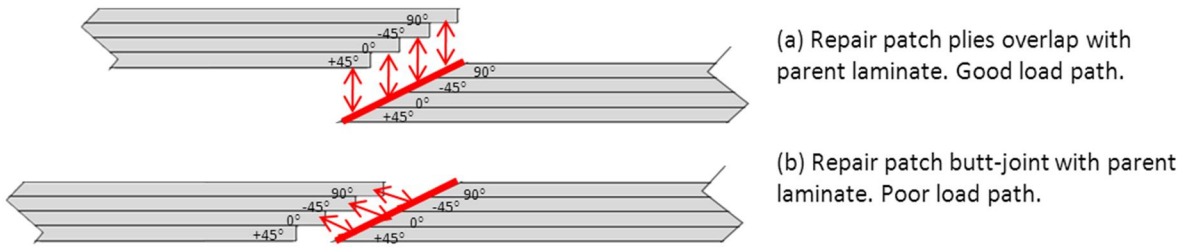


**Figure 3-5: Repair ply application on the parent laminate; (a) shows a good load path transfer as each repair ply is in contact with exposed fibres from the parent laminate; (b) shows poor load path between the repair patch and parent plies due to mismatching ply orientation and no load transfer to the lower repair ply**

In real-life repairs, in-plane air evacuation in the repair patch is not possible due to the three-dimensional nature of the repair; as it is surrounded by parent laminate, hence restricting the air flow during the cure to only through the thickness of the repair patch. To accurately simulate these in-service repair boundary conditions, sealant tape was placed around the laboratory-scale repaired laminate to prevent air evacuation in the in-plane direction. To facilitate the evacuation of gases through the thickness of the repair patch, a fibreglass ply was placed over the repaired laminate and was connected with the breathing cloth, [35]. As shown in Figure 3-6. The fibreglass fabric ply and the breather clothe should extend beyond the repaired laminate and must be in direct contact to allow the transfer of gases from the fibreglass to the breather and subsequently out of the bag by means of vacuum.

The repaired laminates are placed on a toolplate covered with a layer of non-perforated release film to allow for easy removal of the laminate after cure. A 1.54 mm thick composite toolplate was selected instead of the traditional aluminum toolplate used during the parent laminate manufacturing. The reason for selecting a composite toolplate is to minimize the heat sink effects at the toolside of the repair, since composites have relatively lower thermal conductivity than metals; a composite toolplate was deemed a better option to use during the cure of the repair patch.

The bagging configuration of the repaired laminate is shown in Figure 3-7; the repaired laminate is covered by a layer of perforated release film, followed by a fibreglass fabric ply, non-perforated release film and a breather cloth. The heating blanket is then applied and covered by a layer of breather cloth to prevent heat of being potentially conducted through the metallic

vacuum valve. The heating blanket must extend at least 50 mm past the repair patch to ensure uniform heat distribution and to minimize poor heating due to edge effects of the heating blanket. Once the final bagging of the repair was completed, the repair was kept under vacuum at room temperature for 4 hours (debulk process). Following the debulk operation; the repaired laminate was then cured using a heating blanket. During cure, the repaired laminate is kept under 1 atm pressure by means of a vacuum pump to ensure good consolidation.

A cure cycle similar to that used to manufacture the parent laminate was chosen for the repair patch. The heat was ramped 2 °C/min from room temperature up to a dwell temperature of 121°C. The dwell temperature of 121 °C was maintained for 4 hours followed by a ramp down rate of 2 °C/min to reach room temperature.

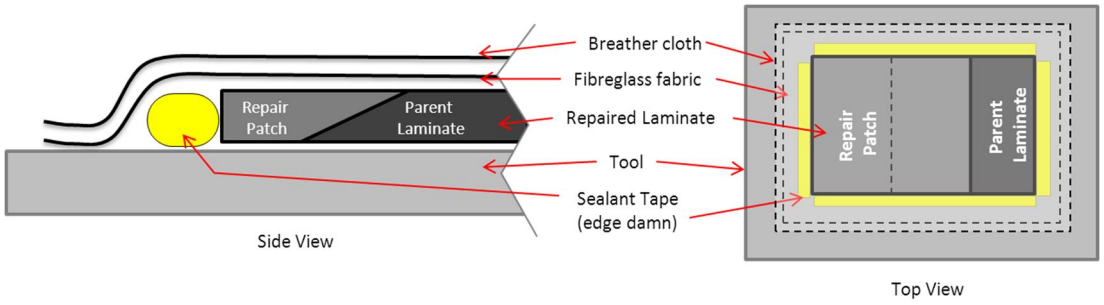


**Figure 3-6: Edge breathing technique to simulate in-service repair boundary conditions by blocking the air flow in the in-plane direction using sealant tape, while facilitating a pathway for evacuation of gases in the transverse direction (through the thickness of the repair patch) by means of the fibreglass and breather cloth**

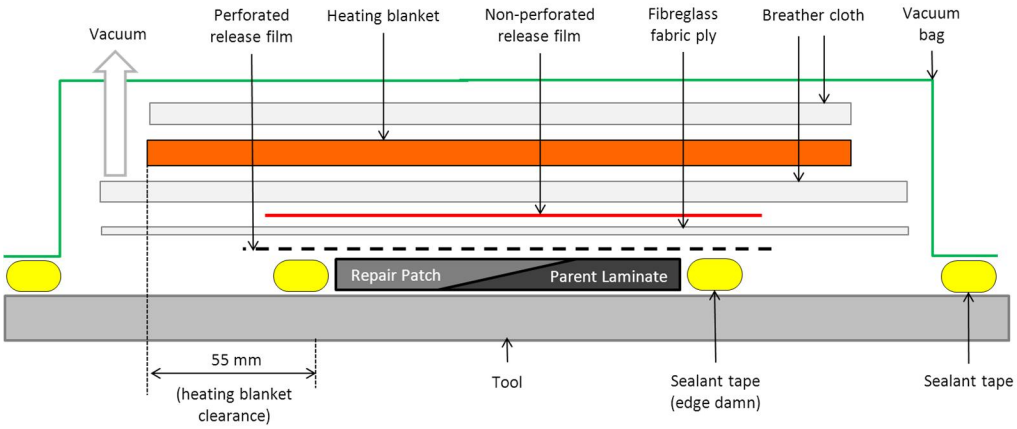


**Figure 3-7: Bagging configuration for repaired laminates**

### 3.1.5 Repair Cure Apparatus

Repaired laminates were cured in a specific apparatus, shown in Figure 3-8, designed to simulate an aircraft structure undergoing a repair; allowing the repair process to be performed on one side; while the other side allows a heat flux exchange with ambient air. The apparatus consists of two aluminum posts that allow the composite toolplate to be clamped vertically.

Since the use of an oven for in-service repair conditions is not always practical (size and location constrains to name a few), in-service repairs are mostly cured by means of a heating blanket. Hence, an in-house hot bond heating system was used to cure all repair configurations. The hot bond system consists of a heating blanket and a PID controller.

The heating blanket used was a 30.5 cm in width and 61.0 cm in length HEATCON® Silicone Rubber heating blanket, with a grid of wound resistance wire vulcanized between two layers of fibreglass reinforced silicone rubber (120V input, 1440W power). Heat is generated when current passes through this network of resistive wires.

The cure cycle for the repair patch was programmed into the PID controller which simultaneously controlled the temperature of the heating blanket via a feedback thermocouple used as an input to the PID controller. The feedback thermocouple was placed directly on the bagside of a repair patch. The location of thermocouples on the repair patch during cure is shown in Figure 3-9. In addition to the feedback thermocouple, three other thermocouples were placed on the repair patch during the cure cycle to monitor the temperature and ensure uniform heat at different locations.

Unlike an autoclave or an oven heating apparatus that surrounds the specimen with equal heat, the one sided heating nature of the heating blanket showed a heat gradient between the bagside and the toolside of the laminate that is dependent on the thickness of the laminate, [36]. For the repair configurations selected, an average of 5% and 15% temperature gradient was expected between the bagside and toolside, with the bagside expecting the higher temperatures as it is the closest to the source of heat. This gradient is a realistic in-service repair deviation that was studied in depth by Bujun hence the usage of the heating blanket for the repairs.

Thermocouples located on the repair as shown in Figure 3-9 were used for all repairs to monitor the temperature gradient during the cure cycle. The resulting temperature plots show a 5°C gradient for 1.54 mm repairs (L1 configuration), and 10°C temperature gradient for 3.1 mm repairs (L2 configuration) through the thickness of the laminate, as shown in Figure 3-10.

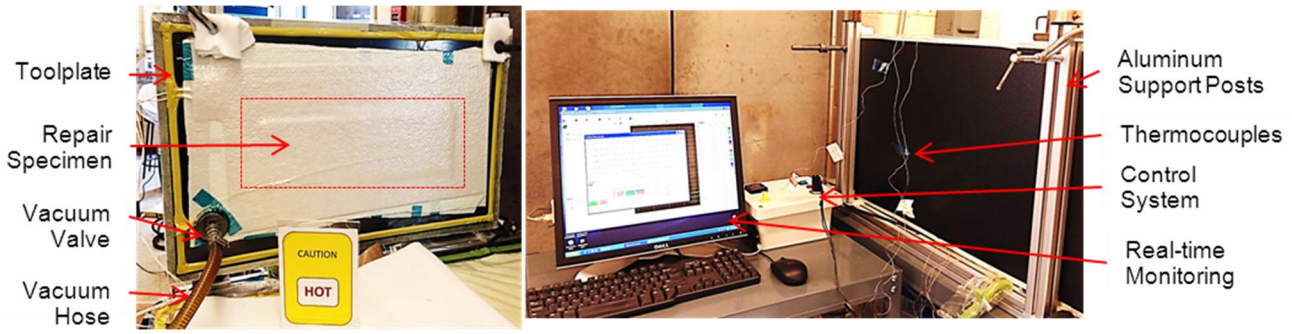


**Figure 3-8: In-house repair cure apparatus**

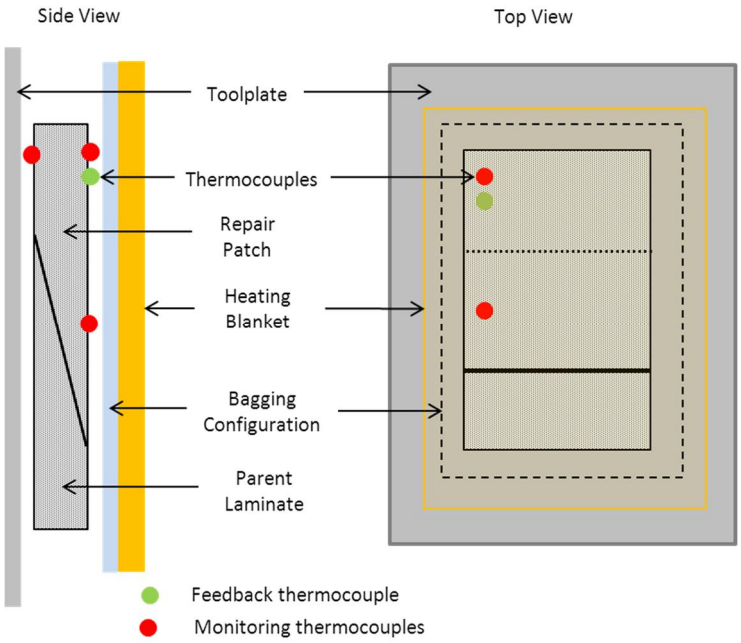


**Figure 3-9: Locations of thermocouples on the repaired laminate for cure cycle monitoring**

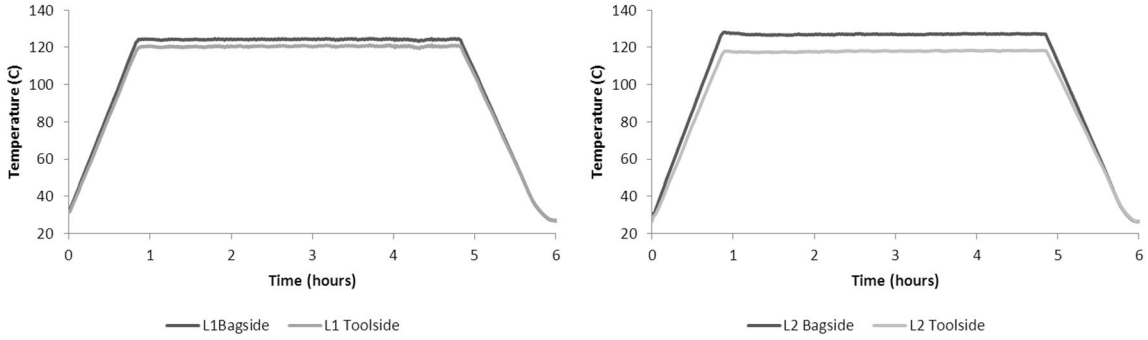


**Figure 3-10: Temperature plot showing the thermocouple data recorded on the bagside and toolside. Left: plot for 1.54 mm repair (L1) shows a 5°C gradient, right: plot for 3.1 mm repair shows an 11°C gradient (L2)**

## 3.2 Temperature Gradient Effect

### 3.2.1 Temperature Gradient Effect on the Film Adhesive

As observed in Figure 3-10, a temperature gradient between the bagside and toolside of the repair was measured. This phenomena would be typical of an in-service repair due to the one sided nature of the heat application, therefore, it is important to understand its effect on the final adhesive and prepreg resin system. Changes in the adhesive and resin's thermochemical properties could directly affect the joint's mechanical strength.

The first step was to assess the effect of the temperature gradient on the final degree of cure and the adhesive's viscosity for the FM300-2M bondline. The degree of cure model in Figure 3-11 and the complex viscosity model in Figure 3-12 were derived by using Equations (2-3) and (2-11) in Chapter 2, for a 3.1 mm thickness laminate (the upper bound in the experimental setup herein).

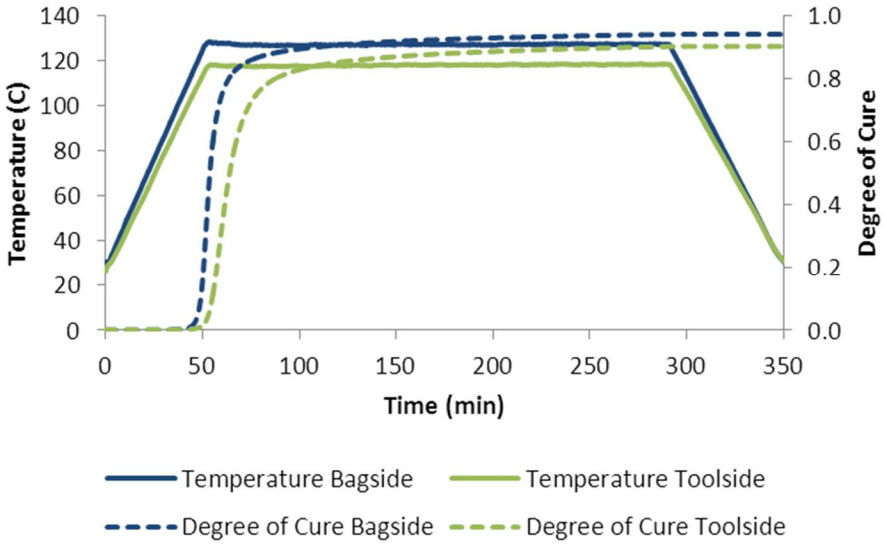


**Figure 3-11: Effect of the temperature gradient on the final degree of cure for as-received adhesive film (FM300-2M)**

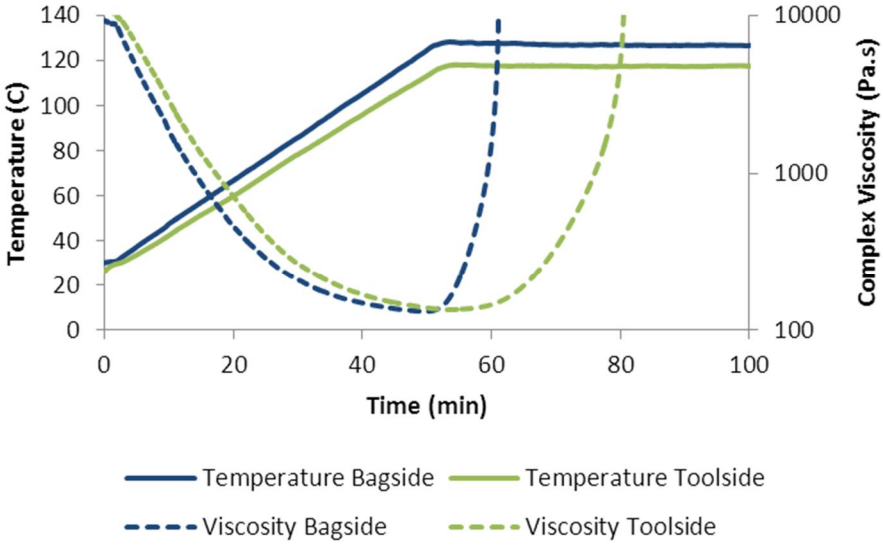


**Figure 3-12: Effect of the temperature gradient on the viscosity of as-received adhesive film (FM300-2M)**

### 3.2.2 Temperature Gradient Effect on the Repair Patch

Nevertheless, void formation as discussed is a byproduct of entrapped air in the prepreg among other sources. Hence, an understanding of the behaviour of the prepreg during cure is necessary to determine the effects of the temperature lag on the final quality of the repair. A cure kinetics model developed by Kratz et al for CYCOM 5320 prepreg was therefore used along with the viscosity model and their respective modelling parameters to determine the final degree of cure and gelation point of the resin, [37]. The cure cycle selected was similar to that used for parent laminate manufacturing; therefore all modelling was based on said cure cycle. The modeling parameters for the cure kinetics model in Equations (2-3) and (2-4), and viscosity model in Equation (2-11) are summarized in Table 3-4.

$$\frac{d\alpha}{dt} = K_1\alpha^{m_1}(1-\alpha)^{n_1}\frac{K_2\alpha^{m_2}(1-\alpha)^{n_2}}{1+exp\left(D\left(\alpha-(\alpha_{C0}+\alpha_{CT}T)\right)\right)} \quad \textbf{(3-1)}$$

$$K_i = A_i\, exp\left(\frac{-E_{Ai}}{RT}\right) \quad \textbf{(3-2)}$$

The degree of impregnation of the resin in the fibres was also determined using the degree of impregnation model developed by Centea et al for the same prepreg system presented in Equation (3 7), the modeling parameters for which are summarized in Table 3-4, [38]. For a prepreg system, the resin viscosity in the initial stage of the cure cycle must be sufficiently low in order to fully impregnate the dry fibre regions of the prepreg. If the resin begins to gel at the early stages, full impregnation might not be achieved hence leaving patches of dry fibres and may potentially contribute to more void formation, [38].

$$\frac{d\beta}{dt} = \frac{K}{\mu R_{tow}^2(1-V_f)}\left(\frac{P_\infty - P_f}{(1-\beta)ln\left({}^{1}/_{1-\beta}\right)}\right) \quad \textbf{(3-3)}$$

where β is the degree of impregnation, K is the transverse tow permeability and $V_f$ the fibre volume fraction. $R_{tow}$ is the outer radius and $P_\infty$ id the corresponding resin boundary pressure. Pf

is the resin pressure at the resin flow front and is calculated as the difference between the gas pressure entrapped within the tow $P_{gas}$ and the capillary pressure $P_c$, values for which can be found in Table 3-4.

**Table 3-4: Summary of input parameters for cure kinetics, viscosity, and degree of impregnation models for CYCOM 5320 PW prepreg**

| | | | |
|---|---|---|---|
| **Cure Kinetics Model Parameters** | | | |
| $A_1 = 8.23 \times 10^7$ | $E_{A1} = 82375$ | $m_1 = 0.75$ | $n_1 = 12.46$ |
| $A_2 = 1.04 \times 10^5$ | $E_{A2} = 6.20 \times 10^4$ | $m_2 = 0.9$ | $n_2 = 2.07$ |
| $D = 40.4$ | $\alpha_{C0} = -1.12$ | $\alpha_{CT} = 4.53 \times 10^{-3}$ | |
| **Viscosity Model Parameters** | | | |
| $A_{\mu 1} = 8.00 \times 10^{-13}$ | $E_{\mu 1} = 93931$ | $A_{\mu 2} = 2.90 \times 10^{-11}$ | $E_{\mu 2} = 8.30 \times 10^4$ |
| $\alpha_{gel} = 0.48$ | $A = 3.20$ | $B = 12.7$ | $C = -29.6$ |
| **Degree of Impregnation Model Parameters** | | | |
| $V_f = 0.71$ | $R_{tow} = 0.0917$ mm | $K = 2.1 \times 10^9$ mm$^2$ | $P\infty = 101325$ Pa |
| | $P_c = 0$ Pa | $P_{gas} = 0$ Pa | |

Figure 3-13, Figure 3-14, and Figure 3-15 show the resulting degree of cure, viscosity, and degree of impregnation (respectively) for the prepreg on the bagside and toolside of a 3.1 mm laminate. The degree of impregnation appears to reach 0.99 (fully impregnated) regardless of the temperature gradient. However, a slight reduction in the final degree of cure of the resin is noted for the toolside (lower cure temperature). The minimum viscosity remains the same despite of the 10°C temperature gradient, however, the gelation point for the bagside (heated side) of the repair occurs at an earlier point than that of the resin at the toolside.

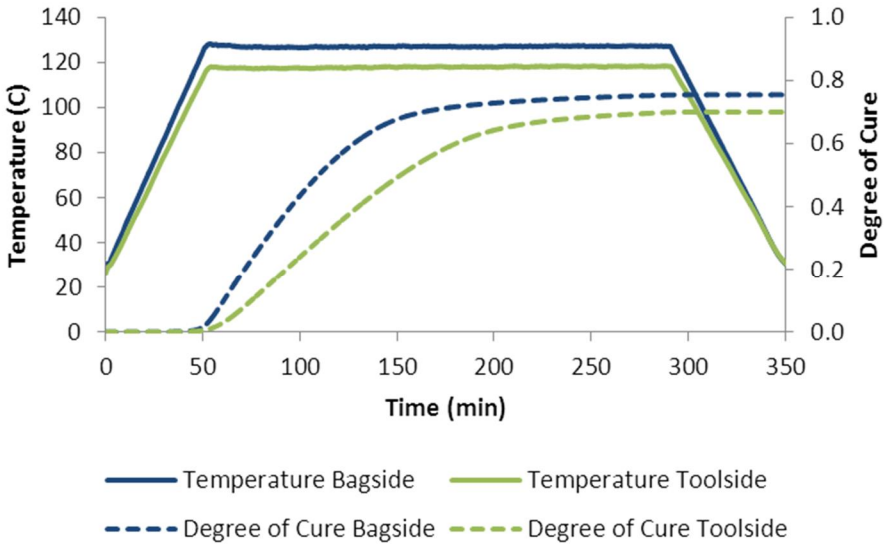


**Figure 3-13: Effect of the temperature gradient on the degree of cure of unconditioned repair patch (CYCOM 5320 prepreg)**

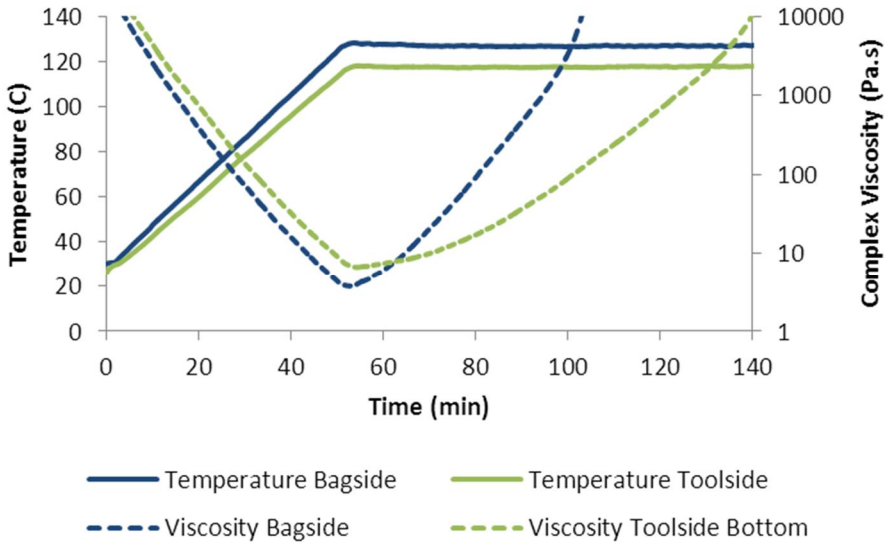


**Figure 3-14: Effect of the temperature gradient on the complex viscosity of unconditioned repair patch (CYCOM 5320 prepreg)**

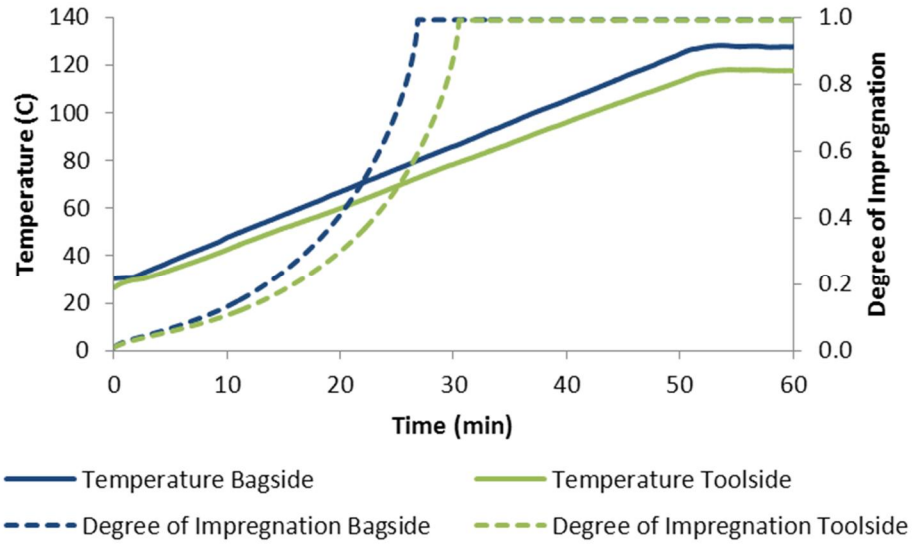


**Figure 3-15: Effect of the temperature gradient on the degree of impregnation of the resin in unconditioned repair patch (CYCOM 5320 prepreg)**

### 3.2.3 Discussion of Temperature Gradient Effects

The final degree of cure and minimum viscosity obtained from the FM300-2M model were not greatly affected by the 10°C temperature gradient between the bagside and toolside of a repair laminate. However, Figure 3-11 shows a slight cure gradient induced throughout the repair patch which is a direct consequence of the temperature gradient that is developed throughout the repair patch due to the one sided heat application. The cure gradient is then translated to a 20 minute delay in the gelation of the adhesive at the toolside with respect to the bagside, as observed in Figure 3-12.

A similar, but more pronounced, thermochemical behaviour was seen for the repair patch (CYCOM 5320 prepreg). Figure 3-13 shows that the degree of cure of the repair on the toolside is 7% lower than that of the plies on the bagside. The cure gradient effect on the gelation of the repair patch plies is also observed in Figure 3-14, where a 40 minute delay in the gelation of the resin in the repair patch at the toolside is noted. The viscosity of the resin also affects the impregnation of the resin in the fibres; as a consequence of the viscosity gradient throughout the

repair patch, more time is required for the resin to fully impregnate the dry fibres furthest from the heat source, as shown in Figure 3-15. However, since the resin flow time is longer than the time required for the repair patch to reach full impregnation, the delay in the impregnation of the fibres for the 10°C temperature gradient is not detrimental. Should the temperature gradient been higher, the resin flow at the bagside would have been shorter which giving the resin less time to fully impregnate the fibres in the repair patch which could potentially result in the formation of voids.

The modeled cure and gel gradient has several implications on the resulting repair patch part quality. First, the model indicates that the surface of the repair patch in contact with the heating blanket (bagside) will gel first while the surface furthest from the heating blanket (toolside) will gel last. As the bagside surface gels, the through thickness permeability of the repair patch decreases consequently blocking the air channels. This behaviour can prevent the escape of volatiles and entrapped air resulting in void formation. Additionally, the model shows that the adhesive gels 40 minutes before the resin in the repair patch. The early gel time of the adhesive could cause void formation in the bondline for repairs with conditioned parent laminates, as the moisture in the parent laminate is diffused into the bondline during the cure cycle and is trapped there when the adhesive gels. This trend is discussed further in section 3.5, Resulting Void Content.

## 3.3 Laboratory Scale Environmental Conditioning

### 3.3.1 Conditioning Chamber Apparatus

The conditioning process of laminates was implemented and monitored using a conditioning chamber built in-house, shown in Figure 3-16, which consists of many components described in this section. The chamber consists of a temperature controlled heating element, salt solution to achieve the desired humidity, and a data logger to monitor the conditions in the chamber in real time.

The chamber structure was assembled using corrosion resistant aluminum sheets fastened onto aluminum frames 61 cm in height and width that was subsequently covered by insulation. To ensure minimal heat transfer, the insulation was designed as two layers of reflective insulation and a layer of breather cloth sandwiched in the middle. The reflective insulation has one layer of 3.175 mm barrier bubble film laminated between two layers of metalized film and has a contact temperature range -51°C to 82°C which makes it ideal for the application.

A strip heater was used as the chamber's heat source; it was identified as the most effective source of air heating. The heating element, Ceramic Insulated Finned Strip Heaters (FSH-180-120), consists of corrosion resistant stainless steel fins that act as radiating surfaces to provide rapid heat transfer to the surrounding air.

The heating element was controlled by a proportional-integral-derivative (PID) temperature controller that executes a specific temperature as entered by the operator. A feedback thermocouple placed in the chamber was used as an input to the PID controller which in turn regulates the amount of current though the heating element until a steady state temperature is reached in the chamber. To ensure the heat in the chamber is indeed at steady state, and to ensure that the chamber does not overheat, a number of thermocouples were strategically placed in multiple locations in the chamber and regularly monitored, including on the door, the far back and the top of the chamber, as shown in Figure 3-17. A temperature and humidity data logger (OM-CP-RHTEMP101A) was used to monitor the humidity in the chamber and to ensure the

temperature enforced by the PID controller was accurate. The logger has a real time clock to ensure that all data is time and date stamped. Commercially available software provided by the manufacturer (Omega Engineering ®) was used to digitally calibrate the logger and to enable real-time monitoring of the conditions in the chamber.

Humidity in the chamber was generated by means of a saturated salt solution made up as a slushy mixture with distilled water and a chemically pure salt. To ensure the desired level of humidity is reached in the chamber, the headspace volume in the chamber (volume above the salt solution) to the surface area of salt solution ratio was kept to an approximate ratio of 10, [21]. An investigation of multiple salts, shown in Figure 3-18, yielded the selection of sodium chloride as the preferred salt, [39]. The salt solution generated an average of 70% relative humidity in the chamber. A corrosion resistant fan was added to ensure constant air circulation thus ensuring stable relative humidity levels in the chamber.

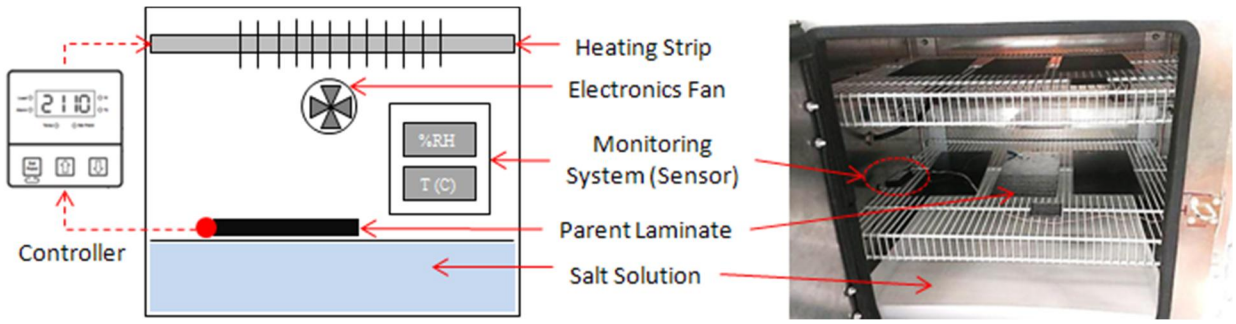


**Figure 3-16: Schematic of the in-house environmental conditioning chamber**

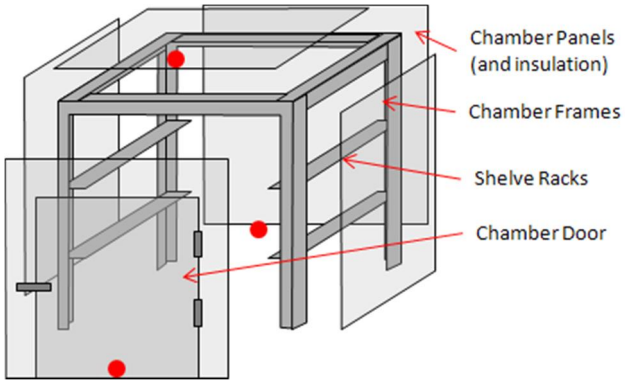


**Figure 3-17: Temperature monitoring in the conditioning chamber. Thermocouples were placed at the top very top and far back of the chamber, as well as on the door (shown as red dots) to ensure proper heat distribution in the chamber**

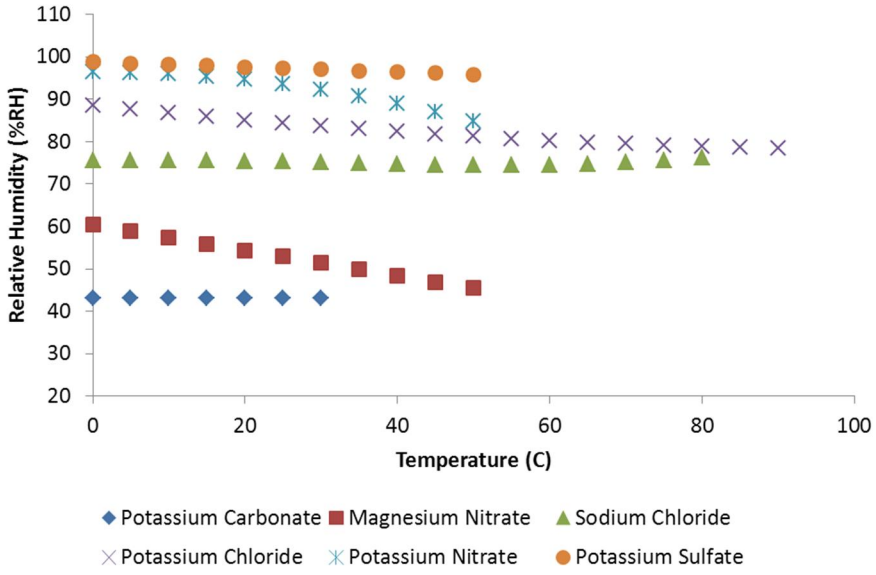


**Figure 3-18: Resulting relative humidity from several saturated salt-solutions at different temperatures [39]**

## 3.4 Moisture Absorption

Void formation due to moisture ingress in different parts of the repair was studied. The different components of the repair (film adhesive, uncured repair patch, and parent laminate) were conditioned as specified in the following sections before bonding. Void content analysis of the resulting repair joints is presented subsequently. Control panels known as the 'baseline' were manufactured with nominal "as-received" materials for later comparison.

**Moisture absorption in the film adhesive**

Uncured film adhesive was conditioned for configuration 'C2a' repair laminates, Table 3-3, to determine the effects of moisture in the film adhesive on the final repair quality and strength. To determine the appropriate exposure time and moisture saturation level of the film adhesive, three samples of uncured film adhesive were conditioned at ambient temperature (21 ± 2°C) at 90 % RH. A schematic of the humidity conditioning glass chamber is shown in Figure 3-19; distilled water was used to create a 90%RH level in the glass chamber. The samples were weighed on regular basis using a Sartorius scale with a 0.01 mg resolution while ensuring no water particles were on the surface of the film to confirm the moisture was absorbed into the film rather than concentrated onto the surface. The samples were conditioned for 16 hours, however it was noted that the samples reached equilibrium with moisture content of 0.25-0.3% after 4 hours of conditioning, as shown in Figure 3-20.

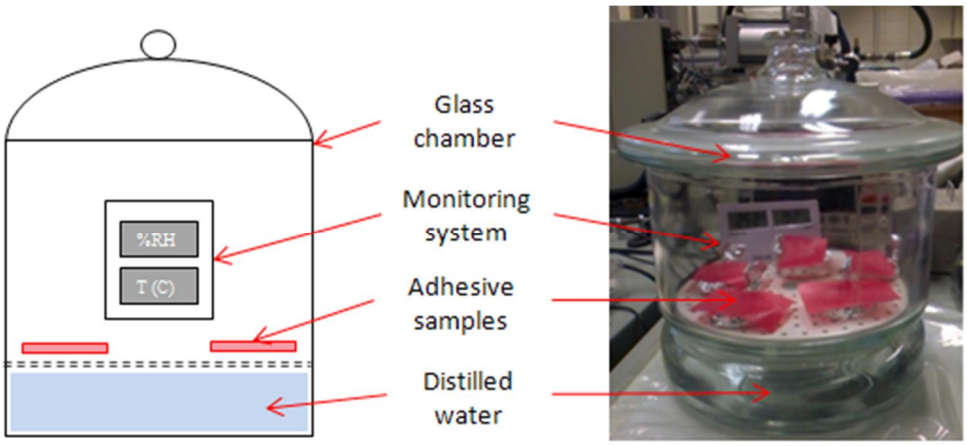


**Figure 3-19: Apparatus used for conditioning adhesive film**

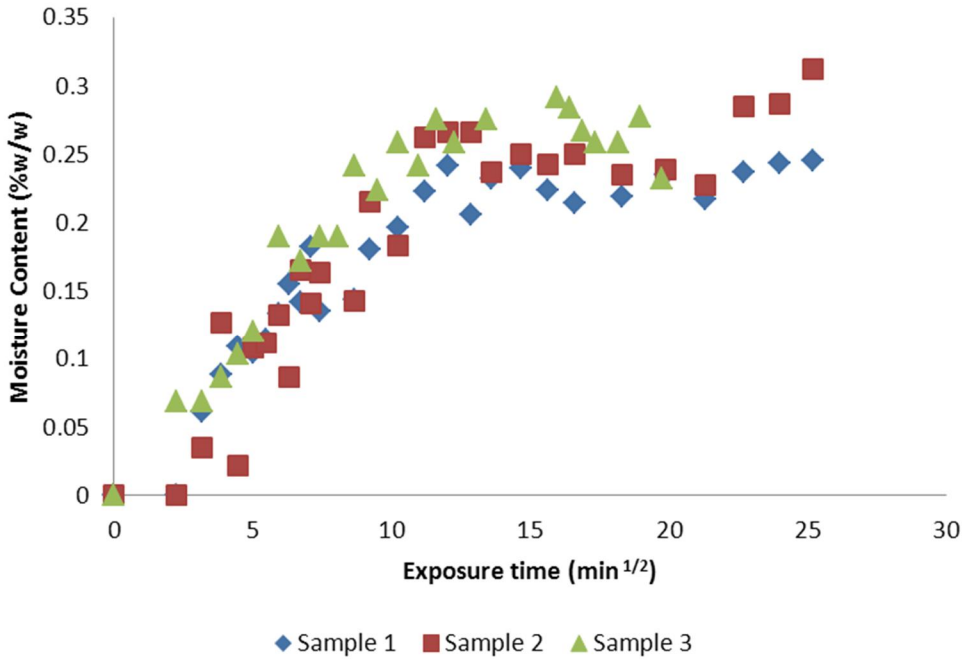


**Figure 3-20: Weight gain curve of several adhesive film samples conditioned up to 16 hours**

Therefore, for configuration 'C2a' repair laminates, the film adhesive ply used for repair was conditioned for 4 hours at ambient room temperature and 90%RH, moisture content in the ply was 0.3% prior to repair.

### Moisture absorption in the repair patch

To determine the effects of pre-bond moisture on uncured repair plies (configuration 'C3a' and 'C3b' repair laminates per Table 3-3); uncured repair laminates were fabricated by cutting the plies to size, placed in the correct quasi-isotropic orientation and step lap length to match that of the parent laminates then placed in the conditioning chamber. Two conditioning levels were examined; one configuration was conditioned at 80%RH and 34°C, and the second configuration was conditioned at 90%RH and 23°C. The samples were weighed on regular basis, however unlike the adhesive film samples (of configuration 'C2a'), they were not conditioned to equilibrium; instead they were conditioned for 24 hours. The resulting moisture is 0.27% and 0.58% for 'C3a' and 'C3b'configurations respectively.

**Moisture absorption in the parent laminate**

The cured panels were stored in normal laboratory conditions (23°C, <30% RH) until required for joint manufacture or conditioning. Laminates repaired with conditioned substrates are referred to as configuration 'C1'.

The conditioned substrates were placed in the conditioning chamber at 65°C and an average of 70% relative humidity. These conditioning parameters were derived from industry standards; it was determined that a reasonable upper-bound value for aircraft design service relative humidity is 85%, whereas the conditioning temperature should be 50°C below the glass transition temperature of the resin, [2].

Traveler coupons representing the parent laminate (same material, thickness and manufacturing parameters) were used in the conditioning procedure to determine the moisture content and to ultimately determine the through-the-thickness moisture absorption properties of the laminate. These coupons are used instead of the parent laminate because they are within the weight and size requirements of the ASTM 5229M method, [22].

The conditioning procedure was conducted as follows: the parent laminates along with their representative travelers were placed in the conditioning chamber. The travelers were weighed immediately after manufacturing, before start of conditioning, and then on a weekly basis using a Sartorius scale with a 0.01 mg resolution. The moisture content in the traveler was determined using Equation (3-4), until the moisture in the traveler reached equilibrium.

$$M_i = \frac{W_i - W_b}{W_b} \times 100\% \quad \textbf{(3-4)}$$

where $M_i$ is the average moisture content and $W_i$ is the specimen's mass at the current time, and $W_b$ is the mass of the specimen as a baseline (oven-dry). Moisture equilibrium, or saturation, is identified when there is no further change in the average moisture content in the traveler, as measured in Equation (3-5), where $M_i$ is the moisture content at the current time and $M_{i-1}$ is the moisture content at a previous time.

$$M_i - M_{i-1} < 0.01\% \quad \textbf{(3-5)}$$

The rate of moisture absorption is controlled by the material property called moisture diffusivity. Diffusion is governed by Equation (3-6),[22] , where c is the concentration of water, t is the time, z in the distance through the t thickness, and $D_z$ is the diffusion coefficient.

$$\frac{\partial c}{\partial t} = D_z \frac{\partial^2 c}{\partial z^2} \quad \textbf{(3-6)}$$

The diffusivity constant for the CYCOM 5320 was then determined from the initial slope of the percentage water gain versus the square-root of time shown in Figure 3-21.

The diffusion parameters were then experimentally measured using Equation (3-7), results summarized in Table 3-5, where h is the thickness of the laminate, $M_1$ and $M_2$ are the moisture content at time $t_1$ and $t_2$ respectively, and $M_m$ is the total moisture in the laminate at equilibrium.

$$D_z = \pi \left(\frac{h}{4M_m}\right)^2 \left(\frac{M_2 - M_1}{\sqrt{t_2} - \sqrt{t_1}}\right)^2 \quad \textbf{(3-7)}$$

**Table 3-5: Measured diffusivity constant for the parent laminate**

| Panel ID | Humidity %RH | Temperature (°C) | Equilibrium moisture level (% w/w) | Diffusion coefficient ($mm^2$/day) |
|---|---|---|---|---|
| **L1** | 70 | 65 | 0.901 | $1.02 \times 10^{-2}$ |
| **L2** | 70 | 65 | 0.896 | $2.91 \times 10^{-2}$ |

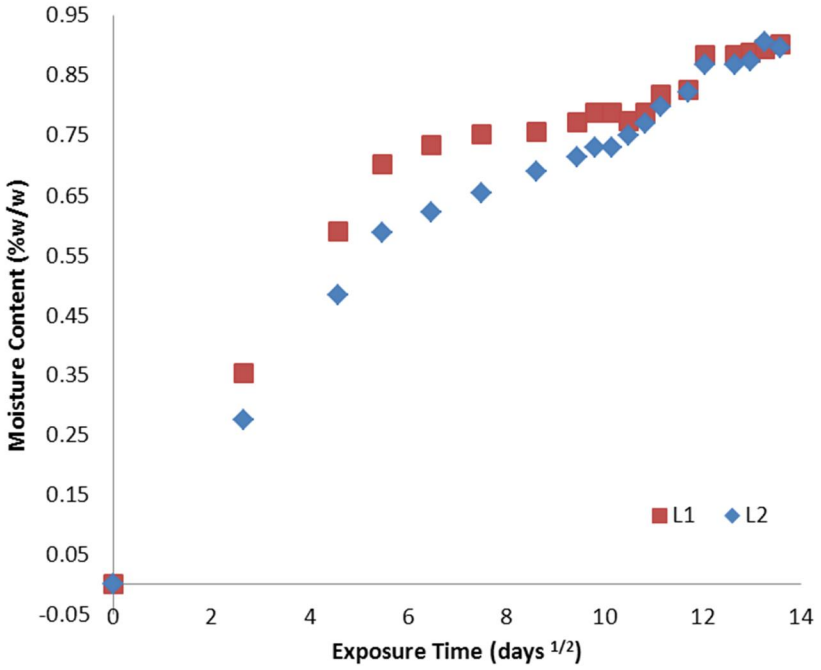


**Figure 3-21: Plot of moisture uptake for parent laminates (1.54 and 3.1 mm thickness)**

Knowing the diffusion coefficient, the initial and equilibrium moisture concentrations, and the dimensions of the panel, the through-thickness moisture profile and the total amount of moisture absorbed can be calculated at any given time.

## 3.5 Resulting Void Content

To determine the void content in the repaired laminate, several specimens 25-50 mm in length were cut from each repaired laminate, and polished using Forcipol 300-1V grinder and polisher instrument with Forcimat head, an automatic specimen mover. Sample cross-sections were gradually polished using Diamond Grinding Discs ranging from 120 to 600 grit, followed by a 1200 grit abrasive paper lubricated gradually with 12.5 μm, 5.0 μm, and 0.3 μm Alumina mixture until a smooth surface is achieved.

Micrographs of the sample cross-sections were taken at 50 times magnification with an optical microscope to assess the quality of the patch and of the bondline for each specimen. The resulting micrographs were composed of many images obtained by an automated movable stage

fitted onto the optical microscope stitched together using a mosaic function of the Clemex Captiva software.

The void content in the total laminate, parent laminate, bondline and repair patch were determined using ImageJ, image processing software. The void volume fraction (or percentage void content) was determined by measuring the void area in the cross-section. Each void was captured using the "magic wand" tool of 8-bits converted images, [35, 40]. An example of the original micrograph is displayed with a post-processed black and white image used for image analysis for void content measurements is shown in Figure 3-22.

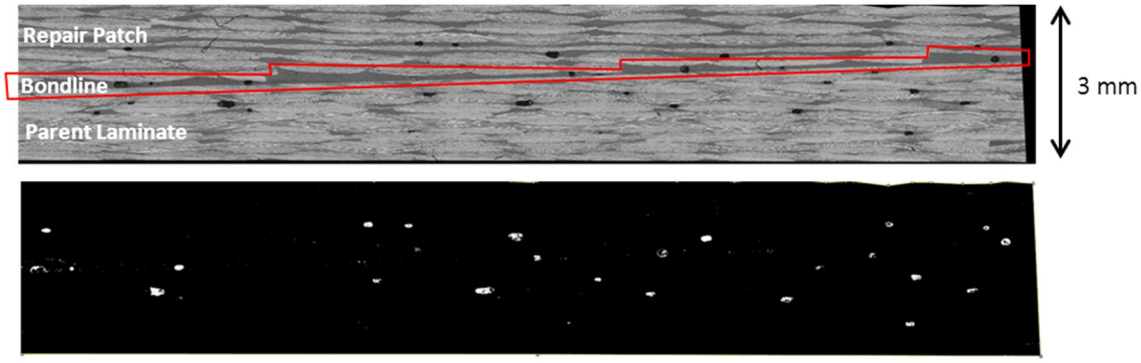


**Figure 3-22: Example of image analysis of a repaired laminate. Top is a micrograph image at 50 times magnification, bottom image is the resulting ImageJ analysis**

The results of the laminate's total percentage void content, obtained from ImageJ software, were plotted against the moisture content for each repair configuration in Figure 3-23 for visual representation. A clear trend is observed; the void content in the repaired laminate increases with the moisture content; most evidently for conditioned patch (configurations 'C3a' and 'C3b'). A summary of the resulting percentage void content in the repair patch, bondline, and the parent laminate along with the moisture content for each of the repair configurations can be found in Appendix A.

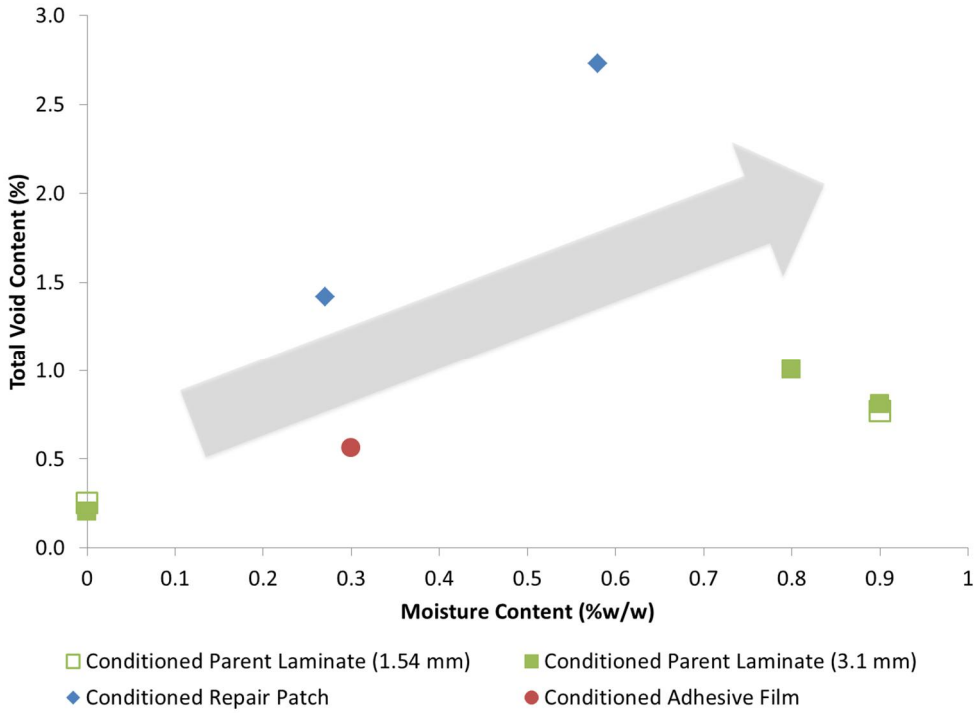


**Figure 3-23: Plot of the total void content in the laminate versus the pre-bond moisture content in the parent laminate, adhesive film, and the repair patch**

Unlike the work done by Preau et al, [35], where various methods were implored to facilitate the in-plane evacuation of the gases from the repair patch and bondline, the repaired laminates herein were manufactured in such a way preventing the in-plane evacuation of gases during the cure process. As discussed earlier, the motivation for this technique was to reflect a basic in-service repair boundary condition. Hence; entrapped moisture from the various conditioning configurations was forced to evacuate through the thickness of the repair patch. By doing so, voids were formed in different regions of the repaired laminate.

Figure 3-24 (a) shows an example micrograph of an L1-C1b repair laminate cross-section; where a high percentage of void content in the bondline is present due to the pre-bond moisture in the parent laminate associated with conditioned configuration ‘C2b’. It is suspected that the moisture entrapped in the parent laminate diffused into the adhesive during the curing process of the repair.

Figure 3-24 (b) on the other hand shows an example micrograph of an L3-C3b repair laminate cross-section. The micrograph shows high void content in both the bondline and the repair patch. This observation can be attributed to the nature of configuration 'C3b', where the uncured repair patch was conditioned. The resulting void content in the patch is formed as the moisture within the repair patch was not fully evacuated during the cure cycle. The entrapment of moisture in the repair patch can be attributed to the low transverse air permeability of the repair patch; it was found by Kratz and Hubert, [41], that the permeability of CYCOM 5320 plain weave prepreg to be two orders of magnitude lower in the transverse direction than in the in-plane direction.

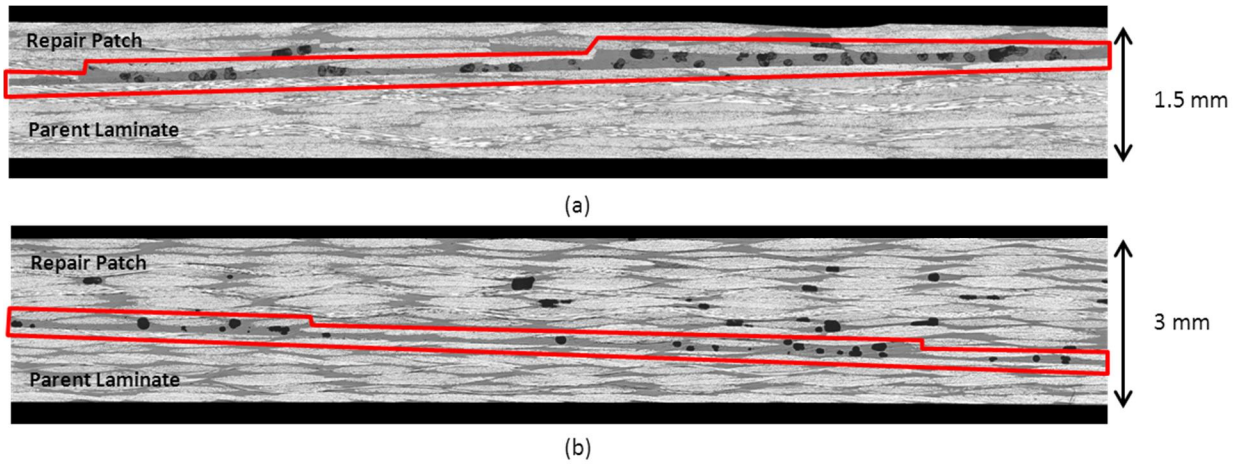


**Figure 3-24: Optical microscopic images of representative sections of L1-C1b and L3-C3b repair laminates. Parent laminates at the bottom of each picture are almost void-free, whereas the bondline (outlined in red) and the repair patch of each configuration exhibit various levels of void content**

Figure 3-25 shows the distribution of the resulting void content in the parent laminate, repair patch and the bondline for all repair configurations for L2 and L3 laminates (3.1 mm thickness). Similar to the results shown in Figure 3-23, an evident increase in the void content in the repair patch and bondline is observed for repair configurations with conditioned parent laminates and conditioned repair patch. For repair laminates with a conditioned parent laminate (configurations 'C1a' and 'C1b'), an increase of the void content in the repair patch up to 8 times of the baseline was noted, and an increase of the void content in the bondline up to 4 times of the baseline was noted. Similarly, for repair laminates with a conditioned repair patch (configurations 'C3a' and 'C3b'), an increase of the void content in the repair patch up to 15 times of the baseline was

noted, and an increase of the void content in the bondline up to 6 times of the baseline was noted. As for repair laminates with a conditioned adhesive film (configurations 'C2a'), the percentage void content in the repair patch increased 3 times the baseline, however no increase in the voids in the bondline were noted.

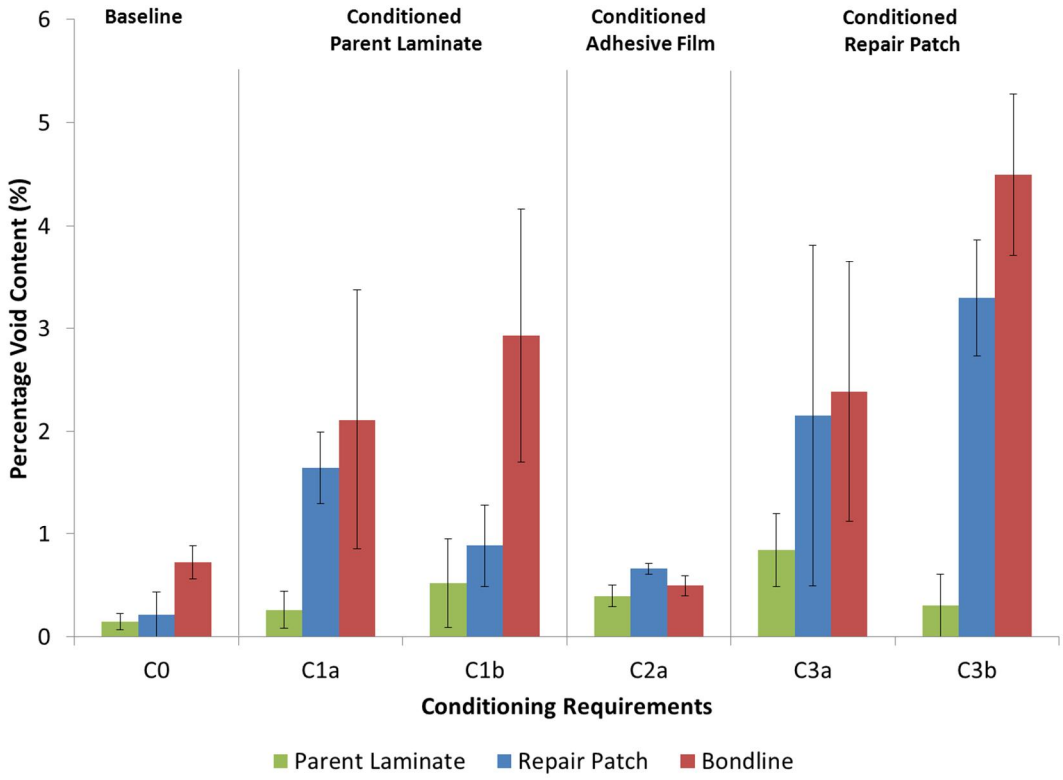


**Figure 3-25: Distribution of resulting void content in the parent laminate, repair patch and bondline for all repair configurations for L2 and L3 laminates (3.1 mm)**

The resulting void content was compared between L1 and L2 laminates (1.54 and 3.1 mm thickness respectively) for conditioned parent laminates (configuration 'C1b') as shown in Figure 3-26. The percentage void content in the repair patch of L2 laminates was 3% higher than that measured in L1 laminates. Similarly, the percentage void content for the bondline of L2 repaired laminates was 16% higher than that of the L1 laminates. Moderately higher void content found in the L2 laminates could be attributed to the thickness of the laminate. As the cure cycle progresses, the absorbed moisture in the parent laminates diffuses into the bondline then into the

repair patch to be evacuated by means of vacuum. It is likely that a higher percentage of the pre-bond moisture could be evacuated for thinner laminates resulting in lower void content in the bondline and the repair patch.

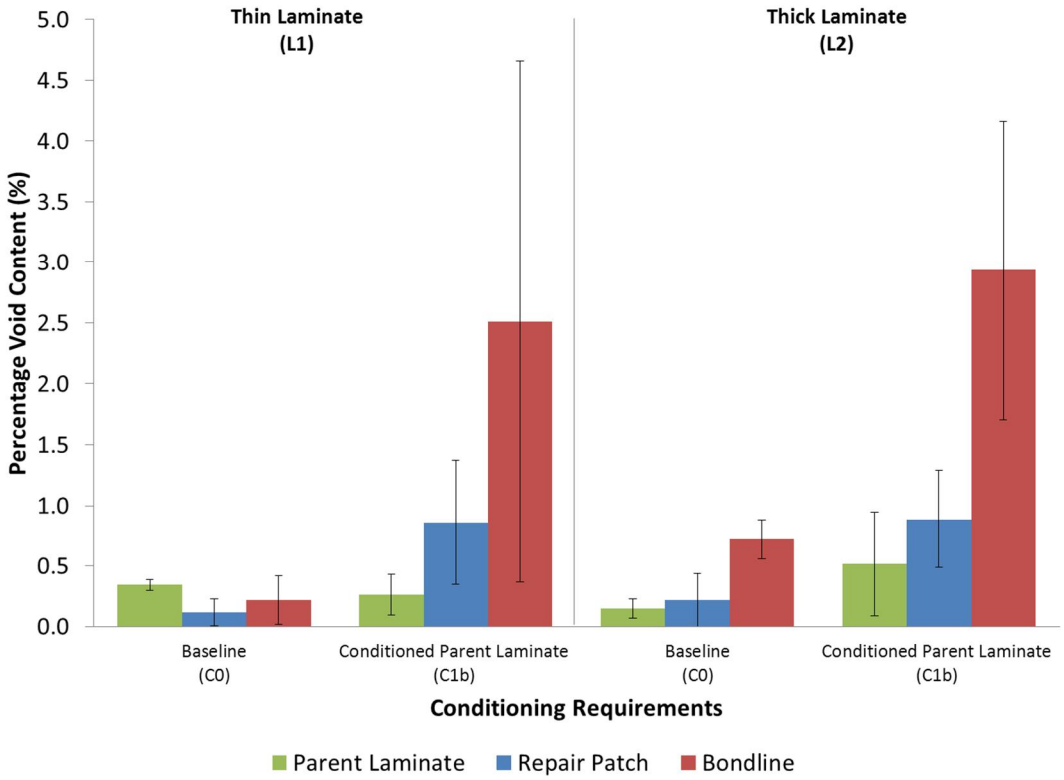


**Figure 3-26: Distribution of resulting void content in the parent laminate, repair patch and bondline for L1 laminates (thin laminates = 1.54 mm) and L2 laminates (thick laminates = 3.1 mm)**

Chapter 4

# Mechanical Testing

Mechanical tests are a necessary step in aircraft design to determine the strength of the structure. Typical aircraft structures are exposed to complex loading that is multidirectional in nature. However, unidirectional testing is the first step to quantify the strength of a structure to be used as input for more complex testing. Unidirectional testing can be either in tension, compression, shear or bending depending on the desired outcome. In the case of bonded joints, the most critical loading in the joint is shear loading in the adhesive itself, which is best achieved by unidirectional tensile testing. For example, the tension load applied on a stepped lap joint specimen, as shown in Figure 4-1, induces shear loading on the bondline which results in the desired failure mode of a bonded joint, which is either adhesive or cohesive shear failure.

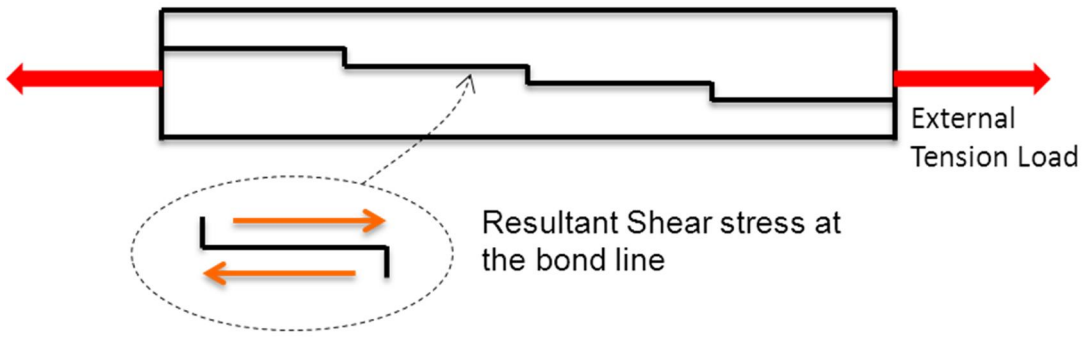


**Figure 4-1: Shear loading in a stepped lap joint**

The failure modes associated with unidirectional tensile testing of adhesively bonded joints can be classified as net section, adhesive, or cohesive failure as shown in Figure 4-2. Each of these failure modes signifies a critical joint design feature, detailed below.

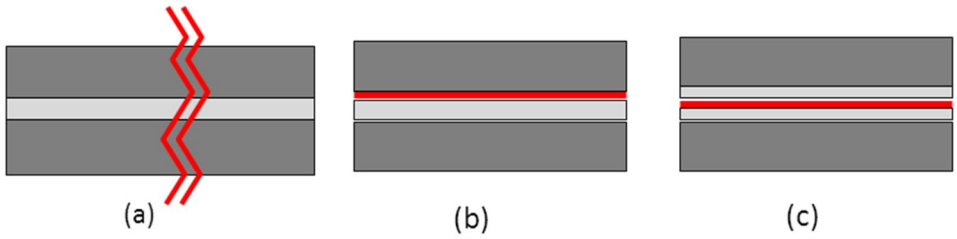


**Figure 4-2: Bonded joint failure modes: (a) net section failure, (b) adhesive failure, (c) cohesive failure**

Net section failure is the tensile failure of the substrate (parent laminate), also known as fibre failure. This failure mode occurs when repair bond line fully restores original strength of the pristine laminate. The bond line shear strength is higher than composite substrate tensile strength resulting in fibre failure of composite substrate.

Adhesive failure is the failure between the substrate (parent laminate) and the adhesive in the bondline. This failure mode occurs when bond between composite substrate and adhesive is not adequate. This can be due to various reasons like poor surface preparation, bond line contamination etc. This is an undesirable failure mode since it typically results in low strength values and indicates that further improvement in bonding process is required.

Cohesive failure is the shear failure of the adhesive. This failure mode occurs when adhesive shear strength is lower than composite tension strength at an applied tension load. This failure mode can occurs when the composite substrate has very high tension strength giving first failure mode as shear of an adhesive.

## 4.1 Experimental Procedure

Mechanical tension tests were performed to evaluate the static strength of repaired coupons. The primary objective was to evaluate the effect of pre-bond moisture on the final repair strength.

The repaired laminates were cut to a rectangular 2.54 (W) x 30.45 (L) cm coupons, which is in agreement with industry standards. Test coupon configuration is shown in Figure 4-3. The hydraulic grip length was maintained at 5 cm, and the distance between the end of the repair scarf and the hydraulic grips was maintained to a minimum of 5 cm to ensure there is no stress field interference between the grip and the scarf. Tabbing was deemed unnecessary; however an abrasive mesh was used for additional friction between the hydraulic grip and the coupon and to eliminate potential slippage of the coupon at higher loads.

The coupons were loaded at a rate of 1mm/sec. Force applied on the coupons was measured using the load cell sensor in the machine, and strain measurements were extracted from a 25 mm extensometer during the initial loading period.

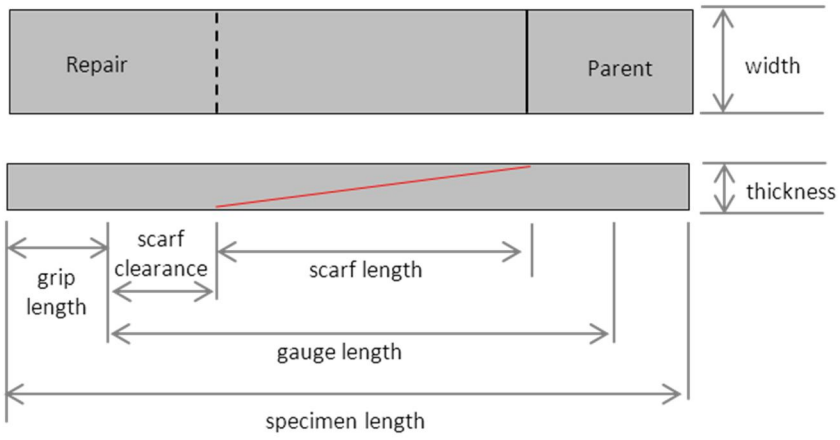


**Figure 4-3: Test coupon configuration**

Four repair variations were tested, as summarized in Table 4-1. One set of repairs was unconditioned and was considered the nominal or baseline repair, the conditioned configurations include coupons with pre-bond moisture in the parent substrate, pre-bond moisture in the

adhesive film, and pre-bond moisture in the repair prepreg plies. Three specimens were tested for each repair configuration to capture the statistical variation.

**Table 4-1: Mechanical testing matrix for all repair laminate configurations**

| Laminate thickness (mm) | Configuration ID | Conditioned parameters | Number of specimens |
|---|---|---|---|
| **1.5 (L1)** | L1-C0 | - | 3 |
| | L1-C1a | parent laminate | 3 |
| | L1-C1b | parent laminate | 3 |
| **3.1 (L2 & L3)** | L2-C0 | - | 3 |
| | L2-C1a | parent laminate | 3 |
| | L2-C1b | parent laminate | 3 |
| | L3-C2a | adhesive | 3 |
| | L3-C3a | repair patch | 3 |
| | L3-C3b | repair patch | 3 |

## 4.2 Analysis and Summary of Results

Simple scarf joint analysis was use to predict the failure load of the repairs. For shallow scarf angles ($\theta < 3°$), the shear stress distribution in the adhesive, shown in Figure 4-4, was uniform if the parent laminate and the repair patch were identical. The shear stress is parallel to the scarf, whereas the normal stress (out-of-plane) is perpendicular to the scarf. The stresses in the joint can be calculated using Equations (4-1), where P is the tensile load, $\theta$ is the scarf angle, $\tau$ is the shear stress, and $\sigma$ is the normal stress [42].

$$\tau = \frac{P}{2t}\sin(2\theta), \quad \sigma = \frac{P}{t}\sin^2(\theta) \tag{4-1}$$

From Figure 4-4 it can be seen that the normal stress in the joint approaches zero and the shear stress τ approaches the shear stress of the adhesive ($\tau_p$) as the joint angle approaches zero. Using this approach, the failure load in the joint (maximum allowable tensile load) can be represented by Equation (4-2). The final joint strength of the repair was calculated to be 1521 MPa using FM300-2M adhesive shear strength of 50.2MPa (obtained from the experimental data in reference [43]).

$$P = \frac{2\tau_p t}{\sin(2\theta)} \tag{4-2}$$

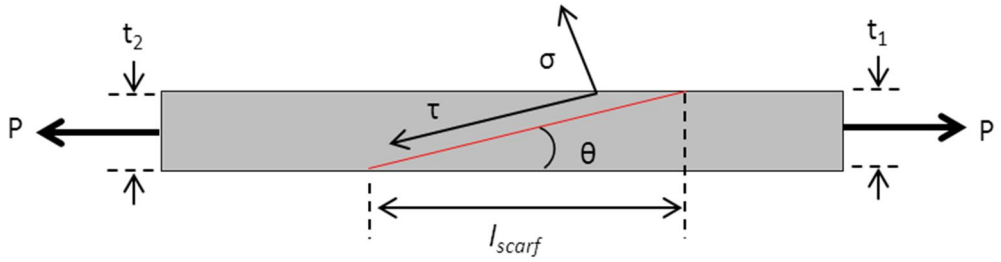


**Figure 4-4: Simple scarf joint analysis**

This analysis method is a simple form, and considers only the elastic region of the adhesive. By setting the plastic zone of the adhesive to zero, the predicted joint failure load is considered conservative; meaning the joint should fail at a much lower load than that predicted.

The un-notched tension strength of the laminate was also calculated (undamaged, unrepaired), which allows the comparison of the repaired joint strength to that of a pristine one. The stiffness of a pristine (unrepaired) laminate was calculated using Cytec-provided data for CYCOM 5320 prepreg, summarized in Table 4-2, and principles of the classical laminate theory, [44]. The theoretical stiffness was calculated to be 48.51 GPa. The pristine strength was obtained by testing and was found to be 650 MPa. The stiffness of the laminates were also extracted from

the experimental data and were found to be on average 45 GPa, which is in close agreement with the calculated stiffness.

**Table 4-2: CYCOM 5320 PW preliminary data, [44]**

| Property | Test method | |
|---|---|---|
| $\mathbf{E_1}$ | 0° Tension Modulus, ASTM D 3039 | 67568 MPa |
| $\mathbf{E_2}$ | 90° Tension Modulus, ASTM D 3039 | 64810 MPa |
| $\mathbf{\upsilon_{12}}$ | 0° Tension Poisson's Ratio, ASTM D 3039 | 0.057 |
| $\mathbf{G_{12}}$ | In-Plane Shear Modulus, ASTM D 5379 | 85736 MPa |
| **t** | Cure ply thickness | 0.19 mm |

### 4.2.1 Summary of results

The force-history plot for all the tensile tests were recorded and summarized in Appendix B, an example is shown in Figure 4-5, the failure load was extracted from the plot and the failure strength of the coupons were calculated based on their exact dimensions. The data from the extensometer was then used to verify the stiffness of the coupons, as shown in Figure 4-6. The experimental failure strength and stiffness results were compared to the predicted failure strengths in the previous section. On average, the experimental failure strengths of the repaired laminate were 90% of the laminate failure strength of the theoretical pristine data, whereas the stiffness of the coupons were determined to be within 5% of the calculated stiffness.

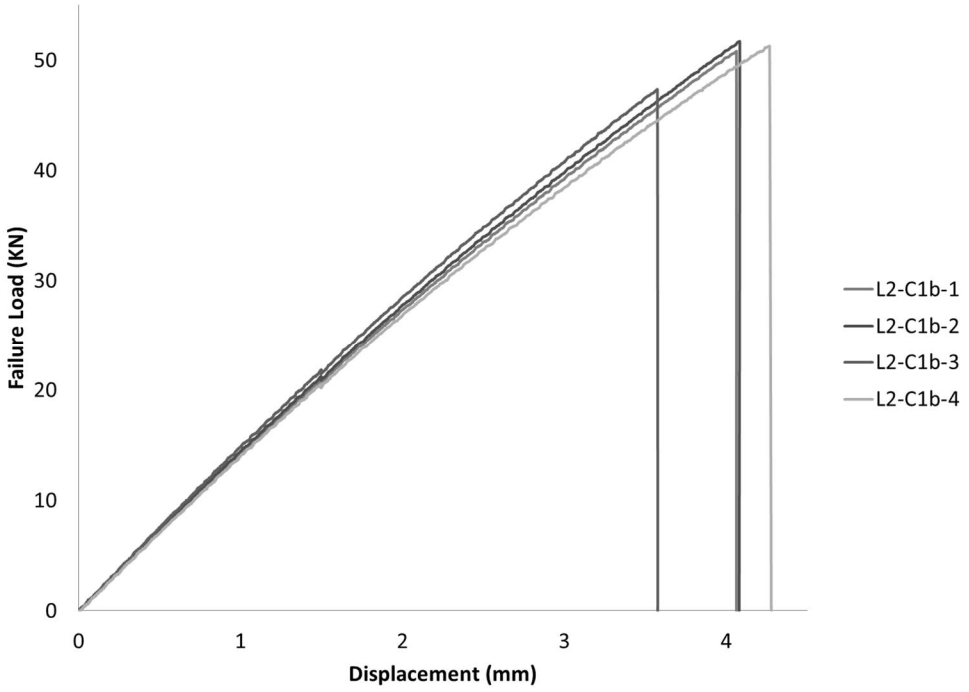


**Figure 4-5: Example of the Force-History plot for three tests of the same configuration. The failure load varies between samples due to slight variation in the width of the coupon. The kink in slope at 20KN corresponds to the removal of the extensometer.**

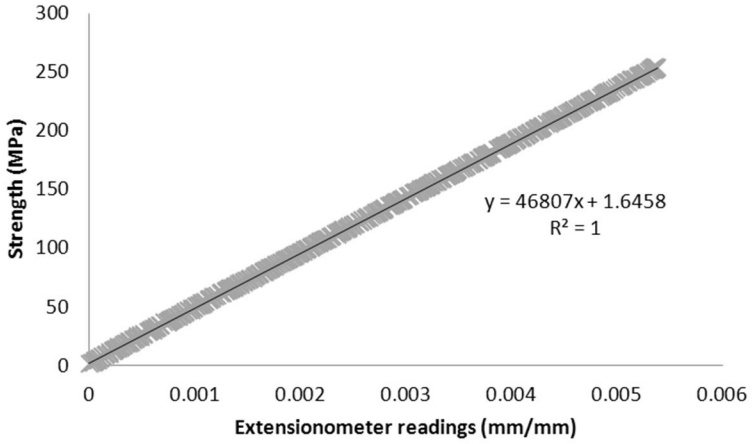


**Figure 4-6: Sample extensometer readings for stiffness verification for coupon L2-C1b-1**

The theoretical allowable strengths calculated earlier indicate that adhesive failure should not occur before laminate as the adhesive allowable elastic strength is much higher than that of the laminate's un-notched tension. The test results indeed support this observation, as all test

coupons failed in the net section of the repair joint. A summary of the different types of net section failure has been summarized in Figure 4-7. A few examples of failed coupons are shown in Figure 4-8. In most cases, the failure of the coupons is representative of that in in Figure 4-8 (a)(b). In some cases, a mix of fibre failure and delamination is noted as shown in Figure 4-8 (c)(d) indicative of a weakened bondline.

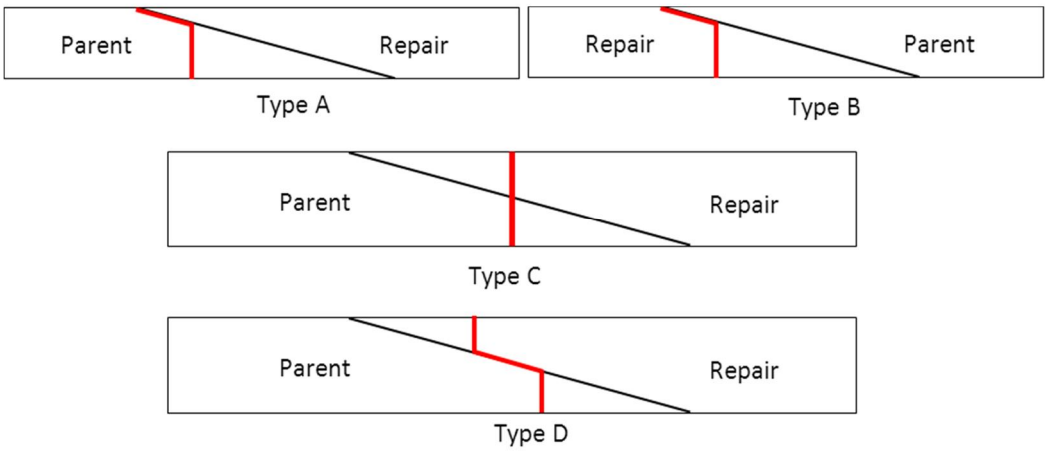


**Figure 4-7: Observed types of net-section failure modes. Type A and B initiate at the topmost repair or parent ply and continue through the thickness. Type B is net section through the thickness. Type D is net section through the laminate that transitions briefly into the bondline.**

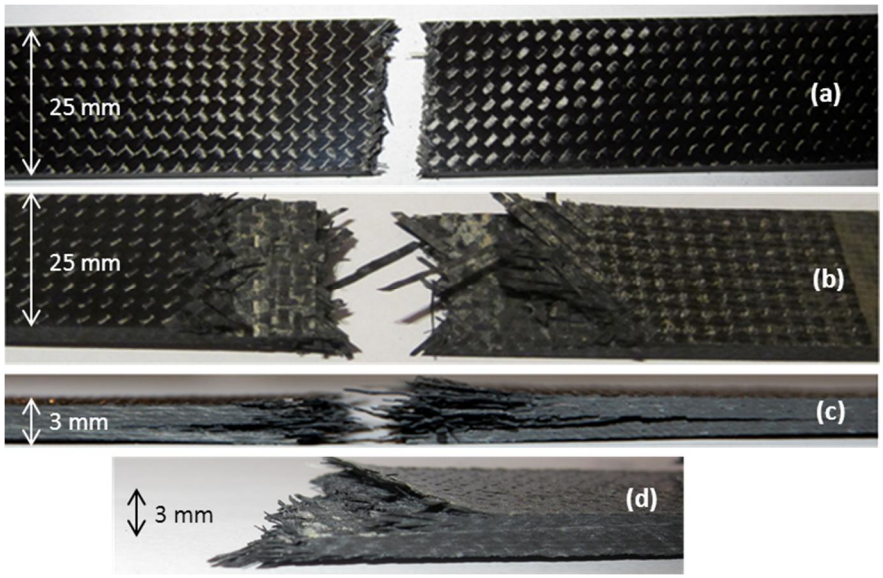


**Figure 4-8: Example of net section failure of test coupons. (a)(c) typical "Type C" net section failure observed for most cases. (b)(d) "Type D" net section failure with delamination in the laminate**

### 4.2.2 Discussion of Results

The results of mechanical tests performed on the repaired coupons have been summarized in Table 4-3 below; results include the average failure strength of the coupons, the type of net-failure observed, and a comparison of the strength result with the baseline coupons. Baseline coupons ate repair joints with no conditioning.

**Table 4-3: Summary of mechanical test results**

| Laminate thickness (mm) | Repair configuration | Failure Strength (MPa) | | Net-section failure type | % difference |
|---|---|---|---|---|---|
| | | average | C.V% | | |
| **1.5 mm (L1)** | L1-C0 | 540.41 | 2.7 | C | Baseline |
| | L1-C1a | 459.96 | 2.1 | A | -15 |
| | L1-C1b | 536.44 | 3.9 | C | -1 |
| **3.1 mm (L2 and L3)** | L2-C0 | 584.80 | 2.3 | C | Baseline |
| | L2-C1a | 578.45 | 1.9 | C | -1 |
| | L2-C1b | 609.28 | 1.0 | C | +4 |
| | L3-C2a | 574.89 | 0.8 | C+D | -2 |
| | L3-C3a | 555.79 | 2.1 | C+D | -5 |
| | L3-C3b | 538.14 | 1.4 | C+D | -8 |

A large decrease in the failure strength of L1-C1a was noted, the pre-bond moisture content in the substrate was 0.81±0.02% at the time of the repair. Initially, it was thought that these results were representative of the failure strength reduction for pre-conditioned substrate, however, a closer look at the failure showed a “Type A” failure. The failure type along with micrographs of the bondline showed that the repair plies were not overlapped with the parent laminate, resulting in a butt-joint configuration with an inadequate load transfer. Hence, the failure strength results obtained for coupon configurations L1-C1a will be omitted from further discussion.

A slight decrease in the failure strength was noted for L2-C1a coupons; the substrate of which was conditioned for the same amount of time as L1-C1a and contains 0.78±0.02% moisture. However, since the decrease in strength was 1%, it was not considered of significance.

The second set of pre-conditioned substrate repair coupons (L1-C1b and L2-C1b) contained 0.90±0.02% moisture by weight and was considered fully saturated. The failure strength results however show a curious trend, where an increase in the failure strength was noted for the thicker

laminates (L2 laminates). This increase in failure strength was not anticipated; however a hypothesis on this anomaly can be made. It is believed that the extended duration of the conditioning of the substrate at elevated temperatures might have increased the through-the-thickness properties of the laminate, a trend that was seen in a study by Charalambides et al, [45]. This increase in the matrix properties could be attributed to a behaviour similar to that of a post-cure; a step used by the manufacturer's to improve the toughness of the resin.

Repair joints manufactured using conditioned adhesive film (L3-C2a) saw a 2% drop in strength, 75% of which failed in the net section of the coupon. One of the four failed coupons however had a "Type D" failure mode; where the failure starts in the laminate, progresses slightly into the bondline, then continues through the laminate. This failure type could be indicative of a weakened bondline due to the increased presence of voids.

The final tested repair configuration was that of a conditioned repair patch prior to bonding. Coupons L3-C3a were conditioned to a 0.28% moisture content in the prepregs prior to cure. The coupons of this configuration failed at a strength 5% lower than that of the baseline results. Most of the coupons failed in the net-section with the exaction of one "Type D" failure mode. As discussed earlier, this change in the failure type could be due to the increased void content in the bondline or the repair patch. Similarly, coupons L3-C3b (0.57% moisture content) failed in the net-section with the exception of one coupon that showed a "Type D" failure behaviour. These coupons had the lowest failure strength, 8% lower than the baseline.

The failure strength was plotted as a function of the percentage void content in the repair patch, the bondline, and the parent laminate as shown in Figure 4-9. A relationship can be observed as the failure strength decreases with increasing void content; the most evident is the effect of void content in the repair patch and the bondline.

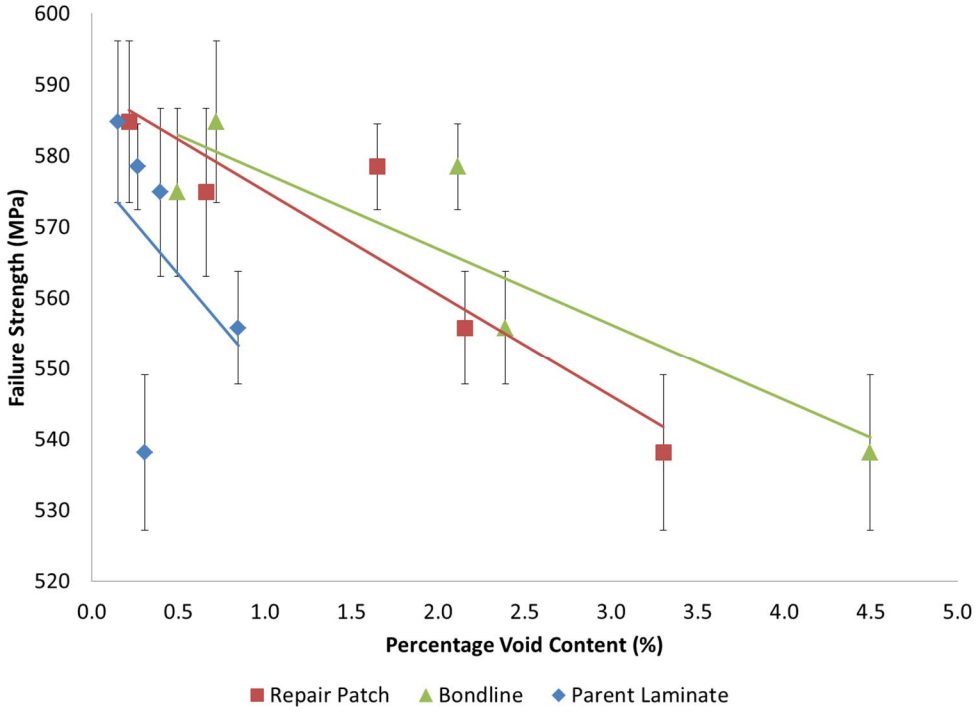


**Figure 4-9: The reduction in average failure strength of the repaired joints is shown as a function of the void content in the repair patch, bondline, and the parent laminate for 3.1 mm (L2 and L3) repairs**

# Chapter 5

# Conclusion

The main objective of this work was to understand the effects of pre-bond moisture on critical in-service repair parameters such as quality and strength. A secondary objective was to characterize and evaluate the structural film adhesive used for the repair application with and to assess the effects of moisture. The following section highlights findings from this research.

**1- Characterization of FM300-2M structural film adhesive**

The thermos-chemical characterization provides important information about the adhesive during the curing process. The adhesive begins to flow at 90°C when the viscosity reaches a magnitude between 100-300 Pa.s and reaches gelation at a degree of cure of $\alpha_{gel} = 0.77$. After gelation, the adhesive's complex viscosity increases by many orders of magnitude, hence closing off the pathway for entrapped air evacuation. A cure kinetics and viscosity models were developed as predictive tools.

**2- Effect of moisture on the FM300-2M cure behaviour**

The effects of moisture on the degree of cure were small but evident nevertheless. An average drop of 10% of the experimental final degree of cure was measured for conditioned DSC samples attributed to the presence of unbound moisture in the adhesive. Meanwhile, moisture in

the samples lowered the complex viscosity for the rheological samples by 100 Pa.s for the 2°C/min ramp rate specimens, and 50 Pa.s for the 3°C/min, whereas the overall rheological behaviour remains the same.

**3- Effect of one sided heat application during repair cure**

A thickness-dependent temperature gradient was measured between the bagside (heated side) and the toolside (non-heated side) of the repair laminate present due to the one-sided nature of a heating blanket hot-bond system. The theoretical thermochemical properties of the laminate due to a 10°C temperature gradient for a 3.1 mm laminate showed that the most affected properties is a drop in the degree of cure and a delay in the gelation point of the non-heated side that may contribute to the void formation in the laminate.

**4- Effect of pre-bond moisture on the final void content**

The percentage void content in the bondline and the repair laminates were measured for all conditioned configurations and a clear increase of voids in the laminate was evident for conditioned samples. Moisture entrapped in uncured repair prepreg had the highest overall effect on the final quality, the void content in the bondline increased six times for repair plies with 0.58% pre-bond moisture content, whereas the void content in the final repair laminate increased 15 times.

**5- Effect of void content on the failure strength**

Mechanical test data showed a decrease in the failure strength of conditioned samples due to the increased presence of voids. For pre-conditioned substrate coupons an increase in the failure strength was noted that can be attributed to potential post-cure of the laminates during the environmental conditioning phase. The most critical observation was made for repair coupons with pre-conditioned repair plies; pre-bond moisture content in the plies of 0.27% resulted in a 5% drop in the final strength, and 0.58% moisture content resulted in an 8% drop in the failure strength.

**6- Effect of the selected repair procedure**

No adhesive failure modes were observed during the mechanical testing phase which indicates a good quality bond between the substrate and the adhesive. This indicates a robust and repeatable repair surface preparation technique.

## 5.1 Conclusive remarks

The objective of this body of work was to address **representative in-service** bonded repair conditions; hence, the test coupons were fabricated using industry standards and techniques that mimic those used in a repair service depot. Therefore, the repairs were cured using a hot bond system with one sided heat application. It was observed that a temperature gradient through the thickness of the repair was present due to this type of heat application. The failure strength results of the repaired coupons include the compounding effects of the thermo-chemical changes in the resin and the adhesive due to the pre-bond moisture effects as well as the temperature gradient during cure.

Suggestions to elaborate on the results of the research would be to investigate alternative cure cycles. Also, non-destructive inspection techniques (NDI) of the failed coupons can be used as more accurate methods to determine void content in the laminate at the location of failure.

## 5.2 Future Work

The present work can be advanced by further investigating the effects of moisture on processing parameters of the laminate and fracture mechanics of the adhesive. The following areas of study are proposed.

**1- The flow of gases in a pre-conditioned repair laminate can be measured**

An instrumented setup can be devised using a pressure sensor to measure the pressure inside the bag of a repair configuration, and a flowmeter can be used to measure the flow of gases from the bag. A calibration procedure could yield the percentage of moisture being evacuated from the bag which can be correlated with the initial moisture in the conditioned laminate. A relationship could then be devised between the pressure, steam flow, and the final void content.

**2- Fracture toughness of the film adhesive can be studied**

The fracture toughness analysis of representative specimens can be performed to obtain $G_{IC}$ for room temperature and conditioned environments. The effect on the $G_{IC}$ of various degrees of cure and pre-bond moisture content can be studied to fully evaluate repair response.

**3- Damage tolerance analysis of the repair laminate can be studied**

Damage tolerance analysis can be performed to evaluate the durability and long term environmental effects on the repair patch. The current results show that for room temperature conditions it is difficult to observe degradation due to pre-bond moisture in the substrate. It is possible that the effect of environment and fatigue can show much different results. Impact testing on the bond region can also be performed to highlight the effect of void and degree of cure on resulting residual strength. Damage tolerance experimental results can also be used to validate any trends found in fracture toughness tests.

# References


1. Kassapoglou, C., *Design and Analysis of Composite Structures*. 2010: John Wiley and Sons.

2. *Military Handbook - MIL-HDBK-17-1F: Composite Materials Handbook, Volume 1 - Polymer Matrix Composites Guidelines for Characterization of Structural Materials*. 2012: SAE International.

3. Tomblin, J.S., Lamia; Davies, Curtis, *CACRC Depot Bonded Repair Investigation - Round Robin Testing*, in *JAMS*. 2009.

4. NLR. *National Aerospace Laboratory Composite Repairs*. 2015 [cited 2015 March 2]; Available from: http://www.nlr.nl/.

5. M2P, *The Costs of Delays and Cancellations - Analysis and Means for Cost Reductions*, in *AGIFORS*. 2006: Dubai.

6. Ackert, S.P. *Basics of Aircraft Maintenance Programs for Financiers*. 2010 [cited 2014; Available from: http://www.aircraftmonitor.com/uploads/1/5/9/9/15993320/basics_of_aircraft_maintenance_programs_for_financiers___v1.pdf.

7. Collings, T., *The effect of observed climatic conditions on the moisture equilibrium level of fibre reinforced plastics.* Royal Aircraft Establishment, 1988.

8. Robson, J.E., F.L. Matthews, and A.J. Kinloch, *The bonded repair of fibre composites: Effect com of composite moisture content.* Composites Science and Technology, 1994. **52**(2): p. 235-246.

9. Armstrong, K.B., *Efforts to standardize aerospace composite repairs, 1988-2003.* Proceedings of the Institution of Mechanical Engineers. Part G: Journal of Aerospace Engineering, 2003. **217**(5): p. 223-236.

10. Blackman, B.R.K., et al., *The Effects of Pre-Bond Moisture on the Fracture Behaviour of Adhesively-Bonded Composite Joints.* The Journal of Adhesion, 2008. **84**(3): p. 256-276.

11. Sage, G.N. and W.P. Tiu, *The effect of glue-line voids and inclusions on the fatigue strength of bonded joints in composites.* Composites, 1982. **13**(3): p. 228-232.

12. Blackman, B.R.K., A.J. Kinloch, and M. Paraschi, *The effect of the substrate material on the value of the adhesive fracture energy, Gc: Further considerations.* Journal of Materials Science Letters, 2001. **20**(3): p. 265-267.

13. Dodiuk, H., L. Drori, and J. Miller, *The Effect of Moisture Content in Epoxy Film Adhesives on their Performance. II. T-Peel and 105°C Lap Shear Strength.* The Journal of Adhesion, 2006. **19**(1): p. 1-13.

14. LaPlante, G. and P. Lee-Sullivan, *Moisture effects on FM300 structural film adhesive: Stress relaxation, fracture toughness, and dynamic mechanical analysis.* Journal of Applied Polymer Science, 2005. **95**(5): p. 1285-1294.

15. Mohan, J., A. Ivanković, and N. Murphy, *Effect of prepreg storage humidity on the mixed-mode fracture toughness of a co-cured composite joint.* Composites Part A: Applied Science and Manufacturing, 2013. **45**: p. 23-34.

16. Gardiner, G. *Out-of-autoclave prepregs: Hype or revolution*. 2011 [cited 2012 January]; Available from: http://www.compositesworld.com/.

17. Brillant, M., *Out-of-Autoclave Manufacturing of Complex Shape Composite Laminates*, in *Department of Mechanical Engineering*. 2010, McGill University.

18. Kardos, J.L., M.P. Duduković, and R. Dave, *Void growth and resin transport during processing of thermosetting — Matrix composites*, in *Epoxy Resins and Composites IV*, K. Dušek, Editor. 1986, Springer Berlin Heidelberg. p. 101-123.

19. Hubert, P., *Processing of Composite Materials (MECH 544) Coursenotes*. 2012, McGill University: Montreal, QC.

20. Grunenfelder, L.K. and S.R. Nutt, *Void formation in composite prepregs – Effect of dissolved moisture.* Composites Science and Technology, 2010. **70**(16): p. 2304-2309.

21. Vodicka, R., *Accelerated Environmental Testing of Composite Materials.* 1998.

22. *ASTM D 5229/D 5229M - Moisture Absorption Properties and Equilibrium Conditioning of Polymer Matrix Composite Materials*. 2002, ASTM International West Conshohocken, PA.

23. Wexler, A., *Relative humidity-temperature relationships of some saturated salt solutions in the temperature range 0 degree to 50 degrees C.* Journal of Research of the National Bureau of Standards, 1954.

24. Parker, B.M., *The strength of bonded carbon fibre composite joints exposed to high humidity.* International Journal of Adhesion and Adhesives, 1990. **10**(3): p. 187-191.

25. Parker, B.M., *The effect of composite prebond moisture on adhesive-bonded CFRP-CFRP joints.* Composites, 1983. **14**(3): p. 226-232.

26. Khoun, L., T. Centea, and P. Hubert, *Characterization Methodology of Thermoset Resins for the Processing of Composite Materials -- Case Study: CYCOM 890RTM Epoxy Resin.* Journal of Composite Materials, 2009. **44**(11): p. 1397-1415.

27. Parker, M.J., *5.09 - Test Methods for Physical Properties*, in *Comprehensive Composite Materials*, A.K. Zweben, Editor. 2000, Pergamon: Oxford. p. 183-226.

28. *ASTM D7028 - Standard test method for glass transition temperature (DMA Tg) of polymer matrix composites by dynamic mechanical analysis (DMA)*. 2007, ASTM International: West Conshohocken, PA.

29. DiBenedetto, A.T., *Prediction of the glass transition temperature of polymers: A model based on the principle of corresponding states.* Journal of Polymer Science Part B: Polymer Physics, 1987. **25**(9): p. 1949-1969.

30. Hickey, C.M.D. and S. Bickerton, *Cure kinetics and rheology characterisation and modelling of ambient temperature curing epoxy resins for resin infusion/VARTM and wet layup applications.* Journal of Materials Science, 2013. **48**(2): p. 690-701.

31. Halley, P.J. and M.E. Mackay, *Chemorheology of thermosets—an overview.* Polymer Engineering & Science, 1996. **36**(5): p. 593-609.

32. O'Brien, D.J. and S.R. White, *Cure kinetics, gelation, and glass transition of a bisphenol F epoxide.* Polymer Engineering & Science, 2003. **43**(4): p. 863-874.

33. Repecka, L., *Vacuum-Bag-Only-Curabble Prepregs That Produce Void-Free Parts*, in *47th International SAMPE Symposium*. 2002.

34. Hoke, M.J., *Adhesive Bonding of Composites*. 2005, Abaris Training Inc: Reno, Nevada, USA.

35. Preau, M., *Out-Of-Autoclave Soft-Patch Breathing Solutions for Low Porosity Repairs*, in *SAMPE Tech*. 2013: Wichita, Kansas, USA.

36. Bujun, K., *Processing Study of in-situ Bonded Scarf Repairs for Composite Structures*, in *Mechanical Engineering*. 2014, McGill University.

37. Kratz, J., et al., *Thermal models for MTM45-1 and Cycom 5320 out-of-autoclave prepreg resins.* Journal of Composite Materials, 2012. **47**(3): p. 341-352.

38. Centea, T. and P. Hubert, *Modelling the effect of material properties and process parameters on tow impregnation in out-of-autoclave prepregs.* Composites Part A: Applied Science and Manufacturing, 2012. **43**(9): p. 1505-1513.

39. *Equilibrium Relative Humidity - Saturated Salt Solutions*. [cited 2014; Available from: http://www.omega.com/temperature/z/pdf/z103.pdf.

40. Rasband, W.S. *Image J*. U. S. National Institutes of Health, Bethesda, Maryland, USA]. Available from: http://imagej.nih.gov/ij/index.html.

41. Kratz, J. and P. Hubert, *Anisotropic air permeability in out-of-autoclave prepregs: Effect on honeycomb panel evacuation prior to cure.* Composites Part A: Applied Science and Manufacturing, 2013. **49**(0): p. 179-191.

42. Hart-Smith, L.J., *Analysis and design of advanced composite bonded joints*. 1974, National Aeronautics and Space Administration Washington, DC.

43. *FM300-2M Adhesive Characterization Results in support of CRIAQ COMP 506 (unpublished)*. 2014, Carlton University.

44. *BA Preliminary Data Summary for CYCOM 5320 (unpublished)*. 2009, Bombardier Aerospace: Montreal, QC.

45. Charalambides, M.N., et al., *Adhesively-bonded repairs to fibre-composite materials I. Experimental.* Composites Part A: Applied Science and Manufacturing, 1998. **29**(11): p. 1371-1381.

46. Kenny, J.M., A. Apicella, and L. Nicolais, *A model for the thermal and chemorheological behavior of thermosets. I: Processing of epoxy-based composites.* Polymer Engineering & Science, 1989. **29**(15): p. 973-983.

47. Ahn, S.-H. and G. Springer, *Repair of Composite Laminates*, DOT/FAA/AR-00/46, Editor. 2000.

48. Tomblin, J.S., C. Yang, and P. Harter, *Investigation of thick bondline adhesive joints*, DOT/FAA/AR-01/33, Editor. 2001, DTIC Document.

49. Baker, A.A.R., L.R.F.; Jones, R. , *Surface Treatment and Repair Bonding*, in *Advances in the Bonded Composite Repairs of Metallic Aircraft Structure*. 2002, Elsevier Science Ltd. .

50. Baker, A.A.R., L.R.F.; Jones, R. , *Certification Issues for Critical Repairs*, in *Advances in the Bonded Composite Repairs of Metallic Aircraft Structure*. 2002, Elsevier Science Ltd.

51. Greenberg, C. *B787 Structural Maintenance Repair*. in *2007 Leasing & Asset Management Conference*. 2007.

# Appendix A

# Void Content Measurements

The resulting moisture content in the parent laminate, adhesive film, and repair patch for each of the conditioning requirements is summarized in Table A-1. A summary of the resulting percentage void content (average) in the repair patch, bondline, and the parent laminate for each of the repair configurations is presented in Table A-2.

**Table A-1: Resulting moisture content for conditioned parent laminate, adhesive film, and repair patch**

| Repair ID *[2] | Moisture content (%w/w) *[1] | Conditioning requirements | Duration | Temperature and Humidity |
|---|---|---|---|---|
| **L1-C0** | 0 | Baseline, no conditioning | - | - |
| **L1-C1b** | 0.9 | Conditioned parent laminate | 180 days | 65°C, 70%RH |
| **L2-C0** | 0 | Baseline, no conditioning | - | - |
| **L2-C1a** | 0.8 | Conditioned parent laminate | 140 days | 65°C, 70%RH |
| **L2-C1b** | 0.9 | Conditioned parent laminate | 180 days | 65°C, 70%RH |
| **L3-C2a** | 0.3 | Conditioned adhesive film | 4 hours | 23°C, >90%RH |
| **L3-C3a** | 0.27 | Conditioned repair patch | 24 hours | 34°C, 80%RH |
| **L3-C3b** | 0.58 | Conditioned repair patch | 24 hour | 23°C, >90%RH |

*1: Note that the resulting moisture herein is measured within ±0.02%

*2: Note that since the repair configuration L1-C1a was deemed ineffective, as discussed in Section 4.2.2, supporting data related to these repairs (conditioning requirements and void content results) have been omitted from this appendix.

**Table A-2: Resulting average void content in the repair patch, bondline, and parent laminate**

| Repair ID | Average Void Content (%) | | | |
|---|---|---|---|---|
| | Patch | Bondline | Parent | Total Laminate |
| **L1-C0** | 0.11 | 0.21 | 0.34 | 0.25 |
| **L1-C1b** | 0.86 | 2.51 | 0.26 | 0.77 |
| **L2-C0** | 0.22 | 0.72 | 0.15 | 0.20 |
| **L2-C1a** | 1.65 | 2.11 | 0.26 | 1.00 |
| **L2-C1b** | 0.89 | 2.93 | 0.52 | 0.81 |
| **L3-C2a** | 0.66 | 0.49 | 0.40 | 0.56 |
| **L3-C3a** | 2.15 | 2.39 | 0.84 | 1.42 |
| **L3-C3b** | 3.30 | 4.50 | 0.31 | 2.73 |

# Appendix B

# Mechanical Test Data

The appendix herein includes the tensile test coupon measurements (measurements in Table B-3 per Figure B-1). It also includes the mechanical test data in Table B-4, including the hydraulic grip pressure, failure load and failure mode, as well as the calculated stiffness for each coupon. Additionally, the force-time history obtained from the raw data for all the mechanical tests have been shown in Figure B-2 through Figure B-10.

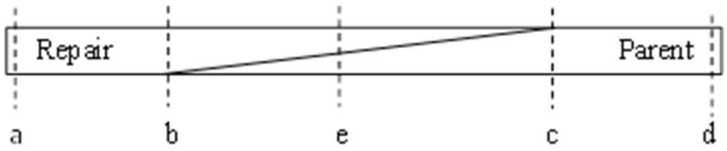


**Figure B-1: Thickness and width measurement locations of the tensile test coupons**

**Table B-3: Actual thickness and width measurements for all tensile test coupons**

| Coupon ID | width (mm) | | | | thickness (mm) | | |
|---|---|---|---|---|---|---|---|
| | a | b | c | d | a | c | d |
| L1-c0-1 | 21.89 | 21.91 | 22.21 | 22.72 | 1.71 | 1.95 | 1.73 |
| L1-c0-2 | 26.28 | 26.90 | 27.74 | 28.33 | 1.63 | 1.97 | 1.72 |
| L1-c0-3 | 24.07 | 25.64 | 25.85 | 25.50 | 1.63 | 2.00 | 1.78 |
| L1-c0-4 | 22.66 | 21.07 | 20.77 | 20.11 | 1.65 | 1.94 | 1.76 |
| L1-c1b-1 | 23.56 | 23.83 | 24.08 | 24.15 | 1.60 | 1.85 | 1.73 |
| L1-c1b-2 | 23.73 | 23.90 | 23.93 | 23.89 | 1.65 | 1.83 | 1.73 |
| L1-c1b-3 | 25.61 | 25.93 | 26.08 | 26.46 | 1.62 | 1.86 | 1.76 |
| L1-c1b-4 | 26.71 | 26.45 | 26.41 | 26.32 | 1.63 | 1.82 | 1.75 |
| L2-c0-1 | 24.68 | 24.51 | 24.50 | 24.62 | 3.27 | 3.52 | 3.35 |
| L2-c0-2 | 24.09 | 24.59 | 24.74 | 24.16 | 3.26 | 3.50 | 3.36 |
| L2-c0-3 | 25.07 | 25.13 | 25.33 | 24.82 | 3.22 | 3.53 | 3.32 |

| Coupon ID | width (mm) | | | | thickness (mm) | | |
|---|---|---|---|---|---|---|---|
| | a | b | c | d | a | c | d |
| L2-c0-4 | 24.68 | 24.59 | 24.35 | 23.95 | 3.26 | 3.48 | 3.32 |
| L2-c1a-0 | 28.57 | 28.11 | 28.22 | 28.29 | 3.21 | 3.41 | 3.33 |
| L2-c1a-1 | 24.92 | 24.84 | 24.38 | 24.41 | 3.22 | 3.52 | 3.37 |
| L2-c1a-2 | 25.40 | 24.89 | 24.74 | 24.56 | 3.21 | 3.53 | 3.35 |
| L2-c1a-3 | 24.84 | 24.46 | 23.77 | 23.52 | 3.21 | 3.53 | 3.37 |
| L2-c1b-1 | 23.81 | 24.49 | 24.81 | 24.81 | 3.22 | 3.57 | 3.35 |
| L2-c1b-2 | 25.38 | 25.12 | 25.00 | 24.57 | 3.24 | 3.67 | 3.31 |
| L2-c1b-3 | 25.84 | 25.88 | 26.05 | 25.95 | 3.22 | 3.65 | 3.33 |
| L2-c1b-4 | 24.84 | 24.87 | 24.67 | 24.41 | 3.23 | 3.72 | 3.35 |
| L3-c2a-1 | 24.70 | 24.83 | 24.52 | 24.45 | 3.15 | 3.53 | 3.26 |
| L3-c2a-2 | 25.12 | 25.08 | 25.26 | 25.20 | 3.14 | 3.56 | 3.27 |
| L3-c2a-3 | 25.78 | 25.59 | 26.30 | 26.11 | 3.14 | 3.52 | 3.31 |
| L3-c2a-4 | 26.73 | 26.51 | 25.73 | 25.28 | 3.16 | 3.56 | 3.28 |
| L3-c3a-1 | 24.80 | 25.67 | 25.52 | 24.63 | 3.19 | 3.55 | 3.26 |
| L3-c3a-2 | 24.07 | 24.33 | 23.81 | 23.80 | 3.14 | 3.54 | 3.28 |
| L3-c3a-3 | 24.91 | 25.22 | 25.50 | 25.36 | 3.19 | 3.52 | 3.23 |
| L3-c3a-4 | 25.91 | 25.79 | 25.07 | 25.01 | 3.15 | 3.54 | 3.22 |
| L3-c3b-1 | 24.59 | 25.20 | 25.86 | 25.96 | 3.16 | 3.59 | 3.33 |
| L3-c3b-2 | 24.70 | 24.57 | 24.89 | 24.94 | 3.14 | 3.55 | 3.30 |
| L3-c3b-3 | 23.90 | 23.88 | 24.05 | 23.97 | 3.13 | 3.54 | 3.30 |
| L3-c3b-4 | 24.31 | 24.62 | 24.62 | 24.64 | 3.14 | 3.54 | 3.30 |

**Table B-4: Actual mechanical test details and results for all tensile test coupons**

| Coupon ID | Grip pressure (psi) | Type of failure mode | failure load (kN) | Failure Strength (MPa) | Experimental Modulus (MPa) |
|---|---|---|---|---|---|
| L1-c0-1 | 550 | C + delam | 20.867 | 524 | x |
| L1-c0-2 | 500 | C + delam | 26.1 | 539 | 43,527 |
| L1-c0-3 | 550 | C + delam | 24.596 | 540 | 43,760 |
| L1-c0-4 | 550 | C + delam | 21.1 | 559 | 42,272 |
| L1-c1a-0 | 1000 | C | 20.73 | 456 | x |
| L1-c1a-1 | 1000 | A | 20.5 | 454 | x |
| L1-c1a-2 | 1000 | A | 20.37 | 474 | x |
| L1-c1a-3 | 1000 | A+C | 20.7 | 456 | x |
| L1-c1b-1 | 550 | C + delam | 22.7 | 550 | 41,793 |
| L1-c1b-2 | 550 | C + delam | 20.94 | 505 | 42,022 |

| Coupon ID | Grip pressure (psi) | Type of failure mode | failure load (kN) | Failure Strength (MPa) | Experimental Modulus (MPa) |
|---|---|---|---|---|---|
| L1-c1b-3 | 550 | C + delam | 24.9 | 548 | 43,868 |
| L1-c1b-4 | 550 | C + delam | 24.9 | 543 | 42,025 |
| L2-c0-1 | 2000 | D | 49.47 | 596 | x |
| L2-c0-2 | 2000 | C | 46.8 | 569 | 43,430 |
| L2-c0-3 | 1500 | C | 49.5 | 588 | 46,224 |
| L2-c0-4 | 1500 | C | 48.03 | 587 | 45,964 |
| L2-c1a-0 | 2000 | D | 53.9 | 574 | x |
| L2-c1a-1 | 2000 | C + delam | 47.78 | 575 | x |
| L2-c1a-2 | 2000 | C + delam | 49.19 | 587 | x |
| L2-c1a-3 | 2000 | C + delam | 46.93 | 577 | x |
| L2-c1b-1 | 1500 | C | 50.9 | 615 | 46,807 |
| L2-c1b-2 | 1500 | C | 51.74 | 607 | 47,060 |
| L2-c1b-3 | 1500 | grip failure | 47.5 | - | 44,658 |
| L2-c1b-4 | 1250 | C + delam | 51.35 | 606 | 45,963 |
| L3-c2a-1 | 1250 | D | 47.6 | 583 | 47,356 |
| L3-c2a-2 | 1250 | C | 48.9 | 585 | 49,795 |
| L3-c2a-3 | 1100 | C | 48.23 | 559 | 47,422 |
| L3-c2a-4 | 1000 | grip slip | 49.7 | 572 | 47,052 |
| L3-c3a-1 | 1050 | C/D | 47.43 | 566 | 47,870 |
| L3-c3a-2 | 1050 | C | 44.37 | 557 | 45,505 |
| L3-c3a-3 | 1050 | C | 45.7 | 546 | 47,845 |
| L3-c3a-4 | 1050 | D | 46.6 | 554 | 45,275 |
| L3-c3b-1 | 1100 | C | 44.98 | 527 | 46,395 |
| L3-c3b-2 | 1100 | C/D | 45.5 | 552 | 45,741 |
| L3-c3b-3 | 1100 | C | 42.33 | 532 | 45,063 |
| L3-c3b-4 | 1050 | C + delam | 44.28 | 542 | 46,449 |

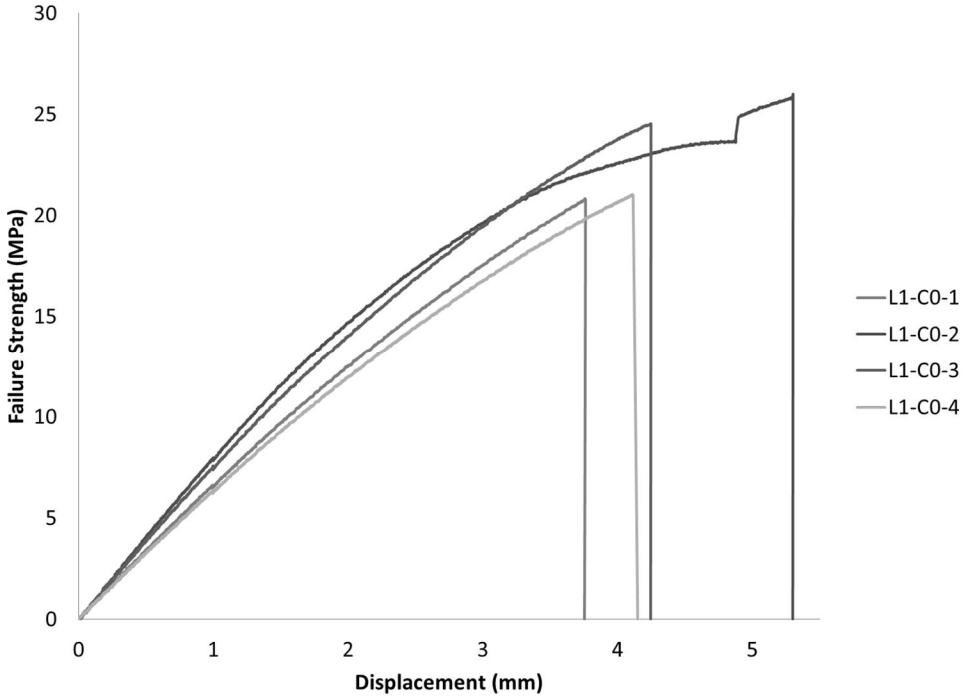


**Figure B-2: Force history for all L1-C0 test samples**

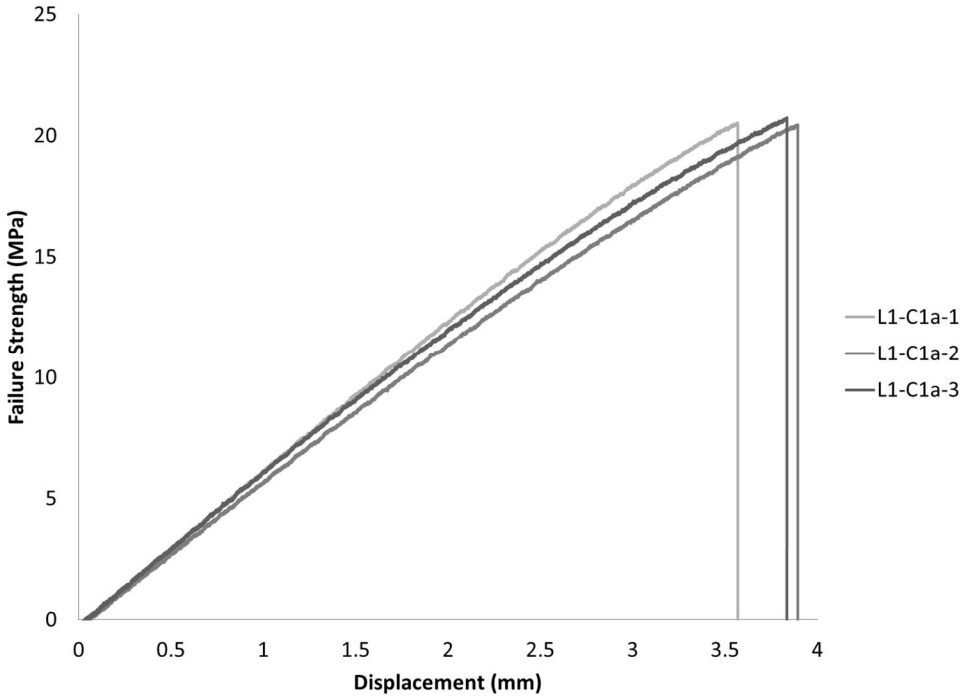


**Figure B-3: Force history for all L1-C1a test samples**

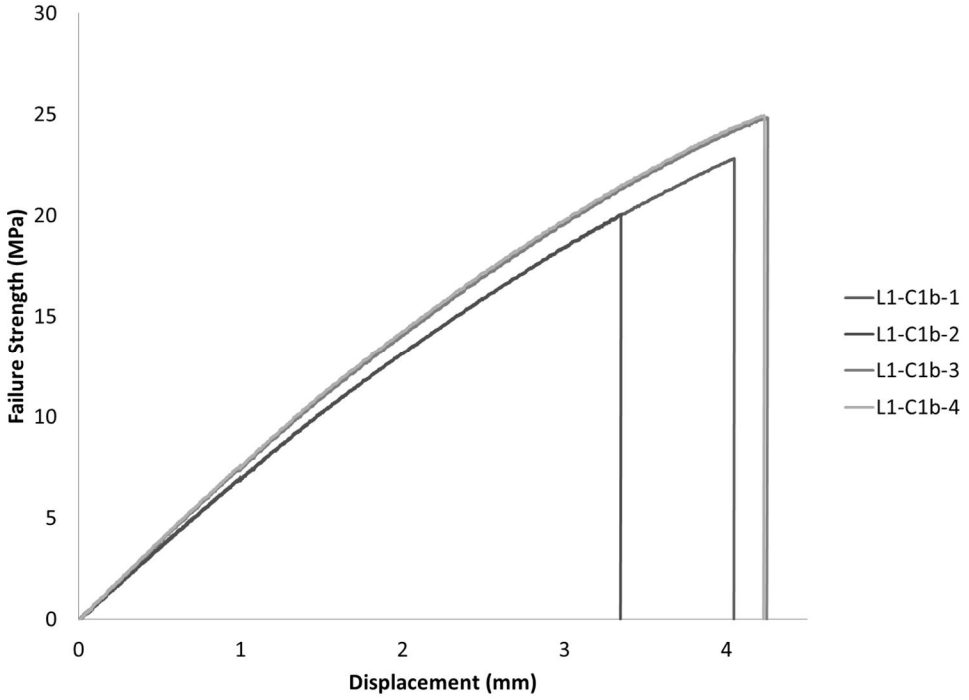


**Figure B-4: Force history for all L1-C1b test samples**

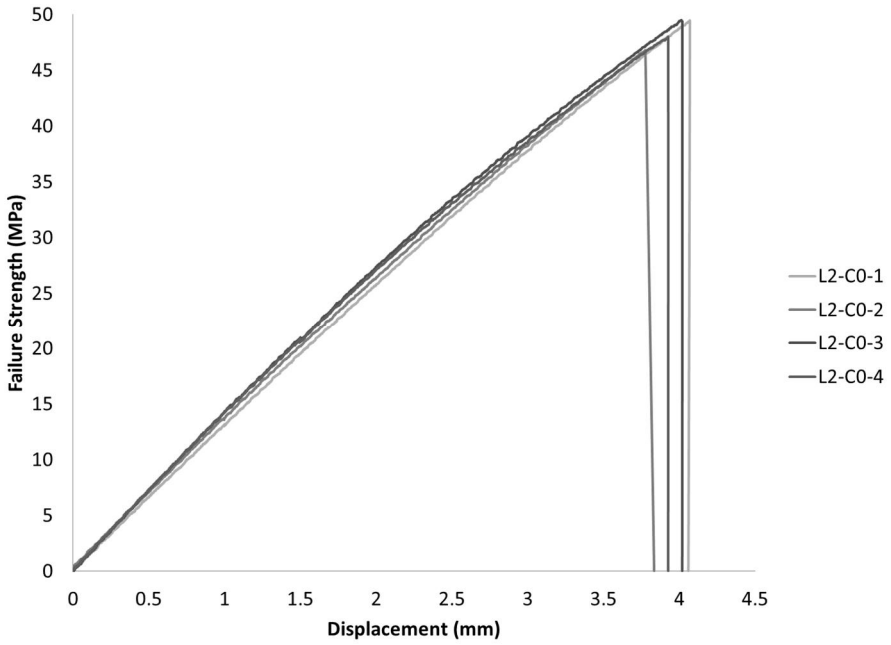


**Figure B-5: Force history for all L2-C0 test samples**

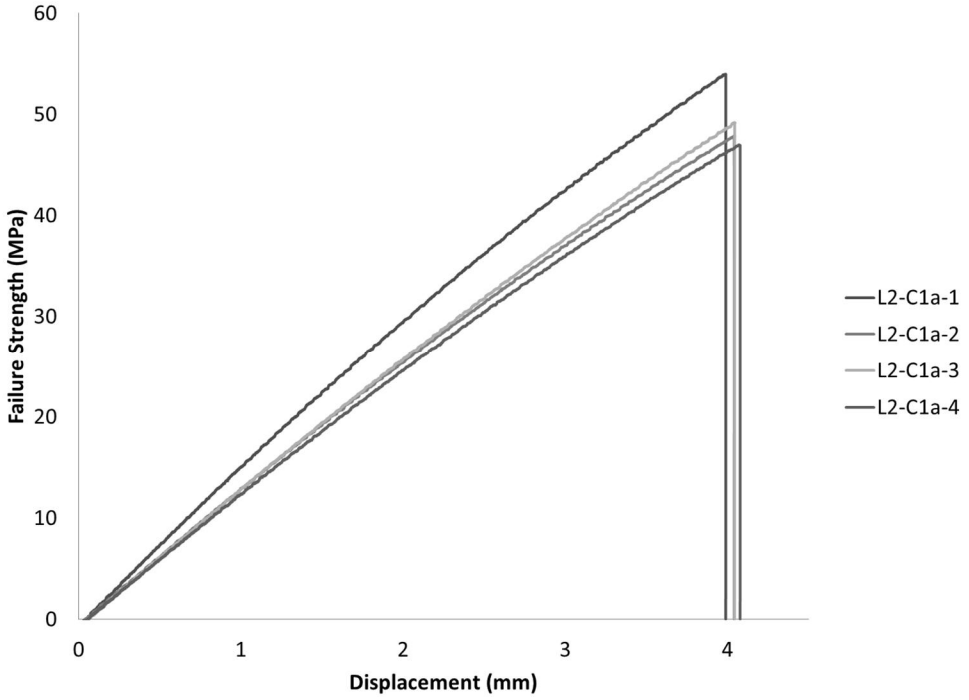


**Figure B-6: Force history for all L2-C1a test samples**

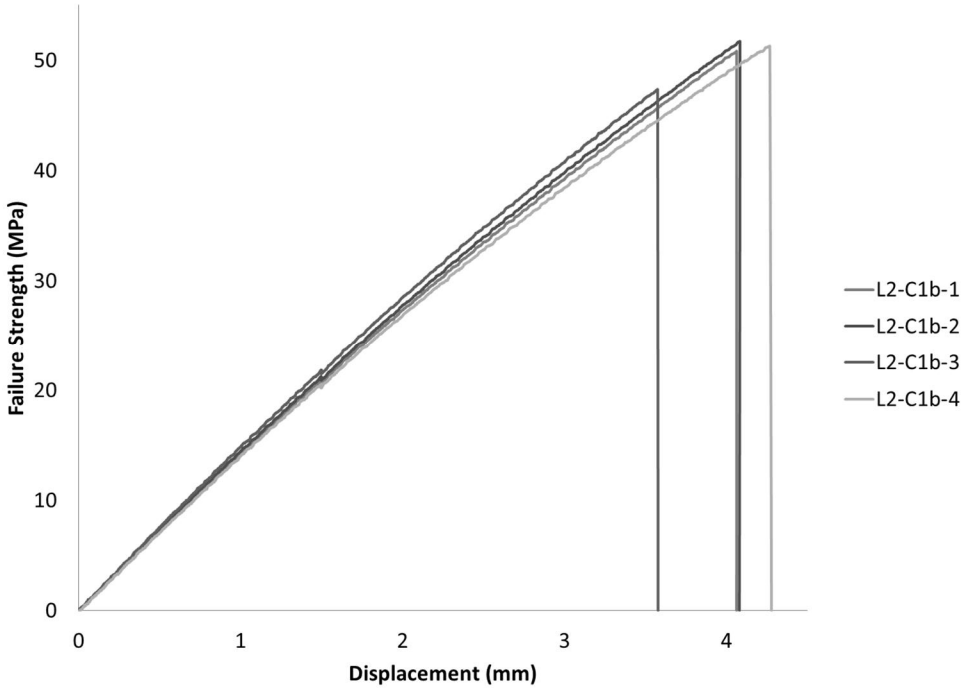


**Figure B-7: Force history for all L2-C1b test samples**

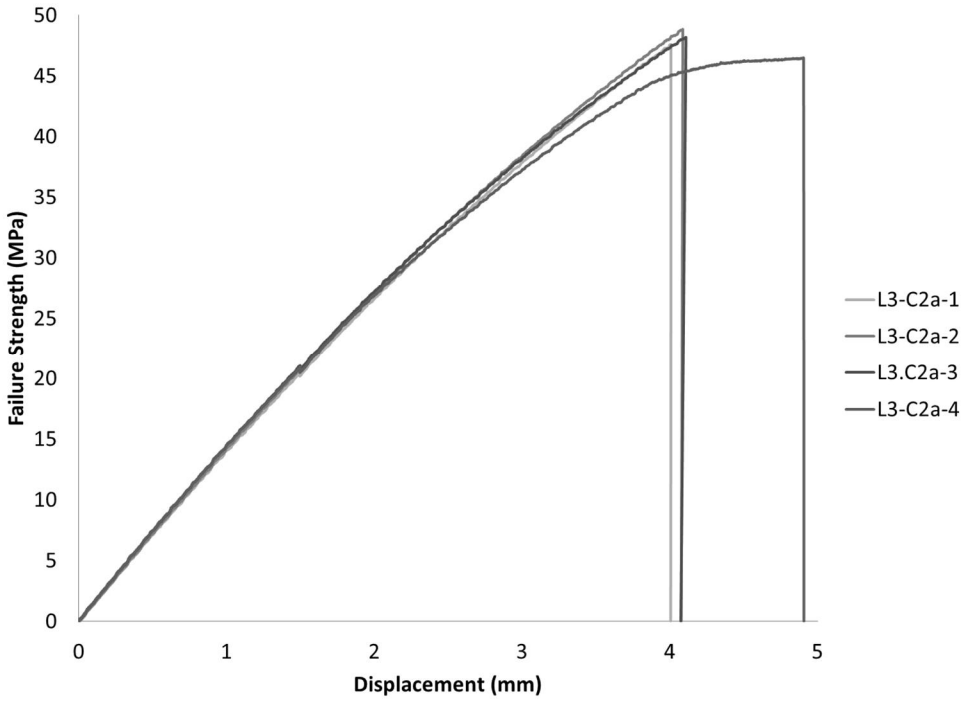


**Figure B-8: Force history for all L3-C2a test samples**

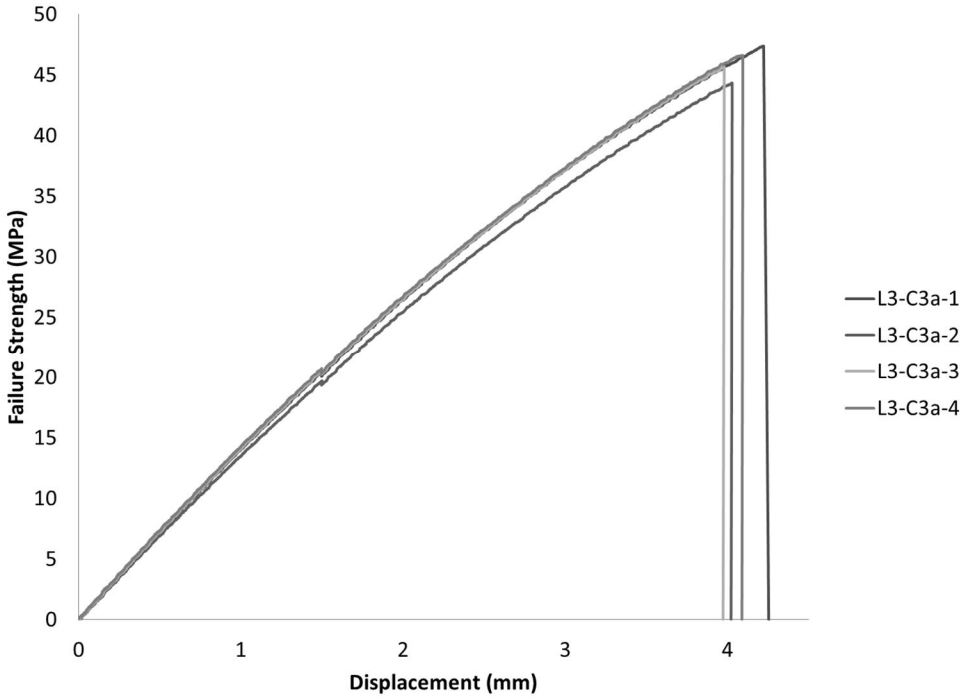


**Figure B-9: Force history for all L3-C3a test samples**

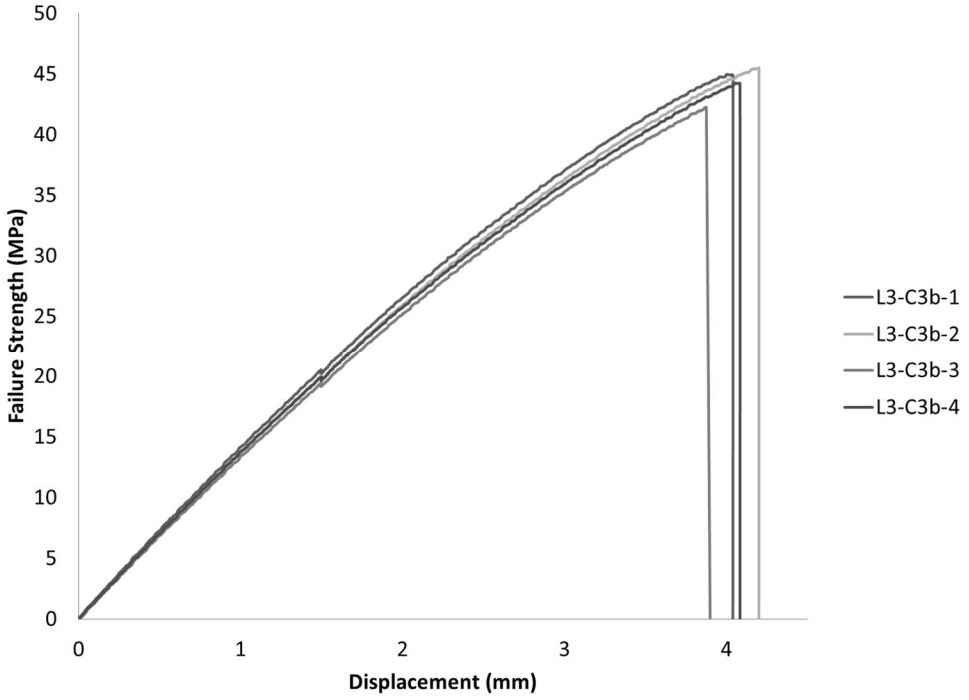


**Figure B-10: Force history for all L3-C3b test samples**